

7-17-2008

# Mechanistic Studies of Specific DNA Cleavage By PvuII Restriction Endonuclease

Xie Fuqian

University of Missouri-St. Louis, fxhb6@umsl.edu

Follow this and additional works at: <https://irl.umsl.edu/dissertation>

 Part of the [Chemistry Commons](#)

---

## Recommended Citation

Fuqian, Xie, "Mechanistic Studies of Specific DNA Cleavage By PvuII Restriction Endonuclease" (2008). *Dissertations*. 548.  
<https://irl.umsl.edu/dissertation/548>

This Dissertation is brought to you for free and open access by the UMSL Graduate Works at IRL @ UMSL. It has been accepted for inclusion in Dissertations by an authorized administrator of IRL @ UMSL. For more information, please contact [marvinh@umsl.edu](mailto:marvinh@umsl.edu).

---

Mechanistic Studies of Specific DNA Cleavage By  
*Pvu*II Restriction Endonuclease

A Dissertation

By

Fuqian Xie

Submitted to the Office of Graduate Studies of  
The University of Missouri St. Louis

In partial fulfillment of the requirements for the degree of

DOCTOR OF PHILOSOPHY

May 2008

Major Subject: Biochemistry

---

## Abstract

Mechanistic Studies of Specific DNA Cleavage by *PvuII* Restriction Endonuclease

(August 2008)

Fujian Xie, B.S., Zhejiang University, P. R. China

Chair of Committee: Dr. C. Dupureur

*PvuII* restriction endonuclease is a homodimeric protein which recognizes and cleaves the palindromic sequence (CAG↓CTG) in the presence of Mg(II) ions. Starting with *PvuII* as a model system, pK<sub>a</sub> calculations with crystallographically defined metal ligated water are applied to PD...D/ExK motif metallonucleases in order to investigate the activation of nucleophile in metal dependent DNA hydrolysis. These results establish the electrostatic contributions of the metal ions and the conserved Lys in lowering water pK<sub>a</sub>. The calculated pK<sub>a</sub> values of metal ligands have been used to simulate the pH dependence of Mg(II) binding to *PvuII*. The bell shaped pH-rate profile is dissected into three ionizations. One is recognized as from the metal ligands, and the other two have pK<sub>a</sub>'s similar to calculated metal ligated water pK<sub>a</sub> in the absence of DNA. The determined pH profiles agree well with previous pH dependence studies on metallonucleases, and the correlation with pK<sub>a</sub> calculations indicates the direct involvement of metal activated water in catalysis.

---

The different metal occupancies observed in crystal structures lead to controversy regarding the number and function of metal ions involved in DNA hydrolysis by type II restriction endonucleases. Quench flow experiments are used to monitor Mg(II) dependent single and multiple turnover DNA cleavage reactions with *PvuII*. Several models which differ in order of binding and the number of metal ions supporting catalysis are examined by global fits using DynaFit. The best fitted model has a preference of binding order in the reaction scheme and supports one-metal ion catalysis with 50 fold reduced activity compared with two-metal ion catalysis. The same model is also found to account for multiple turnover data in fits and simulations. A unique reaction scheme for *PvuII* is established to interpret the determined Mg(II) dependence of kinetic data, which provides an insight into Mg(II) participation in substrate binding, catalysis and product dissociation by restriction endonucleases.

---

## DEDICATION

I dedicate this work to my Mom, who encourages me to complete my Ph.D and support me along the way.

---

## ACKNOWLEDGEMENTS

I would like to thank my advisor, Dr. Cynthia M. Dupureur, for the guidance and help on my projects. I switched from a polymer chemist to a biochemist after five years studies in her laboratory. Dr. Dupureur has made the greatest contributions to my conversion. I also thank Dr. Dupureur for her help with my English writing and speaking, which is important for my scientific career in the future as well. I would like to thank Dr. Jim Briggs in University of Houston. His assistance is essential for the completion of my first project. He provided us all the programs and protocols for  $pK_a$  calculations. I would like to thank Dr. Chung F. Wong who is a computational biochemist for instructive discussion with my  $pK_a$  calculation works. I would like to thank the rest of committee members Dr. Keith J. Stine and Dr. Michael R. Nichols for helpful scientific discussions and suggestions on my dissertation. I thank Dr. Wesley R. Harris for helpful suggestions with my dissertation proposal and presentations. I thank Dr. Peter Kuzmic and Honggao Yang for trouble shooting the program DynaFit.

I thank the former lab member Dr. Lori Bowen. She helped me to get started in the lab and taught me lots of experimental techniques. I thank the former lab member Dr. Julie King who started the computational works, and her notes used to be very helpful. I also thank the former lab member Dr. Shabir H. Qureshi who started the kinetic work and modeling, and his kinetic data is included in my dissertation. I would like to thank Greg Papadakos for the contribution of kinetic data to my dissertation and helpful suggestions to my projects. He also helped me get familiar

---

with spectrofluorimeter to complete my last experiment. I am grateful to the rest of my lab members, Charu Prasannan, Supratik Dutta and Binod Prasad Pandey for their help in my work and being good friends.

Finally, I would like to thank Department of Chemistry and Biochemistry in UMSL providing me the opportunity and financial support for five years Ph.D studies. I would like to thank NIH for funding to do research.

---

## TABLE OF CONTENTS

	Page
ABSTRACT	ii
DEDICATION	iv
ACKNOWLEDGEMENTS	v
TABLE OF CONTENTS	vii
LIST OF FIGURES	ix
LIST OF TABLES	xii
LIST OF SCHEMES	xv
I. INTRODUCTION	
Restriction Endonuclease	1
Divalent Metal Cofactors Mg(II)	16
pK <sub>a</sub> Calculation and Its Correlation With pH Dependence Studies.	18
Kinetics Studies in Enzymology.	26
Overview of Dissertation	30
II. MATERIALS AND METHODS	
Materials	32
Purification and Preparation of <i>Pvu</i> II Restriction Endonucleases	33
Preparation and Quantitation of Oligonucleotides	36
Radio-labeling of Oligonucleotides	40
Quantitation of Metal Ions Stocks by Atomic Absorption	42
Determination of <i>Pvu</i> II Endonuclease-DNA Equilibrium Constants	42
Using Fluorescence Anisotropy	
Quench Flow	44
The Application of Swiss Pdbviewer	44

---

UHBD Program	46
Dynafit Program	49
III. ELECTROSTATIC CONTRIBUTIONS TO WATER ACTIVATION IN PD...(D/E)xK METALONUCLEASE	
Introduction	52
Experiments and Methods	61
Results	67
Discussion	102
Conclusions	111
IV. METAL DEPENDENCE STUDY AND KINETIC MODELING	
Introduction	112
Experiments and Methods	117
Results	121
Discussion	170
REFERENCES	184
APPENDIX	193
VITA	199

---

## LIST OF FIGURES

	Page
Figure 1.1. The biological function of restriction endonuclease as a part of restriction modification system in bacteria	2
Figure 1.2. The crystal structures of type II restriction endonucleases as a homodimer and its association with cognate DNA duplex	4
Figure 1.3. Conserved PD...D/ExK catalytic motif in endonuclease family	6
Figure 1.4. The general mechanism for the hydrolysis of phosphodiester bond	9
Figure 1.5. One-Metal Ion Mechanism	11
Figure 1.6. Two-Metal Ion Mechanism	12
Figure 1.7. Superposition of <i>PvuII</i> with <i>BglII</i> , <i>BamHI</i> and <i>EcoRV</i>	14
Figure 1.8. Three-Metal Ion Mechanism	15
Figure 1.9. Environment effects on $pK_a$ of titratable sites	24
Figure 2.1. Purification of WT <i>PvuII</i> endonucleases using heparin sepharose	35
Figure 2.2. Structure of the fluorescent dye of Hex, Rhodamine and Dansyl Fluorophore	39
Figure 2.3. PAGE Gel and kinetic analysis of <i>PvuII</i> endonucleases activity for single turnover assay and steady state assay	41
Figure 2.4. The configuration of SFM-4 quench flow instruments	45
Figure 2.5. The application of DynaFit in global fit	50
Figure 3.1. Possible roles of metal ions and the activation of water molecule in the DNA hydrolysis by endonuclease	54

---

	Page
Figure 3.2. The general mechanism of phosphodiester bond hydrolysis by type II restriction endonucleases	59
Figure 3.3. A two site interacting model fits well with experimental pH titration of WT using $^{25}\text{Mg}(\text{II})$ NMR	74
Figure 3.4. The metal ion occupancies in the <i>PvuII</i> active sites	76
Figure 3.5. The defined metal ligated water molecules in <i>PvuII</i>	79
Figure 3.6. pH dependence of single turnover rate constant	94
Figure 3.7. pH dependence of steady state kinetics	96
Figure 3.8. Simulated pH-rate profiles for single turnover and steady state reaction by derived pKa and kinetic parameters in corresponding global fits and local fits	101
Figure 3.9. Superposition of <i>BamHI</i> and <i>PvuII</i> active site	104
Figure 3.10. The water activation in the presence and without the presence of substrate	110
Figure 4.1. The resolved metal binding sites in <i>PvuII</i>	113
Figure 4.2. DNA binding affinity is dependent on $\text{Ca}(\text{II})$ concentration	122
Figure 4.3. The Hill analysis of $\text{Mg}(\text{II})$ dependence of DNA association rate constants	131
Figure 4.4. Dependence of single turnover rate constants on metal ion Concentrations	133

---

	Page
Figure 4.5.	141
A. Simulated Mg(II)- $k_{obs}$ profiles from the best fit based on model	
A and B are plotted with experimental Mg(II)- $k_{obs}$ profile.	
	142
B. Global fits of single turnover time courses at 0.1, 0.5 and 1 mM	
Mg(II)	
Figure 4.6.	151
Simulated Mg(II)- $k_{obs}$ profiles from the best fit based on model	
C1, C2 and C3 are plotted with experimental Mg(II)- $k_{obs}$ profile.	
Figure 4.7.	153
A typical burst phase observed in specific DNA cleavage by <i>PvuII</i>	
under pre-steady state kinetics conditions	
Figure 4.8.	155
Mg(II) effect on the weak interactions between protein and	
product using fluorescence anisotropy binding assays	
Figure 4.9.	159
The best fit to the Mg(II)-steady state velocity profile by two	
models B1-1 and B1-2.	
Figure 4.10.	161
Global fit of pre-steady state time courses under various Mg(II)	
concentration	

---

## LIST OF TABLES

	Page
Table 1.1. Crystal structures of type II restriction endonucleases which belong to PD...D/ExK family and exceptions.	8
Table 1.2. The ionizable groups in proteins and their model pK <sub>a</sub> 's	19
Table 2.1. Oligonucleotides Sequences Used In the Assays	37
Table 3.1. Summary of pK <sub>a</sub> predictions for apo enzyme	70
Table 3.2. Summary of pK <sub>a</sub> calculations for PvuII variants	72
Table 3.3. Summary of pK <sub>a</sub> calculations in the presence of Mg(II)	77
Table 3.4. Summary of pK <sub>a</sub> calculations of Mg(II) ligated water molecules	80
Table 3.5. Summary of water pK <sub>a</sub> calculations with WT and K70A variants	83
Table 3.6. Summary of pK <sub>a</sub> calculations with other nucleases with conserved Lys	85
Table 3.7. The pK <sub>a</sub> calculation of metal ligated water in the presence of nucleotides and neutralization of DNA backbone	88
Table 3.8. The pK <sub>a</sub> calculation of attacking water molecules in <i>EcoRV</i> upon S substitution on non-bridging O of 3' phosphate	91
Table 3.9. The pK <sub>a</sub> of metal ligated water dependence on salt concentration and protein dielectric constant	92
Table 3.10. The summary of global fits and local fits with pH profiles of single turnover and steady state kinetics.	100

---

	Page
Table 4.1. Experimental measurements and corresponding global fits on the equilibrium constants in Scheme 4.1.	125
Table 4.2. Measured dissociation rate constants for DNA binding equilibrium of <i>PvuII</i>	128
Table 4.3. Estimate Mg(II) dependent DNA association rate	130
Table 4.4. The dissociation rate constants for metal ion binding	137
Table 4.5. Global fit results with single turnover reaction courses as a function of Mg(II) concentrations.	139
Table 4.6. The investigations of two distinct sites on metal binding properties and cooperativity	149
Table 4.7. The best fit results of steady state and pre-steady state kinetics with model B1-1 and B1-2.	162
Table 4.8. The potential influence of weak equilibrium between apo enzyme and product on global fit results	165
Table 4.9. Best fit derived metal binding equilibrium constants and product release rate for DNA binding, single turnover kinetics, steady state kinetics and pre-steady state kinetics.	168
Table 4.10. A. Mg(II) binding affinities of enzymes	172
B. The comparison of Mg(II) and Ca(II) binding affinities for the same enzyme.	173

---

	Page
Table 4.11. The summary of distance between two metal ions in the crystal structures of nucleases	175
Table 4.12. Summary of Ca(II) and Mg(II) dependence on DNA binding affinity	176
Table 4.13. The summary of measured <i>PvuII</i> enzyme activity for different mixing protocols	179

---

## LIST OF SCHEMES

	Page
Scheme 3.1. The kinetic model scheme for equation 3	66
Scheme 3.2. The general kinetic model for single turnover and steady state reaction	98
Scheme 4.1. Model of Metal Ion Participation In Metal Dependence of DNA Binding Equilibrium.	123
Scheme 4.2. Proposed candidate kinetic models for global fits to Mg(II) dependent single turnover progressive courses	134
Scheme 4.3. Proposed candidate models to dissect two metal binding site A and site B	147
Scheme 4.4. The proposed candidate models to fit Mg(II) dependent steady state and pre-steady state experimental data	157

---

## CHAPTER I. INTRODUCTION

This mechanistic study of specific DNA cleavage by *PvuII* restriction endonucleases combines computational and experimental approaches to investigate the nucleophile activations in the catalytic mechanism and Mg(II) participation in DNA association, catalysis and product dissociation. The biophysical characterizations are particularly important to study enzyme behaviors, which provide the most reliable evidences to understand the catalytic mechanism or build up the reaction scheme. Besides those conventional experimental approaches, the computational methods in biophysics are developing rapidly since they provide new scopes to those issues which are beyond the reach of experiments. Based on protein crystal structures, the  $pK_a$  calculations can predict the  $pK_a$ 's for those catalytic residues. Now kinetic modeling greatly depends on the application of some data fitting programs (Scientist, Origin, DynaFit and etc), which provide more freedom and convenience in modeling, and are able to derive those critical kinetic parameters which are not measurable experimentally. This chapter includes a brief description of restriction endonucleases, structural and functional features of metal cofactor,  $pK_a$  calculation methods and kinetic studies in enzymology.

### **Restriction Endonuclease**

The biological function of type II restriction endonucleases is to protect the host DNA by cleaving the invading phage DNA into fragments as a part of restriction modification system (**Figure 1.1**) (Tock & Dryden, 2005). DNA cleavage reactions

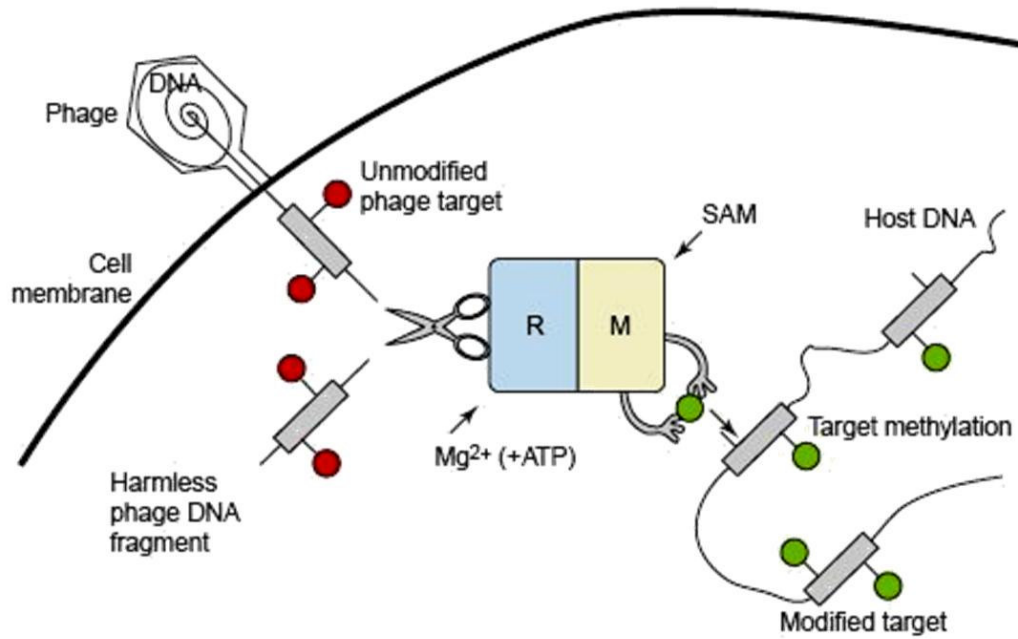


**Figure 1.1. The biological function of restriction endonuclease as a part of restriction modification system in bacteria.** The methylated host DNAs are highlighted as green spheres attached to host DNA backbone. The invading phage DNAs as the recognition and cleavage target by restriction endonuclease are marked red spheres. Type II restriction endonucleases only require Mg(II) as cofactor for hydrolytic activity (Tock & Dryden, 2005).

---

catalyzed by type II restriction endonucleases occur specifically at the recognition sites and generate products with 3'-hydroxyl and 5'-phosphate. The recognition site usually is a palindromic sequences with 4~8 base pairs on both strands of a duplex and the products can have either blunt ends (ex. *EcoRV* and *PvuII*) or a 5' or 3' overhang (*EcoRI* and *BglI*) depending on the cleavage sites on the top and bottom strand. The type II restriction endonucleases are typically homodimers, binding to the DNA duplex. Dramatic conformational changes in the protein occur during DNA association coupled with DNA bending (Hiller, et al., 2003; Dupureur, 2005). The substrate binding and cleavage is accomplished by one catalytic domain on each subunit and one binding domain, which consists of five stranded  $\beta$  sheets flanked by two  $\alpha$  helices (**Figure 1.2**).

*Metal Cofactor Required In Specific DNA Association and Cleavage.*

According to crystal structures of DNA bound complexes, metal cofactors mediate the specific DNA association by type II restriction endonucleases and the direct contact between scissile phosphate and metal binding sites of enzyme has been visualized (Horton, et al., 1998; Horton & Cheng, 2000). The binding experiments also indicate that the specificity of DNA binding is greatly enhanced in the presence of a metal cofactor such as Ca(II) (Engler, et al., 1997; Martin, et al., 1999a; Conlan & Dupureur, 2002b). DNA binding affinities from pico to nanomolar in the presence of Ca(II) have been determined by various methods including fluorescence

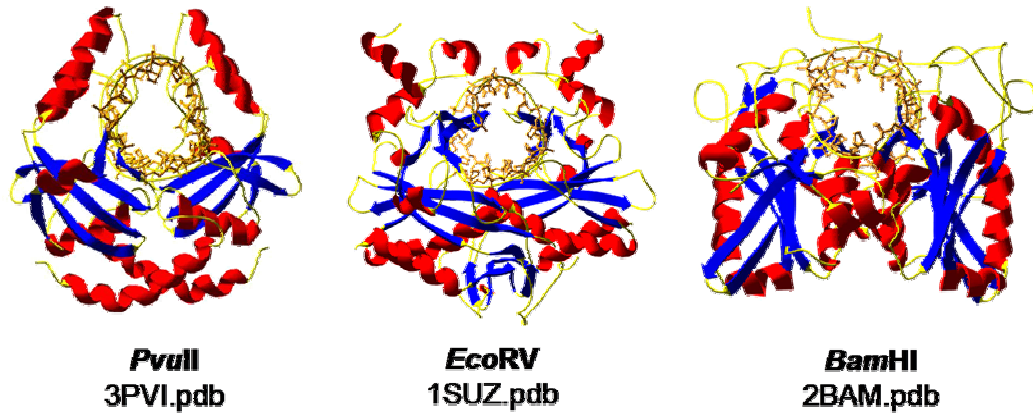


**Figure 1.2.** The crystal structures of type II restriction endonucleases as a homodimer and its association with cognate DNA duplex. The crystal structures of *PvuII*, *EcoRV* and *BamHI* bound with cognate DNA duplex have been shown from left to right. The pdb codes of those structures are indicated at the bottom of figure.

---

anisotropy, nitrocellulose filter binding and gel shift assay (Nastri, et al., 1997; Conlan & Dupureur, 2002b). The metal cofactors are essential for specific DNA cleavage reactions by type II restriction endonucleases, but the number of metal ions required in the hydrolysis is still controversial (Pingoud, et al., 2005). Cofactors which support the hydrolysis are Mg(II) (native divalent metal cofactor), Co(II) and Mn(II) (Bowen & Dupureur, 2003). The metal dependence of enzymatic activity on specific DNA cleavage has been determined for *EcoRV* (Groll, et al., 1997). A sigmoidal shaped metal dependence has been obtained, which implies multiple metal ion involvement in DNA cleavage and the possibility of metal binding cooperativity (Vipond, et al., 1995b; Groll, et al., 1997; Sam & Perona, 1999b).

*Conserved PD...D/ExK Catalytic Motif In Endonuclease Family.* The active sites of a few endonucleases featured with this motif are shown in **Figure 1.3**. Since divalent metal cofactors are essential for hydrolytic activity of cognate DNA by restriction endonucleases, the metal binding sites of acidic residues Glu and Asp residues are conserved in the active sites of restriction endonucleases. However, the number of metal ions bound in the active site is not unique for all type II restriction endonucleases. *EcoRI* is found to bind one metal ion in its active site (JenJacobson, et al., 1996), but *BamHI*, *EcoRV* and *PvuII* are observed to bind two metal ions with two acidic residues Asp and Glu (Horton, et al., 1998; Viadiu & Aggarwal, 1998; Horton & Cheng, 2000). In the presence of cognate DNA, it is observed that the scissile phosphate can function as an additional metal binding ligand (Horton, et al., 1998; Horton & Cheng, 2000). The metal binding affinities

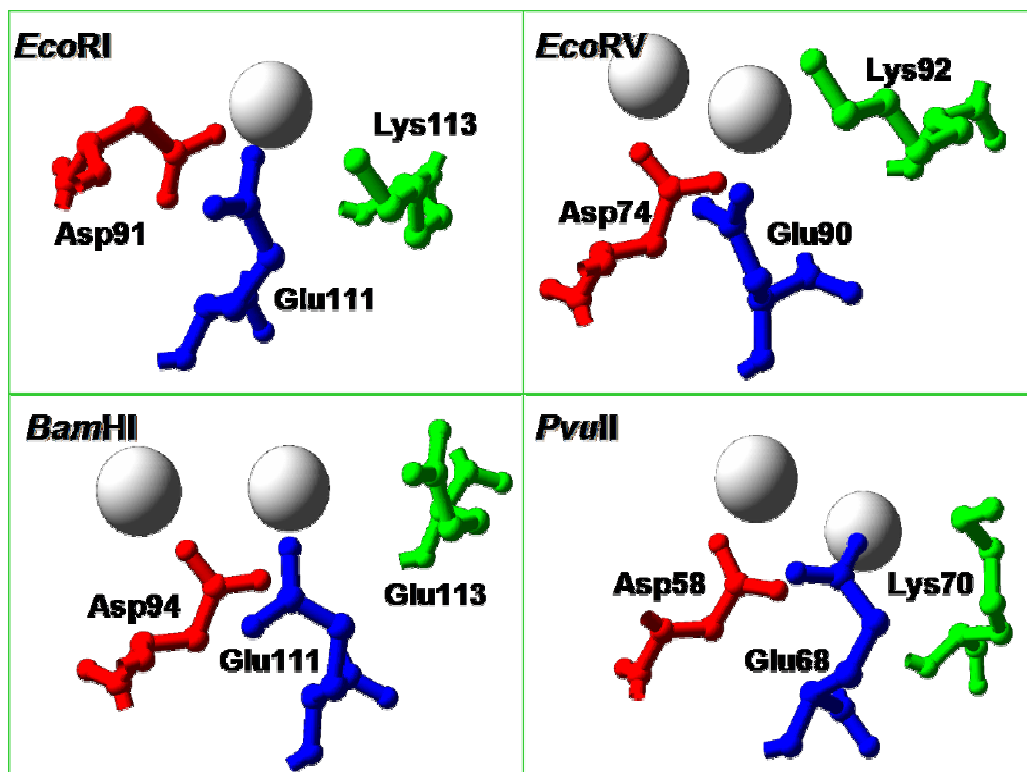


**Figure 1.3.** Conserved PD...D/ExK catalytic motif in endonuclease family. The active sites of *EcoRI* (1QPS), *EcoRV* (1BSS), *BamHI* (2BAM) and *PvuII* (1F0O) are indicated with conserved residues and metal ions.

---

determined for Mg(II) and Ca(II) are from a few hundred micromolar to millimolar (Jose, et al., 1999; Dupureur & Conlan, 2000). Besides the acidic residues conserved in the active site, the nearby Lys is also conserved and its structural function remains controversial. According to the *PvuII* crystal structure, this conserved Lys is within hydrogen bonding distance to metal ligated water molecules, and Ala mutation at this position destroys the enzymatic activity effectively (Horton & Cheng, 2000). Not all the type II restriction endonucleases belong to this family with conserved PD...D/ExK catalytic motif, *BamHI* and *BglIII* are exceptions, and in them the conserved Lys residue is replaced with Glu and Gln, respectively (Horton & Cheng, 2000). Some of the endonucleases with conserved PD...D/ExK catalytic motif are summarized in **Table 1.1** including the active site, DNA recognition sites and crystal structure information.

*Catalytic Mechanism of DNA Hydrolysis By Restriction Endonucleases.*

Although structural and biophysical studies reveal metal ion stoichiometry, there is no universally accepted mechanism for the DNA hydrolysis reaction. Generally, the hydrolysis of the phosphodiester bond consists of nucleophilic attack, the stabilization of pentavalent transition state and the departure of 3' hydroxyl group (**Figure 1.4**). The metal ions which ligate the carboxylate groups (Asp or Glu) conserved in the catalytic center function to activate the attacking water molecule and neutralize the negative charge developed by the pentavalent transition state (Horton, et al., 1998; Martin, et al., 1999b; Horton & Cheng, 2000).

**Table 1.1. Crystal structures of type II restriction endonucleases which belong to PD...D/ExK family and exceptions.**

<b>Enzyme</b>	<b>Catalytic motif</b>	<b>pdb code for enzyme-M(II)-DNA complex</b>
<b>PD...D/ExK family</b>		
EcoRI	Asp91;Glu111;Lys113	1QPS
NgoMIV	Asp140;Glu201;Lys187	1FIU
TnsA (Tn7transposase)	Glu63;Asp114;Lys132	1F1Z
BglI	Asp116;Asp142;Lys144	1DMU
EcoRV	Asp74;Asp90;Lys92	1AZ0, 1B94, 1RVA, 1BSS, 1SUZ, 1SX8, 1STX, 1SX5, 1RVB,
HincII	Asp114;Asp127;Lys129	1HXV
PvuII	Asp58;Glu68;Lys70	1F0O
T7 endonuclease I	Asp55;Glu65;Lys67	1M0I
<b>Exceptions</b>		
BamHI	Asp94;Glu111;Glu113	2BAM
BglIII	Asp84;Glu93;Gln95	1DFM

The table is adapted from the review about restriction endonucleases (Pingoud, et al., 2005).

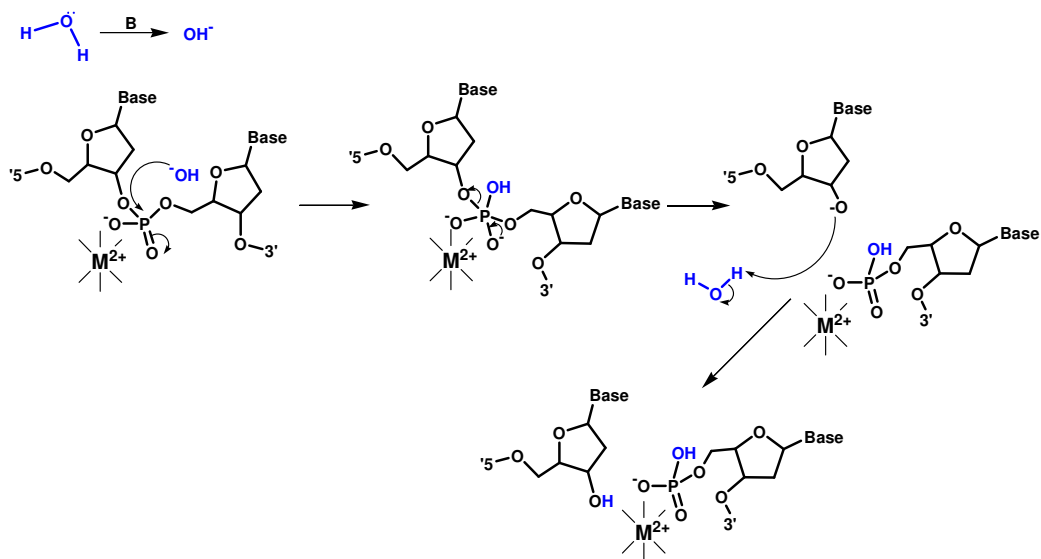


**Figure 1.4. The general mechanism for the hydrolysis of phosphodiester bond.** The scissile phosphate is hydrolyzed to form the 5' phosphate and 3' hydroxyl group. "B" represents the general base to abstract the proton from the attacking water molecule. Two water molecules are included; one serves as a general base to form the hydroxide and attack the scissile phosphate; the other serves as a general acid to protonate the 3' hydroxyl group.

---

The major controversy regarding the mechanism of DNA cleavage by restriction endonucleases is about the number of divalent metal ions involved in the catalytic process (Pingoud, et al., 2005). The proposed mechanistic models are named after the number of metal ions involved in the catalysis including one-metal ion, two-metal ion and three-metal ion mechanisms.

*One-metal ion mechanism.* This mechanism is mainly supported by *EcoRI* and *BglIII* co-crystal structures with a single divalent metal ion at the active site since there is no evidence of binding a second metal ion at the catalytic center in any case (Grigorescu, et al., 2004). The proposed one-metal ion mechanism (**Figure 1.5**) requires that the single metal ion acts to stabilize the negative charge of the transition state, and the deprotonation of water molecule is accomplished with the assistance of 3' phosphate. This mechanism is also called substrate assisted catalysis (Jeltsch, et al., 1993; Horton, et al., 1998).

*Two-metal ion mechanism.* This mechanism has been adapted for numerous reactions in metalloenzymes including nuclease, polymerase, and ribozymes (Aqvist & Warshel, 1990; Pyle, 1993; Steitz & Steitz, 1993; Vipond, et al., 1995a; Wilcox, 1996). An ideal two-metal ion mechanism features the two metal ions 4 Å apart from each other, which is the most efficient to reduce the electrostatic repulsion between negative charges that accumulate at the transition state (Pingoud, et al., 2005) (**Figure 1.6**). One metal ion ligates with one attacking water molecule to favor its deprotonation, and the other interacts with a second water molecule involved in protonation of the leaving group (Horton & Cheng, 2000). Horton compared the two

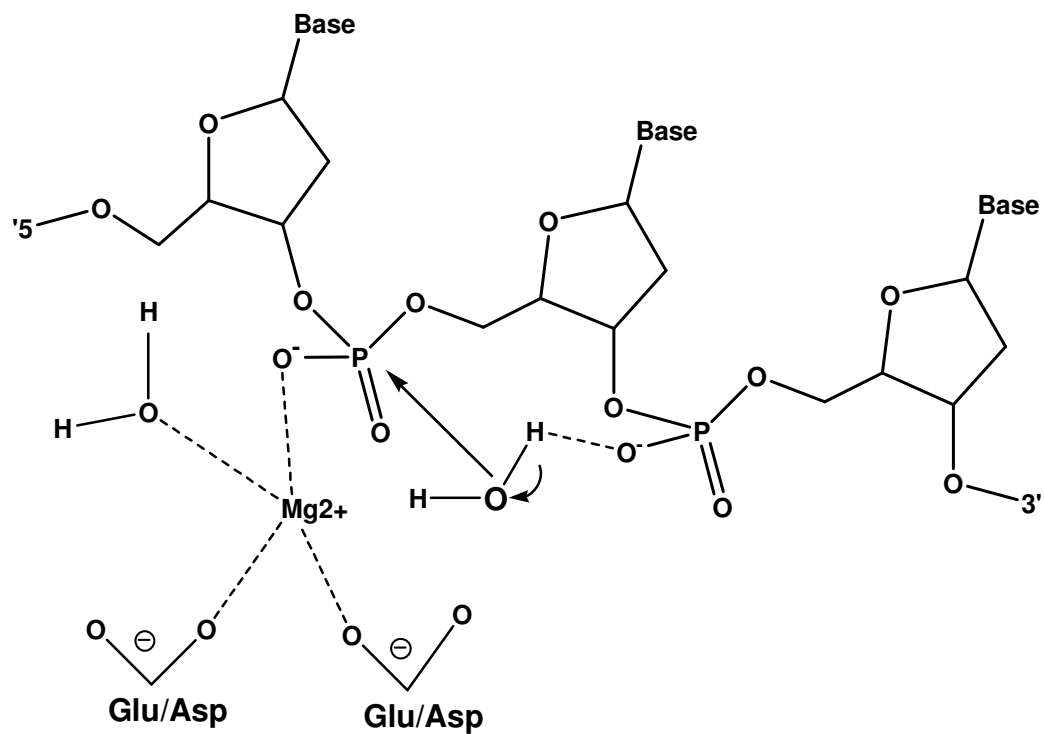


**Figure 1.5. One-Metal ion mechanism.** The 3' phosphate serves as a general base to deprotonate the attacking water molecules. The second water molecule that ligates with  $Mg(II)$  ion serves as a general acid to protonate the 3' leaving group.

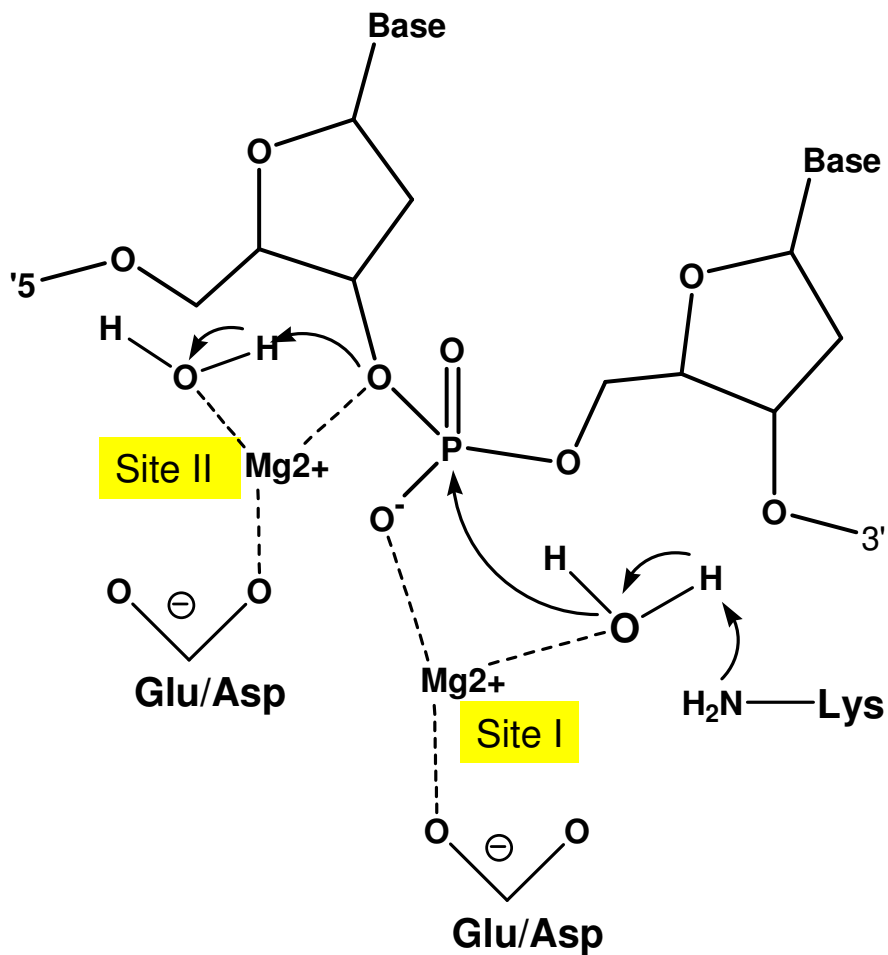


**Figure 1.6. Two-Metal ion mechanism.** One metal ion ligates with one attacking water molecule to favor its deprotonation, which is assisted by a general base such as Lys or Glu. The other metal ion interacts with second water molecules involved in protonation of the leaving group for its departure. Both metal ions are required to stabilize the negatively charged transition state and they should lie in parallel with apical direction of trigonal bipyramidal transition state (Horton & Cheng, 2000; Pingoud, et al., 2005).

---

Ca(II) sites in *PvuII*-Ca(II)-DNA complex with other restriction endonucleases and concluded that site A in *PvuII* is commonly conserved in all well characterized structures of type II restriction endonucleases (**Figure 1.7**), including BamHI and BglIII (Horton & Cheng, 2000). The site B in *PvuII* does not overlap with that in BamHI and BglI which have the same second metal binding sites, while it is very similar with the third metal binding site in *EcoRV* (**Figure 1.7**) (Horton & Cheng, 2000). The distance between two Ca(II) ions in *PvuII* is 3.5 Å, which is shorter than 4.3 Å in *BglI* and *BamHI* (Horton & Cheng, 2000).

*Three-metal ion mechanism.* This mechanism has been proposed for *EcoRV* based on the multiple crystallographic structures which feature three distinct metal ion binding sites, although those three sites have never been occupied simultaneously (Horton & Cheng, 2000; Horton & Perona, 2004) (**Figure 1.8**). Compared with two-metal ion mechanism, two metal ions initially occupy site I and site II which are equivalent to those two sites in two-metal ion mechanism, acting to generate the nucleophilic hydroxide, stabilize the transition state and facilitate the ionization of a second water molecule to protonate the 3' oxyanion. The metal ion in site III shifts to site II later, together with the movement of scissile phosphate deeper into the active site cleft. During this rearrangement, the metal ion in site I still maintains the contact with scissile phosphate and the intermediate has been observed in pre-reactive crystal structures with occupied site I and site II (Horton, et al., 1998; Horton, 2000).

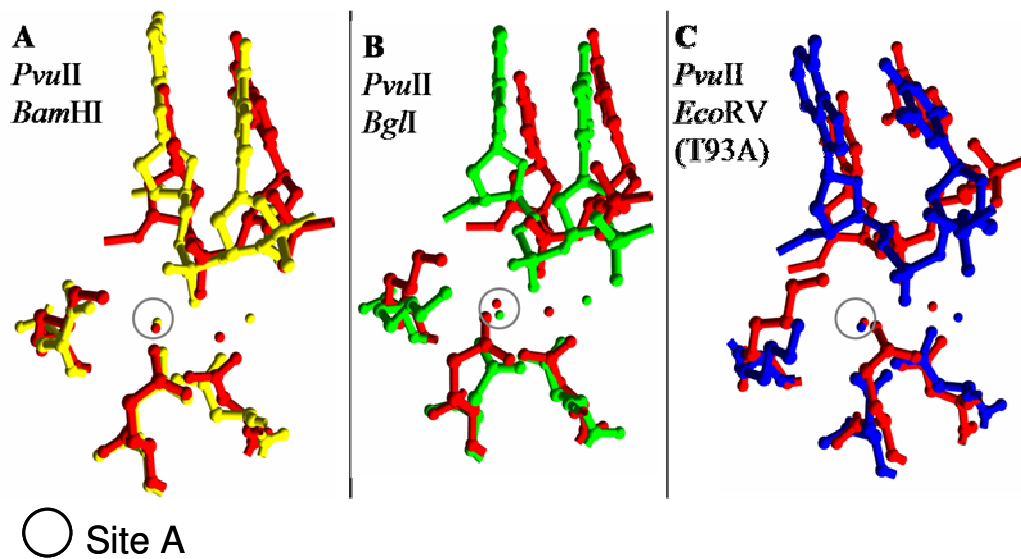


**Figure 1.7. Superposition of *PvuII* with *BglII*, *BamHI* and *EcoRV*.** A. *BglII* (1DMU) (Newman, et al., 1998), B. *BamHI* (2BAM) (Viadiu & Aggarwal, 1998), and C. *EcoRV* T93A mutant (1BSS) (Horton, et al., 1998). The comparison is based on the structural alignment of three active site amino acid residues (Asp58, Glu68, and Lys70) plus two Ca(II) ions in subunit B of *PvuII* (1F0O) and their structural equivalents in *BamHI*, *BglII*, and *EcoRV*, respectively (Horton & Cheng, 2000). Structure of *PvuII* is in red; *BamHI*, *BglII*, and *EcoRV* are in green, yellow and blue. Spatially equivalent metal ions are circled in each case, which is referred to site A and the other is site B.

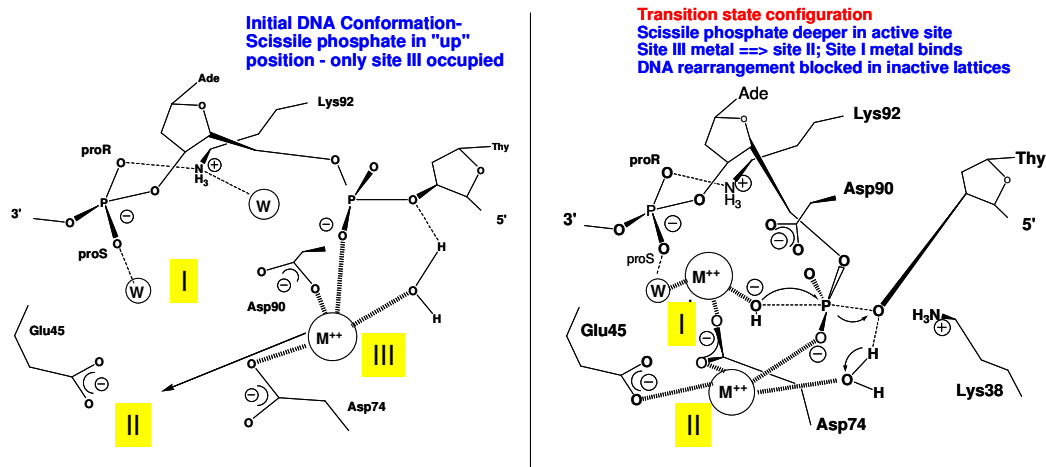


**Figure 1.8. Three-Metal ion mechanism.** Three metal binding sites are indicated as site I, II and III (Horton & Perona, 2004). In left panel, site III is occupied and the metal ion in site III make the direct phosphate contact. This metal ion will move to occupy site II in the following transition state configuration, which is indicated by arrow. Right panel depicts the transition configurations in the catalysis, which still follows up a two-metal ion mechanism. Site I and site II are equivalent to the site A and site B in a two-metal ion mechanism and site III probably just serves a structural role. This figure is provided by Dr. Dupureur from personal communication with Perona.

---

## Divalent Metal Cofactors Mg(II)

Many biological activities are dependent on the participation of metal cofactors. Some metal cofactors experience the change of oxidation state during a redox reaction cycle such as iron and copper, which is beyond our scope. Here, we focus only on the Mg(II) ion involved in protein-DNA interactions and DNA hydrolysis. Mg(II) ion follows an octahedral coordination and is heavily hydrated, which assists its binding with protein or nucleic acid through outer sphere complexation (Cowan, 1998). The catalytic functions that Mg(II) is essential for the hydrolysis of DNA include: 1) Mg(II) can stabilize the developed negative charge in the formation of transition state to lower the energy barrier for catalysis; 2) Mg(II) can effectively lower the  $pK_a$  of a water molecule which ligates to it and facilitate its deprotonation to form the attacking nucleophile. The distance of Mg(II)-O (oxygen in ligand) in coordination complex is about 2.0 Å and the determined  $pK_a$  of Mg(II) ligated water molecule is 11.4 (Dahm, et al., 1993).

*Mg(II)-Protein Interaction.* It is known that Mg(II) can bind with endonucleases, pyrophosphatase, polymerase and farnesyltransferase with binding affinity from 1 mM to 10 mM but there are some proteins such as parvalbumin which has a micromolar affinity (Cowan, 1997; Henzl, et al., 2003). Mg(II) itself is spectroscopically silent and it causes no dramatic conformational change for CD or UV studies when it is bound to protein, which makes the Mg(II) binding studies more difficult than other metal ions such as iron and copper. Intracellular and extracellular Mg(II) concentrations were reported via ion selective microelectrode (Lanter, et al.,

---

1980). The competition binding assay using Mg(II) sensitive mag-fura-2 is used to determine the Mg(II) binding affinities for *PvuII* endonuclease and its variant (Papadakos, et al., 2007). <sup>25</sup>Mg NMR has also been used to determine the Mg(II) binding affinities with *PvuII* endonuclease (Dupureur & Conlan, 2000). ITC is also employed to determine Mg(II) binding affinities with parvalbumin coupled with a competition assay using the metal chelator EDTA (Henzl, et al., 2003).

*Mechanism Studies Of Mg(II) Dependent Enzymatic Activity.* The Mg(II) dependent mechanism has been investigated by crystal structures and biochemical characterizations of restriction endonucleases, exonucleases III, ribonuclease H, general nucleases, polymerases and phosphatase and integrases (Cowan, 1998). It is widely observed that Mg(II) promotes the enzymatic activity at low concentrations but inhibits enzymatic activity gradually at higher concentrations (>20 mM). This is interpreted as due to the non specific Mg(II) binding to the substrate and inhibition of enzyme substrate interactions (Cowan, 1998). A series of catalytic mechanisms have been proposed to address the number of metal ions required and distinct roles of those metal ions in catalysis (Pingoud, et al., 2005). The Mg(II) ions may shuffle among three metal binding sites of *EcoRV* during the DNA association and cleavage, based on multiple crystal structures corresponding to various reaction phases (Horton & Perona, 2004).

*Mg(II)-DNA Interaction And Its Catalytic Role In Ribozyme.* Mg(II) is known to bind with DNA through phosphate groups or oxygen atoms on the base, which has been observed in the crystal structures of metal DNA complexes and

---

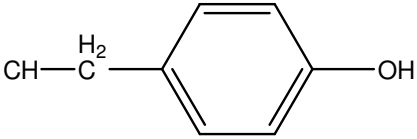
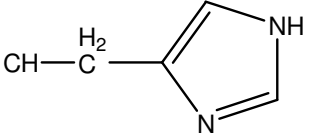
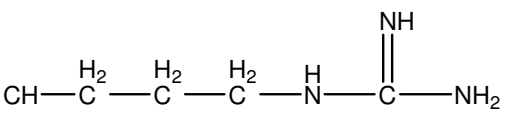
interpreted as random binding (Minasov, et al., 1999). Mg(II) is found to serve as a Lewis acid in ribozymes when it coordinates with water molecules or stabilizes particular folded conformations critical for catalysis (Dahm, et al., 1993; Sreedhara & Cowan, 2002). Unlike endonucleases, more divalent ions can mediate ribozyme catalysis, which allows metal substitution experiments and investigations of  $pK_a$ 's of metal ligated water molecule for various metal ions (Dahm, et al., 1993; Lott, et al., 1998; Roychowdhury-Saha & Burke, 2006). The mixed metal experiments can be used to dissect the structural and functional roles of distinct metal ions in the active site. In a mechanistic study of the hammer head ribozyme, a two-metal ion mechanism was concluded by assigning the role of the first Mg(II) ion to lowering the  $pK_a$  of the 2' attached proton and the role of the second Mg(II) ion to absorbing the negative charge accumulated in the transition state (Lott, et al., 1998).

### **$pK_a$ Calculation and Its Correlation With pH Dependence Studies.**

Proteins consist of natural amino acids, and those with ionizable side chain are divided into acidic and basic groups. The ionization states of the amino acid groups determine the important protein properties like pI value. **Table 1.2** lists all the ionizable groups considered in  $pK_a$  calculations with proteins.

*pK<sub>a</sub> Calculation Methodology.* Most of the  $pK_a$  calculations depend on the solution of the Poisson-Boltzmann equation to calculate the electrostatic energies for a given protein structure. The electrostatic interactions serve a critical role in protein-ligand binding and protein stabilities (Honig & Nicholls, 1995). The

**Table 1.2. The ionizable groups in proteins and their model pK<sub>a</sub>'s.**

Residue	Structure of side chain	Model pK <sub>a</sub> <sup>a</sup>
Asp	$\text{CH}-\overset{\text{H}_2}{\text{C}}-\overset{\text{O}}{\parallel}{\text{C}}-\text{OH}$	4.0
Glu	$\text{CH}-\overset{\text{H}_2}{\text{C}}-\overset{\text{H}_2}{\text{C}}-\overset{\text{O}}{\parallel}{\text{C}}-\text{OH}$	4.4
Cys	$\text{CH}-\overset{\text{H}_2}{\text{C}}-\text{SH}$	9.5
Tyr		9.6
His		6.3
Lys	$\text{CH}-\overset{\text{H}_2}{\text{C}}-\overset{\text{H}_2}{\text{C}}-\overset{\text{H}_2}{\text{C}}-\overset{\text{H}_2}{\text{C}}-\text{NH}_2$	10.4
Arg		12

a. The model pK<sub>a</sub> values for UHBD calculations.

---

developed software packages to calculate electrostatic energies include Delphi, GRASP, WHAT IF and UHBD (Vriend, 1990; Nicholls & Honig, 1991; Nicholls, et al., 1991; Antosiewicz, et al., 1996b). Most of the  $pK_a$  calculation programs are now embedded into those software packages because the  $pK_a$  predictions are also need to deal with site-site interactions among multiple titratable sites in proteins, and related methods have been developed to minimize the possibilities (Honig & Nicholls, 1995).

Accuracy of  $pK_a$  predictions is always of major concern since it is related to the validation of the electrostatic model and applied atomic parameters (charges and radii). NMR experiments combined with pH titration of specific ionizable groups in ribonucleases and lysozyme was used to measure experimental  $pK_a$  values (Mandel, 1964; Mandel, 1965). The comparison of experimental and predicted  $pK_a$  values can be used to validate the methodology and estimate the accuracy of  $pK_a$  calculations for other systems in which the experimental  $pK_a$  is not available (Antosiewicz, et al., 1996b). Factors that may affect  $pK_a$  calculations include protein structures used in the calculations (X-ray structure or solution structure), the assignment of the dielectric constant in protein, the conformational flexibility of the protein structure and the influence of ligands (ions and organic group) (Antosiewicz, et al., 1996b).

*Solution Structure vs. Crystal Structure.* The  $pK_a$  calculations based on 41 lysozyme crystal structures indicate that the crystallization conditions and resolutions of crystal structure are not helpful in selecting a reliable structure for  $pK_a$  calculations, even the applications of optimization methods such as energy minimization and molecular dynamics simulation would not effectively improve the  $pK_a$  calculation

---

results (Nielsen & McCammon, 2003). Although NMR structure reflects the dynamic information and seems more applicable than the crystal structure, it is not conclusive that the solution structure can provide a better accuracy than crystal structure (Antosiewicz, et al., 1996b).

*Empirical Dielectric Constant For Proteins.* The dielectric constant can be calculated from the dipole moment of a protein molecule and a low value (2~5) is estimated (Gilson & Honig, 1986). The argument lies in whether the contribution of the ionizable groups should be included or not in the calculations of dipole moments (Antosiewicz, et al., 1994). Applying a single site model in UHBD, the calculated pK<sub>a</sub> values with an empirical value of dielectric at 20 show better agreement with experimental pK<sub>a</sub> values than using a dielectric constant of 4 (Antosiewicz, et al., 1994; Antosiewicz, et al., 1996b). However, the pK<sub>a</sub> calculation results could be improved assuming dielectric constant of 4 using a more detailed charged model (full site model) (Antosiewicz, et al., 1996a). pK<sub>a</sub> calculations on staphylococcal nuclease with UHBD indicate that the calculated pK<sub>a</sub> values show little dependence on dielectric constant when using a value above 20, and a value of 20 still gives the best agreement between calculations and measurements for most surface ionizable groups. The predicted pK<sub>a</sub> values obtained when assigning the dielectric constant to 10 seem to be the best for buried ionizable groups.

*Conformational Flexibility.* Protein flexibility has been taken into account for pK<sub>a</sub> calculations to reflect protein fluctuations in the real environment. The strategy is to generate enough possibilities in order to determine either the

---

conformation with the lowest energy or conformationally averaged protonation status for titratable sites (Zhou & Vijayakumar, 1997). You and Bashford investigated the effects of local side chain conformational change by sampling the torsion angle of Asp, Glu and Tyr residue side chains and generating a library including 36 conformers. The application of this multiple conformers strategy on hen lysozyme proved to be a significant improvement on the predicted  $pK_a$  values as compared to the single conformational calculation (You & Bashford, 1995). A similar strategy of flipping the side chain of Asn, His and Gln around their  $\chi^2$  and  $\chi^3$  torsion angles to optimize the hydrogen bond network resulted in better calculation results on hen lysozyme and superoxide dismutase (Nielsen, et al., 1999). The conventional molecular dynamics and Monte Carlo simulations are employed to generate the multiple conformations used to determine the averaged protonation states of the titratable sites as a function of pH. The calculated  $pK_a$ 's with yeast iso-1-ferricytochrome c are in good agreement with experimental  $pK_a$  values (Zhou & Vijayakumar, 1997). Except for the position changes of heavy atoms on the side chains (O, N and C), the change of proton positions is considered protonation flexibility. Alexov and Gunner coupled the proton position at the titratable site with orientation of neighboring hydroxyl groups to generate a series of conformers and determined their distributions by Monte Carlo sampling (Alexov & Gunner, 1997; Alexov & Gunner, 1999). All the methods mentioned above deal with local conformational variability in proteins. The effect of global structural variability can be examined by long time (1 ns) molecular dynamics simulation (Gorfe, et al., 2002). By using four trajectories in a calculation

---

on an engineered leucine zipper, the error of calculated  $pK_a$  values was reduced to 0.25 pH units (Gorfe, et al., 2002).

*pK<sub>a</sub> Perturbations In Proteins.* There are three factors which can effectively perturb the  $pK_a$  values of ionizable groups: charge-charge interaction, a hydrophobic environment and hydrogen bonding. As shown in **Figure 1.9**, a negatively charged environment (neighboring residues) will increase the  $pK_a$  of a titratable site since the negative charge stabilizes the protonated state of an acidic ionizable group, and destabilizes the protonated state of a basic group (Lys) (Nielsen, et al., 2001). For the positive charged environment, the effect is to decrease the  $pK_a$  of a titratable site. The hydrophobic environment will elevate the  $pK_a$  of an acidic group but lower the  $pK_a$  of a basic group because it always favors the neutral state and destabilizes the ionized state. In a folded protein, those factors which perturb the  $pK_a$  values of ionizable groups may all exist. However, in a denatured protein there are fewer local electrostatic interactions, and the measured  $pK_a$  is very close to the model  $pK_a$  of a given amino acid (Laurents, et al., 2003). Following those principles, the  $pK_a$  shift can be predicted in the mutagenesis studies when charged residues are neutralized by introducing Ala substitution. The apparent  $pK_a$  shift has been observed experimentally when Ala mutation occurs in the active site on *PvuII* (Dupureur & Conlan, 2000). In the case of pH dependence studies of *MunI*, the derived apparent  $pK_a$  of the same ionizable moiety in the active site is elevated upon DNA association as an effect of the negatively charged phosphate on the DNA backbone (Haq, et al., 2001).

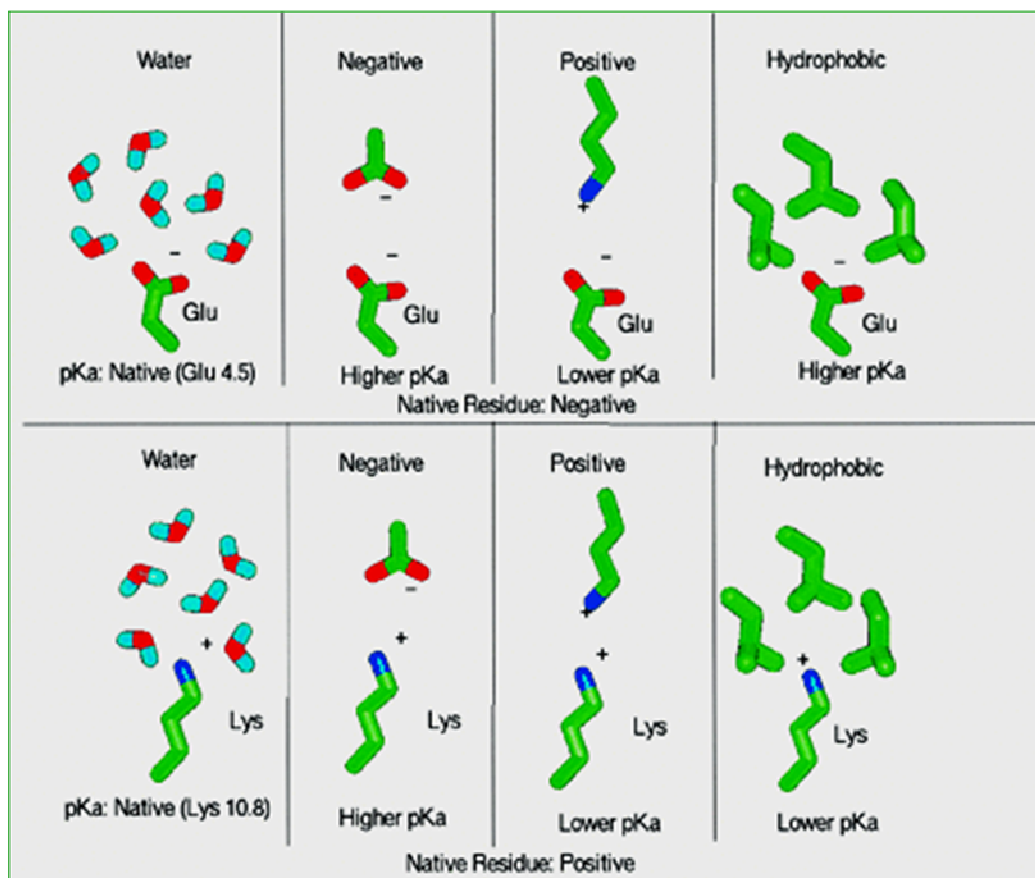


**Figure 1.9. Environment effects on  $pK_a$  of titratable sites.** The effects of placing a titratable site in a negative, positive and hydrophobic environment are indicated. The figure is adapted from reference (Nielsen, et al., 2001).

---

*Surface Groups vs. Buried Groups.* It is reported that the  $pK_a$  values of surface residues are much less disturbed (less than one pH unit) than buried ones (Huyghues-Despointes, et al., 2003). Since they are solvent exposed and do not form hydrogen bonds, the perturbations are mainly from long range electrostatic interactions (Huyghues-Despointes, et al., 2003). The long range electrostatic interactions can be screened by increasing the salt concentration, which has been observed in the  $pK_a$  calculations with two His residues in RNase Sa and its variant (Laurents, et al., 2003).  $pK_a$  perturbation of buried groups is more complex and has to be correlated with specific electrostatic environments. Short range electrostatic interactions are expected if charged residues can be identified in close proximity to each other in the crystal structures. For example, that a water molecule can elevate the  $pK_a$  of a buried His via hydrogen bonding, and such a elevation can not be screened by increasing the salt concentration (Huyghues-Despointes, et al., 2003). More than 90% of buried groups are predicted to be ionizable based on MCCE (multiple-conformation continuum electrostatic) calculations with 490 proteins (Kim, et al., 2005). The factors which stabilize the ionizable states of those buried groups have been shown to include ion pair interactions, interactions between backbone dipoles, polar interactions between side chains and hydrogen bond donors (Kim, et al., 2005). Staphylococcal nuclease (SNase) has been used as a model to calculate the  $pK_a$  values of buried groups such as Lys66 and Glu66, and the determined  $pK_a$  values were found to be highly perturbed (5.7 for Glu and 8.8 for Lys) (Fitch, et al., 2002). The polarity is rationalized to be the main cause of  $pK_a$  perturbations because Glu66

---

is hydrogen bonding to an internal water molecule which is observed in the crystal structure. In the case Lys66, the water penetration probably occurs since there is no internal water molecule visualized in the crystal structure. The calculations show that internal water molecules can modulate  $pK_a$  values of buried groups.

### **Kinetics Studies in Enzymology.**

The kinetic studies discussed below include not only the measurements of enzymatic activities under various reaction conditions, but also the dynamic studies of substrate or ligand association, dissociation and conformational changes during the reaction.

The enzymatic activity measurements determine steady state and single turnover rate constants, which are widely used to distinguish the residues critical for catalysis in mutagenesis studies (Groll, et al., 1997; Sam & Perona, 1999a). The single turnover condition can be described as the saturation of bound substrate using excess amounts of enzyme to reach the maximal activity so that the measured rate constant is independent of the substrate binding process and best reflects the rate of the chemistry step. The steady state kinetics provides the apparent rate constant for the overall reaction pathway, which is probably partially or fully limited by the slowest step. To elucidate the details of a reaction mechanism, the measurements of single turnover and steady state kinetic parameters are not sufficient. Basic questions have to be addressed regarding the complexity of catalytic mechanism. Is the reaction reversible or irreversible? What is the rate limiting step in the overall reaction pathway? Is there any intermediate formed in the course of the reaction

---

pathway? Is the reaction following a random binding mechanism or a sequential binding order when a cofactor is present? Kenneth A. Johnson pointed out that transient kinetics and kinetic programs were very powerful tools to establish a complete reaction scheme (Johnson, 1998).

*Transient Kinetics Approaches.* The application of stopped flow and rapid quench flow instruments allows monitoring fast processes during a reaction. The chemistry steps or binding processes can be monitored in a time scale of milliseconds. The individual rate constant for a specific event can be derived from the kinetic analysis of reaction progress curves.

*EcoRV* is a well-characterized type II restriction endonuclease, and transient kinetics have been conducted with *EcoRV* to study DNA association, DNA bending, enzyme transfer from a nonspecific to a specific site on the plasmid and cleavage reactions. In experiments tracking tryptophan fluorescence signal during a single turnover DNA cleavage reaction by *EcoRV*, the increase of the fluorescence intensity was regarded due to the effect of a fast conformational change occurring simultaneously with DNA binding to *EcoRV*. The subsequent slow decay was attributed to DNA cleavage since the derived rate constant was similar to the determined single turnover rate constant (Baldwin, et al., 1995). With fluorescence resonance energy transfer assays using a double labeled DNA duplex (rhodamine and fluorescein), DNA bending is found to occur simultaneously with DNA binding to *EcoRV* and the rate constants are determined to be  $1.46 \sim 1.6 \times 10^8 \text{ M}^{-1} \text{ s}^{-1}$  (Hiller, et al., 2003). Through the combination of quench flow techniques and data fitting, it was

---

found that *EcoRV* could scan and locate the specific site on a plasmid at an extremely rapid rate of  $5 \times 10^5$  bases per second (Erskine, et al., 1997). As the measured plasmid association rate was  $1.2 \times 10^8 \text{ M}^{-1}\text{s}^{-1}$ , the binding was proposed to be a diffusion controlled process (Erskine, et al., 1997). The quench flow techniques were also applied to monitor rapid cleavage reactions by *EcoRV* with radiolabeled short oligonucleotides in the cleavage studies under pre-steady state conditions in the presence of Mg(II) or Mn(II) (Sam & Perona, 1999b). The appearance of a burst phase indicated that product release step was partially or completely rate limiting step for *EcoRV* catalyzed DNA cleavage reactions. Those examples show the applications of rapid mixing techniques in characterizing the fast processes in the case of restriction endonucleases.

*Data Analysis of Kinetics Studies.* Kinetic studies generally yield time dependent signal which accounts for the substrate disappearance or the product appearance. The first order equation is often fit to a reaction course under single turnover conditions and a Michaelis-Menten equation is usually fit to data sets of velocities as a function of substrate concentration under steady state conditions. Pre-steady state reaction courses are usually fit to an equation integrating a burst phase with a linear phase. Those kinetic equations are expressed in exponential or linear terms of the enzyme and substrate concentrations, and they can be derived from a simple reaction scheme (Fierke & Hammes, 1995).

There are some situations in which a reaction scheme contains multiple ligands, cofactors and multiple binding sites. This can involve non equivalent

---

activities or multiple phases such as conformational changes or iso-forms of enzyme. In order to fit the kinetic data to the whole reaction scheme, global fits are employed to distinguish the kinetic models and estimate the unknown kinetic parameters with the assistance of fitting programs. Unlike fitting data to derived equations, fitting programs usually provide a friendly interface to construct kinetic models or reaction schemes, allowing user to assign initial value and constraints to unknown kinetic parameters and quantitate fitting qualities for evaluation. Simulations by these programs can be conducted prior to experiments to guide experimental design. The widely used global fitting programs are KinTek Global Kinetic Explorer (KinTek Corporation, [www.kintek-corp.com](http://www.kintek-corp.com)) and DynaFit (BioKin, Ltd, [www.biokin.com](http://www.biokin.com)).

Kinetic analysis using global fits has been performed with several metalloenzymes. The transient kinetic data of yeast cytosine deaminase (a zinc metalloenzyme) have been globally fit using DynaFit to derive the rate constants of the chemical step and the product release, and the simulation results are consistent with measured steady state kinetic parameters (Yao, et al., 2005). Another example of using DynaFit is in the case of MutT pyrophosphohydrolase (a  $Mg^{2+}$  dependent enzyme). Both single and multiple turnover data globally fit to a uni-bi-iso kinetic mechanism yield all the nine rate constants in the reaction scheme (Xia, et al., 2005). DynaFit has also been also used to distinguish the models for observed data by comparing the qualities of global fits (Moss, et al., 1996). According to Kenneth A Johnson, the simplest model is always proposed as long as it accounts for experimental data. New steps incorporated into a reaction scheme should be

---

supported by sufficient experimental evidence (Johnson, 1998).

### **Overview of Dissertation**

The characterization of WT *PvuII* restrictions endonuclease and variants has been conducted in Dr. Dupureur's lab for several years, and substantial biophysical data have been collected including DNA binding equilibrium constants, DNA association and dissociation rate constants, and Ca(II) and Mg(II) binding affinities with enzyme (Dupureur & Conlan, 2000; Conlan & Dupureur, 2002b; Conlan & Dupureur, 2002a). Those kinetic data, combined with metal dependent activity measurements, provide the possibility to establish a complete reaction scheme regarding participation of the metal cofactor for the specific DNA cleavage reaction. It was attempted to fit all the experimental data to a single and complete kinetic model. pH dependence studies of Mg(II) binding and enzymatic activities provide an insight to ionizable groups critical for catalysis in *PvuII* active site. On the basis of the pK<sub>a</sub> calculation package embedded in UHBD, the nearly neutral apparent pK<sub>a</sub> of general base derived from pH-rate profiles can not be correlated with the calculated pK<sub>a</sub>'s of any active site residues, but is correlated with the calculated pK<sub>a</sub> of metal ligated water molecule in the absence of DNA. The factors which lower the pK<sub>a</sub> of metal ligated water have been investigated by a computational approach, and the major electrostatic contribution appears to be the effect of the metal ions and nearby Lys.

Chapter II describes preparations of experimental materials, experimental techniques and computational methodology.

Chapter III describes the pK<sub>a</sub> calculations with *PvuII* active site residues and

---

metal ligated water, rationalizing the factors which effectively perturb their  $pK_a$  values. It also includes the pH dependence studies of *PvuII* activity and the corresponding dissection of ionizations reflected from pH profiles. The  $pK_a$  calculations with metal ligated water have been applied to metallonucleases featuring the PD...D/ExK catalytic motif, which provides an insight into the water activation mechanism in DNA hydrolysis reactions. The hypotheses of possible water activation mechanisms and related computational studies on *BamHI* are also discussed as an exception.

Chapter IV deals with metal dependent kinetic studies of single turnover, steady state and pre-steady state reactions and the corresponding global fits using various candidate models. The various kinetic models are presented and examined with respect to observed experimental data. Finally, a unique reaction scheme is concluded with detailed information about metal ion participation in binding, catalysis and product dissociation. The properties of two distinct metal binding sites are investigated by global fits, and the data seems to fit best to a two-equivalent site model with positive cooperativity.

---

## CHAPTER II. MATERIAL AND METHODS

### MATERIALS

In the purification and preparation of *PvuII*, the following reagents were used: M9 salts ( $\text{Na}_2\text{HPO}_4 \cdot 7\text{H}_2\text{O}$ ,  $\text{KH}_2\text{PO}_4$ ,  $\text{NaCl}$ ,  $\text{NH}_4\text{Cl}$ ), Buffer D ( $\text{KH}_2\text{PO}_4$ ,  $\beta$ -mercaptoethanol,  $\text{KCl}$ ,  $\text{EDTA}$ ), Lysis buffer ( $\text{KH}_2\text{PO}_4$ ,  $\beta$ -mercaptoethanol,  $\text{KCl}$ ,  $\text{EDTA}$ ), glucose, IPTG, ampicillin, ammonium sulfate, phosphocellulose and heparin sepharose which was used to prepare the column.

Most reagents were purchased from Fisher with ACS grade or higher purity such as most of the salts used in the preparation of buffer, acids, bases and organic solvents. The Puratronic  $\text{MgCl}_2$  and  $\text{CaCl}_2$  used to prepare the metal cofactor stock were also purchased from Fisher. The absolute ethanol (99.99%) used to rinse the curette was purchased from stock room in the chemistry department.

In the PAGE gel preparation, the reagents such as acrylamide (electrophoresis grade), TEMED (N,N,N',N'-Tetramethylethylenediamine) and ammonium persulfate were purchased from Fisher or Sigma/Aldrich. The PAGE gel running buffer 5X TBE was prepared by dissolving Tris, boric acid and  $\text{EDTA}$  in the MilliQ water.

Water used to make solutions was distilled and deionized by MilliQ Biocel A10 from Millipore (Billerica, MA). Chelex resin was purchased from Biorad (Hercules, CA) and used to remove the metal ions in the buffer. All buffers were prepared using deionized water and subsequently flowed through Chelex resin

---

(Hercules, CA). To prepare the buffer of the desired pH, several concentrations of acids/bases were prepared (typically 100 mM, 1 M and 6 M).

## **METHODS**

**Purification and Preparation of *PvuII* Restriction Endonucleases.** The recombinant *PvuII* expression systems in *Escherichia coli* PR1206 (pBBE) for wild type (WT in abbreviation) were kindly provided by Dr. Paul Riggs of New England Biolabs.

On the first day, media in the cell culture, nutrient cocktails and MgCl<sub>2</sub>/CaCl<sub>2</sub> are prepared and sterilized with the necessary glasswares. The recipes of media and nutrient cocktails are recorded in protocol “*PvuII* purification”. 8 L of buffer D containing 30 mM potassium phosphate and 50 mM KCl is also prepared. The transfected cells from a single colony were cultured overnight with addition of ampicillin (0.10 mg / mL media) in about 100 mL nutrient cocktails and M9 media. The flasks were placed in incubator at 37 °C shaking at 225 rpm.

On the second day, overnight cultures were scaled up to 1 L. IPTG (0.036g/ml) was added to initiate the induction when OD<sub>600</sub> of culture reached 0.6~0.8, then cells continued to grow 3~4 more hours. The culture was then harvested by centrifugation and stored as a frozen pellet.

On the third day, the frozen pellet is resuspended in lysis buffer (50 mM KPhosphate, 15 mM β-mercaptoethanol, 1 mM EDTA, pH 7.4). The overall volume of resuspended cell was kept below 100 mL for 10 L of original culture. After the cell lysis using a French press, the pellets were centrifuged for several times until the

---

supernatant was clear. The pellets were discarded. The nucleic acids were precipitated by addition of streptomycin sulfate to a final concentration of 25% w/v. Ammonium sulfate was added up to 45% w/v to precipitate the proteins in the solution. The precipitated protein could be recovered by centrifugation and dialysis in buffer D (30 mM potassium phosphate and 50 mM KCl, pH 7.4 at 4 °C).

On the fourth day, the purification was accomplished by ion exchange chromatography using a phosphocellulose column. The column was precycled with buffer D until pH of the buffer flowing in and out of the column both were about 7.4 (7.37~7.43). The pH of protein was also adjusted to pH 7.4 (7.37~7.43) and loaded onto the column. Following a wash, the pure protein was eluted using linear gradients of 0.05 M KCl~0.8 M KCl at 2 mL/min over 600~800 mL, and 6 mL fractions were collected. The proteins concentrations were monitored by UV absorbance at 280 nM. The collected fractions were analyzed using a 17% SDS PAGE gel. The purest fractions were selected to run heparin sepharose column. The protein fractions were pooled and dialyzed again overnight.

On the fifth day, the protein was purified by heparin sepharose column. The pH flowing in and out of the column was assured to be around 7.4 (7.37~7.43). The dialyzed protein was adjusted to the same pH and eluted by linear gradients of 0.05 M KCl~0.8 M KCl. Pure protein was reported to be eluted from the heparin column at 240~530 mM KCl (Dupureur & Hallman, 1999). 6 mL fractions were collected and analyzed on a 17% SDS PAGE gel. The chromatography of purification and SDS gel image are shown in **Figure 2.1**.

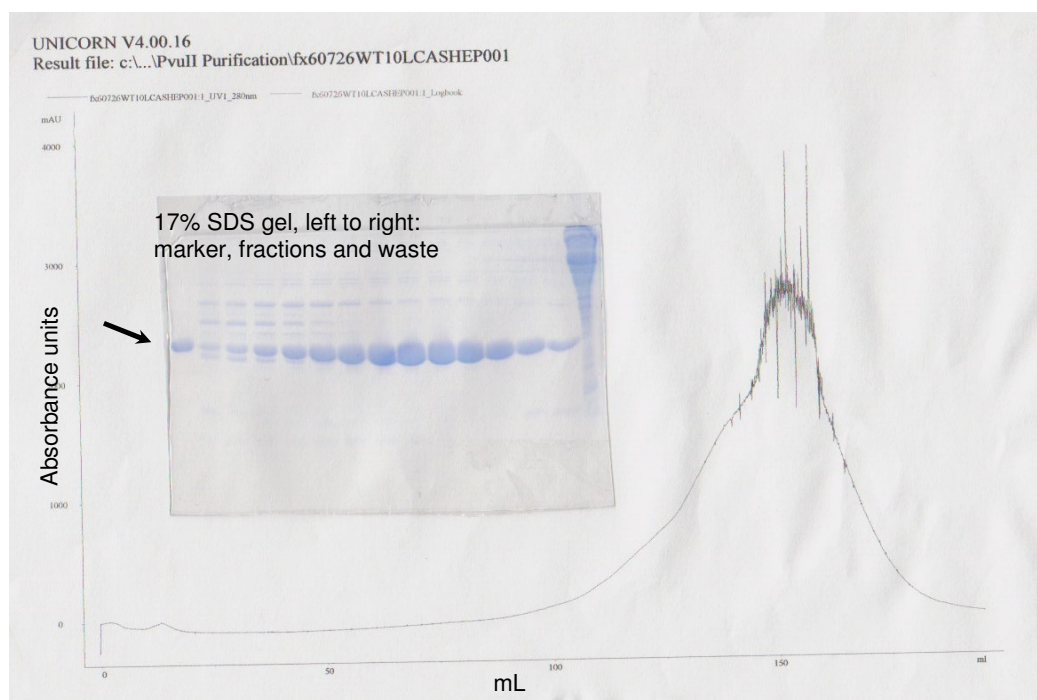


**Figure 2.1. Purification of WT *PvuII* endonucleases using heparin sepharose.** A typical FPLC is shown. Pooled fractions containing enriched protein from the phosphocellulose column were dialyzed into 0.03 M potassium phosphate pH 7.4, 15 mM  $\beta$ -mercaptoethanol, 1 mM EDTA, 0.05 mM KCl. Protein was eluted by using a linear gradient of 0.05 M KCl ~ 0.8 M KCl over 300 mL with 6 mL each fraction. The inset shows the 17% SDS gel image used to determine the purity of fractions. From left to right: *PvuII* marker, fractions 17 ~ 30 and the waste. The arrow indicates the position of purified protein.

---

The proteins was either lyophilized or prepared for assays. To get rid of the high concentrations of salt, the protein was dialyzed in a Slide-A-Lyzer Dialysis Cassette (0.5-3 mL, 10,000 MWCO, purchased from PIERCE) twice with metal free buffer (100 mM NaCl, 50 mM Tris, pH 7.5 at 25 °C). The proteins could also be concentrated using Amicon Centricon and Microcon concentrators (Millipore Corporation, Billerica, MA).

The proteins were measured UV absorbance at 280 nM and its concentration in monomer was calculated using  $\epsilon_{280} = 36,900 \text{ M}^{-1}\text{cm}^{-1}$  (Pace, et al., 1995). The protein concentration could be expressed either as monomer or dimer depending on binding or cleavage assay.

**Preparation and Quantitation of Oligonucleotides.** The unlabeled or Hex-labeled oligonucleotides were purchased from IDT (Coralville, Iowa) and rhodamine or dansyl labeled oligonucleotides were purchased from Midland Certified Reagent Company (Midland, Texas) (**Table 2.1**). If the purchased oligonucleotides were not HPLC purified, they had to be purified by PAGE gel and recovered by Elutrap (Schleicher and Schuell, Keene, NH). The oligonucleotides were quantitated by monitoring the UV absorbance at 260 nm. The extinction coefficient of oligonucleotides used was either from the vendor or calculated using  $6600 \times$  the number of nucleotides in the DNA. Duplexes were prepared by mixing complementary single strand at a molar ratio of 1:1, heating up to 95 °C then cooling the mixture to room temperature.

---

**Table 2.1 Oligonucleotides sequences used in the assays.**

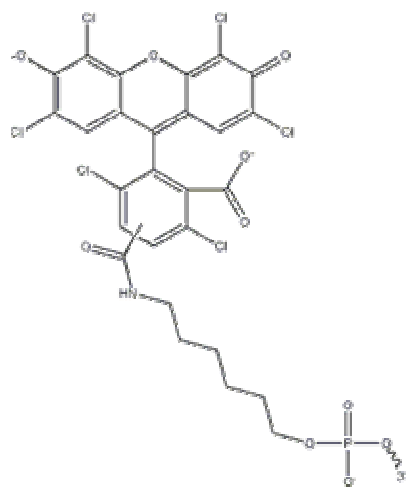
---

	Sequence	Modification
Sq3121-1	5'-CAG GCA GCT GCG GA -3'	None
Sq3121-2	5'-TCC GCA GCT GCC TG -3'	None
Rs1086-a	5'-Phos CTG CGG TCG CG -3'	Phosphate
Rs1086-b	5' Hex-CGC GAC CGC AG -3'	Hex
Sq1126-1	5'HEX- CAG GCA GCT GCG GA -3'	Hex
Sq2100-2	5'Rhoda (C6amino) CAG GCA GCT GCG GA -3'	Rhodamine
Fx0970	5'-CGC GAC CGC AG -3'	None
Fx09101	5' Dansyl (C6amino) CGC GAC CGC AG -3'	Dansyl
Fx09102	5'-Phos CTG CGG TCG CG -3'	Phosphate

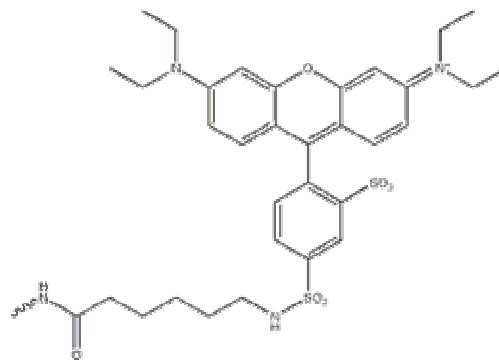
---

---

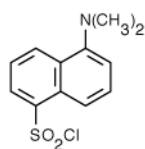
Hexchlorofluorescein (Hex), rhodamine and dansyl Chloride (**Figure 2.2**) were used as fluorescent tags. According to the Molecular Probes Handbook ([www.probes.com](http://www.probes.com)), hex and rhodamine offer lots of desirable properties, including good photostability, high extinction coefficients ( $>75,000 \text{ cm}^{-1}\text{M}^{-1}$ ) and high fluorescence quantum yields. Moreover, the fluorescence of their conjugates are completely insensitive to pH between 4 and 9. The dansyl fluorophore has a lower quantum yield than hex or rhodamine, which allows the use of higher concentrations without inner filter effects. The more weakly absorbing dansyl probe was used to study the weak interactions between enzyme and product. In an emission experiment, an inner filter effect refers to an apparent decrease in emission quantum yield as a result of reabsorption of emitted radiation. In order to avoid inner filter effects, the optical density of the absorbing species should be less than 0.1 absorbance units at the emission wavelength (Lakowicz & Thompson, 1983).



Hexachlorofluorescein



5' RhodamineRed



dansyl

**Figure 2.2. Structures of the fluorescent dye of Hex, Rhodamine and Dansyl fluorophore.** The structure of dansyl fluorophore was obtained from [www.probes.com](http://www.probes.com). Hex and rhodamine structures were obtained from [www.idtdna.com](http://www.idtdna.com).

---

**Radio-labeling of Oligonucleotides.** In the PAGE gel activity assay, the oligonucleotides were radio-labeled so as to be visualized by the Storm phosphoimager. The radio-label reaction was initiated by addition of 1 or 2  $\mu\text{L}$  [ $^{32}\text{P}$ - $\gamma$ ] ATP (33 pmoles of a 6000 Ci/mmol stock, purchased from Perkin Elmer, Boston, MA) and T4 polynucleotide kinase (New England Biolab), then incubated at 37 °C for half an hour. The radio-labeled duplexes was diluted by 10 fold (final concentration is about 200 nM) and purified by Sephadex G-50 resin (Sigma, St. Louis, MO).

**Assay of *PvuII* Endonucleases Activity.** The hydrolysis reaction at different time points could be monitored by loading denatured samples into PAGE gel. The denatured PAGE gel was prepared by addition of TEMED (N,N,N',N'-Tetramethylethylenediamine) and 10% APS (ammonium persulfate) into the 20% acrylamide/8 M Urea/0.5X TBE (buffer containing Tris, Boric acid and EDTA) solution. The gel was formed in the template between two glass plates with 20 wells on top (35X45 cm with 0.4 mm spacer). The sample is run in the gel for about 4 hours at 1500 Voltage till the substrate and product band were clearly separate. The amount of product and substrate were subsequently visualized by the Storm Phosphoimager (GE Healthcare, Piscataway, NJ) and the scanned image could be further quantitated by ImageQuant (GE Healthcare, Piscataway, NJ).

The reaction conditions varied depending on the kinetic study (i.e. single turnover, steady state and pre-steady kinetics). The typical single turnover reactions conditions were 2  $\mu\text{M}$  enzyme, 300 nM DNA (**Figure 2.3**).

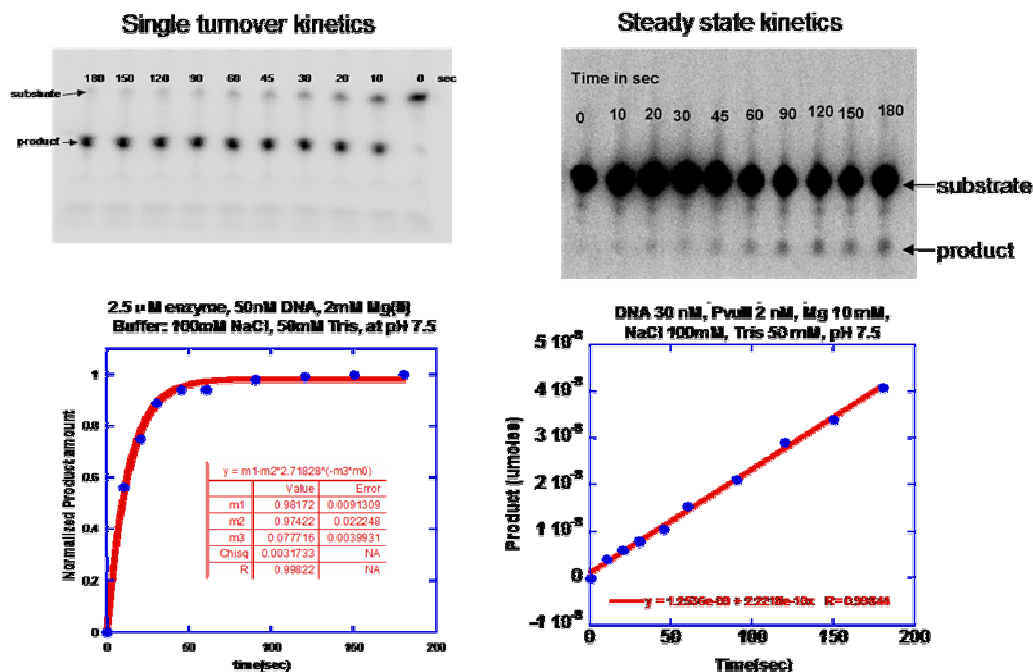


**Figure 2.3. PAGE gel and kinetic analysis of *PvuII* endonucleases activity for single turnover assay and steady state assay.** The top panel shows the separation of radio-labeled substrate and product in a 20% polyacrylamide gel with 8 M urea, running for 4 hours in 0.5 TBE buffer. The bottom panels show the kinetic curve fit for typical single turnover and steady state reactions. The single turnover reaction conditions: 2  $\mu$ M enzyme, 50 nM DNA, 2 mM Mg(II), Buffer: 100 mM NaCl, 50 mM Tris, at pH 7.5, 37  $^{\circ}$ C. Steady state reaction condition: 2 nM enzyme, 30nM DNA, 10 mM Mg(II), Buffer: 100 mM NaCl, 50 mM Tris, at pH 7.5, 37 $^{\circ}$ C. The single turnover data was fit to a first order rate equation and the steady state data was fit to a linear equation to calculate the reaction velocity.

---

For the steady state kinetics, 1 or 2 nM enzyme was usually used and DNA concentration varied from 5 nM to 200 nM. Pre-steady state conditions usually were the same as steady state at low Mg(II) concentrations (below 3 mM). At high Mg(II) concentrations (above 3 mM), a much higher enzyme to substrate ratio of 3~5 was applied so that the product could be visualized.

For the investigation of Mg(II) dependence of reaction rates, the typical buffer system consisting Tris (50 mM) and NaCl. The concentration of NaCl was adjusted according to Mg(II) concentrations to keep the ionic strength as constant as buffer with 100 mM NaCl/50 mM Tris/10 mM Mg(II) and pH was typically 7.5 at 37 °C. For the investigation of pH dependent activity study, a triple buffer system consisting of 80 mM NaCl/50 mM Tris/25 mM NaAc/25mM MES was used, which was designed to keep ionic strength as constant at a broad pH range (4~9) without changing any components concentrations (Lagunavicius, et al., 1997).

#### **Quantitation of Metal Ions Stocks by Atomic Absorption.**

Concentrations of MgCl<sub>2</sub> and CaCl<sub>2</sub> stocks solution were determined by flame atomic absorption spectroscopy using a GBC model 904BT double beam atomic absorption spectrometer. Standard solutions were purchased from Fisher (Pittsburgh, PA) and appropriate dilutions were made into 5% HNO<sub>3</sub> to produce the standard curves.

#### **Determination of *Pvu*II Endonuclease-DNA Equilibrium Constants**

**Using Fluorescence Anisotropy.** The fluorescence anisotropy measurements reflect the target molecule's intrinsic properties or its local environment. The measurements have been conducted using a Fluorolog-3 (SPEX) spectrofluorimeter

---

equipped with a polarization assembly. Depending on the fluorophore labeling oligonucleotides, the excitation and emission spectra were collected to determine the wavelength of emission and excitation during the measurement. For example, the excitation/emission wavelength is 540/556 nm for hex, 553/578 nm for rhodamine and 350/543 nm for dansyl. The target molecules, which usually are fluorophore labeled oligonucleotides, are placed in a nitric acid cleaned cuvette (NSG Scientific, Farmingdale, NY) with filtered buffer containing the appropriate metal cofactor concentration, and the solution in the cuvette is kept stirring at 25 °C using a water bath and a thermostatted cell holder. Filtered enzyme was titrated into the oligonucleotides in the cuvette, allowing about 5 minutes incubation to reach equilibrium. The intensity of polarized fluorescence in both parallel and vertical direction are measured and anisotropy values are obtained in triplicate and automatically calculated from **equation 2.1**.

$$A = (I_{\parallel} - I_{\perp}) / (I_{\parallel} + 2I_{\perp}) \quad (2.1)$$

where I is recorded as intensity at the indicated polarizer orientation (perpendicular and parallel). Normalized anisotropy values were plotted as a function of added protein concentration and then fit to an appropriate binding model.

For *PvuII* endonuclease-DNA binding, it was assumed that one dimer of *PvuII* endonuclease binds to one duplex of DNA (**equation 2.2**).



where  $[ED] = [E][D] * K_a$ ,  $K_a$  is the association constant, E and D represent *PvuII* endonuclease dimer and DNA duplex, respectively. This one-site equilibrium model

---

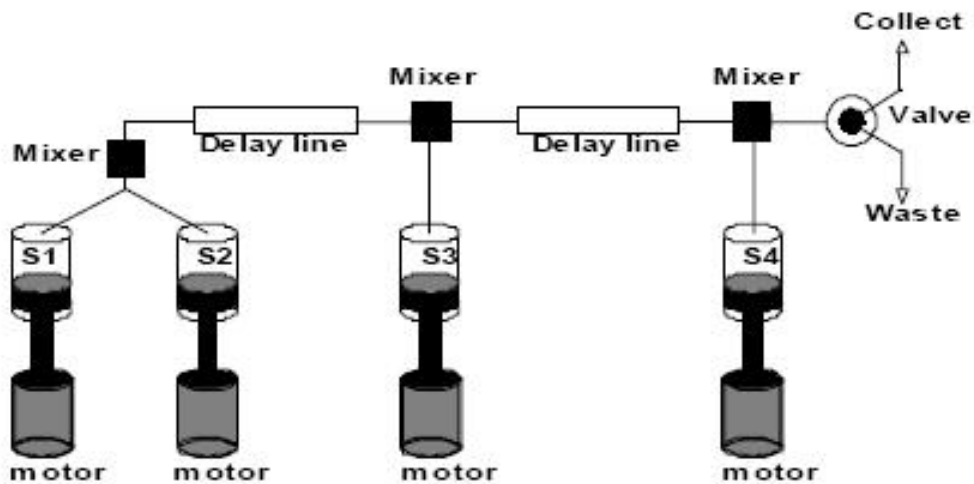
can be fit to the Langmuir isotherm (**equation 2.3**) using KaleidaGraph software.

$$\theta = K_a[E]/(1 + K_a[E]) \quad (2.3)$$

where  $\theta$  is bound fraction (normalized anisotropy values) and  $[E]$  is the concentration of enzyme in dimers.

**Quench Flow.** The quench flow is used to monitor the reaction or process on the millisecond time scale. SFM4/Q quenched-flow device has four syringes ports and it can process two mixing events (Bio-Logic Science Instruments, Knoxville TN). For *PvuII* endonuclease cleavage reactions, typically port 1 and port 2 were filled with enzyme and DNA, respectively. The reaction was initiated at inter-mixer 1 by mixing equivalent volumes of solutions from port 1 and 2, then after flowing through the designated delay lines, the reaction was quenched by addition of 100 mM EDTA solution from port 4 (**Figure 2.4**). The accessory includes delay lines with various volumes and can be easily combined and replaced. MPS software was used to program the driving sequence and monitor the injection volume and flowing rates. The reaction time is the interrupt phase time plus the aging time in the delay lines. The aging time can be calculated using the volume of delay line and solution flowing rate. The typical delay line combination for *PvuII* cleavage reactions were 17  $\mu$ L and 90  $\mu$ L, and the flow rates was 0.5 mL/sec, therefore the minimum reaction time was about 200 ms.

**The Application of SwissPdbviewer.** Swiss-PdbViewer (version 3.7) (Guex & Peitsch, 1997) is application software that provides a user friendly interface allowing visualizing and modifying protein structures. The proteins can be



### SFM-4 quench flow mode

**Figure 2.4.** The configuration of SFM-4 quench flow instruments. The configuration of SFM-4 quench flow mode is adapted from stop flow manual of Bio Logic Science Instruments. Quench flow consists of four syringe ports (S1, S2, S3 and S4), two delay lines and three inter-mixers. Typically S1 and S2 are filled up with enzyme and DNA, S4 is filled up with EDTA. The reaction is initiated at the first inter-mixer and quenched at the third inter-mixer. Each syringe plunger is driven by electric motor and its motion can be programmed.

---

superimposed in order to deduce structural alignments and compare their active sites or any other relevant parts, which is used to compare the Ca(II) and Mg(II) binding sites available in the different *PvuII* crystal structures. Amino acid mutations, distances between atoms, shifting atoms in the active site and addition of water molecules as metal ion ligand can also be accomplished using the intuitive graphic and menu interface. In the pK<sub>a</sub> calculations of *PvuII* endonucleases, the mutations and the shift of metal ions or ligated water molecules were all conducted by SwissPdbviewer. The distance information between atoms is easily obtained using the distance tools in the menu.

**UHBD Program.** The electrostatics-based computational methodology implemented in the University of Houston Brownian Dynamics (UHBD) program (Antosiewicz, et al., 1994; Antosiewicz, et al., 1996a) was used to predict pK<sub>a</sub> values of all ionizable groups and molecules in the type II restriction endonuclease *PvuII*. UHBD is used to compute the electrostatic potential and the electrostatic free energy for a given charge distribution in an arbitrary dielectric medium by solving the Poisson-Boltzmann equation using a finite-difference method. In this approach, each ionizable group is assigned to a model pK<sub>a</sub> value which represents the pK<sub>a</sub> of that group in solution. For Mg(II)-ligated water molecules, 11.4 was used as the model pK<sub>a</sub> (Dahm, et al., 1993). According to a thermodynamic cycle of ionization in solution and in a protein, prediction of the apparent pK<sub>a</sub> value of an ionizable group in the protein environment is computed from the difference in electrostatic free energy ( $\Delta\Delta G$ ) for protonating such a group in solution vs. in its environment in the

---

protein (**equation 2.4**) (Briggs, et al., 1989).

$$\Delta\Delta G = \Delta G_{\text{protein}}^{\text{el}} - \Delta G_{\text{solution}}^{\text{el}} \quad (2.4)$$

where  $\Delta G^{\text{el}}$  is the electrostatic free energy difference for ionization of a given site in a molecule in the solution and in the protein with all other groups in their neutral state.

The intrinsic  $\text{pK}_a$  is defined by the **equation 2.5** (Briggs, et al., 1989):

$$\text{pK}_a^{\text{intrinsic}} = \text{pK}_a^{\text{model}} - \gamma \Delta\Delta G / 2.303RT \quad (2.5)$$

where  $\gamma$  is -1 for an acidic group and +1 for a basic group.

The electrostatic work for the ionization is calculated by use of the linearized Poisson-Boltzmann equation implemented in UHBD. The determination of  $\text{pK}_a^{\text{intrinsic}}$  consists of two electrostatic contributions. One is the desolvation energy when the ionizable group is transferred from bulk solution to its environment in the protein, the latter of which exhibits a low dielectric environment. The other contribution is from the ionization energies assuming that all of the other titratable groups are neutral. The electrostatic energy is determined by the interaction with all of the background charges in the protein when all amino acids are in their neutral state.

In reality, of course, the protein has multiple titratable sites, so  $\text{pK}_a^{\text{intrinsic}}$  is not equal to  $\text{pK}_a^{\text{apparent}}$  because all other ionizable residues will not be neutral. Therefore, to calculate the electrostatic energy from the charge-charge interaction between the given ionizable group and all other titratable groups, it is essential to evaluate the ionization states of each site at various pH values. This multiple titration state problem requires the evaluation of numerous protonation patterns. This problem can be treated using a Monte Carlo method, which samples

---

combinations of protonation states using a Metropolis algorithm, resulting in a Boltzmann distribution of protein protonation states and their associated electrostatic free energies. The Monte Carlo method provides a list of pKa apparent and pKa intrinsic values for all ionizable groups in the protein. Since the number of protein ionization states is huge (on the order of  $2^N$ , where N is the number of ionizable groups in the protein system), it is difficult to adequately sample the possibilities. Therefore, a different approach was also taken to address this coupled titration problem, which was a hybrid divide-and-conquer Tanford-Roxby method (Gilson, 1993). In this approach, titratable residues that strongly interact are put in the same cluster and the coupled titration problem is solved exactly within each cluster, supplemented by an inter-cluster interaction term.

The single site approach was used to describe the ionization in the titratable group upon protonation or deprotonation. This approach neglects the fact that the partial charge distribution changes upon ionization and treats ionization by adding or subtracting a full charge to one atomic position in the group. The atomic ionization sites are atom CG in Asp, CD in Glu, CZ in Arg, NZ in Lys, OH in Tyr, NE2 in His and OW in H<sub>2</sub>O, where the unit charge is added upon protonation or deprotonation. Ionizable groups were switched “off” by changing the atom type to nonionizable. Due to the somewhat rough description of ionization in the single site model and the neglect of conformational flexibility, the error in the pKa prediction is ca. one pH unit (Antosiewicz, et al., 1994).

In the pKa predictions, atomic partial charges and radii from the

---

CHARMM22 force field were used in all calculations (Follope & Alexander D. Mackerell, 1999). Solvent and protein dielectric constants were 80 and 20, respectively. The ionic strength (150 mM), ionic radius (2 Å), surface probe radius (1.4 Å), and temperature (293 K) were chosen to reflect the experimental conditions.

**DynaFit Program.** DynaFit is the program to perform nonlinear least-squares regression of chemical kinetic and ligand-receptor binding data. The interface consisting of three windows as reaction scheme, data graphic and status (**Figure 2.5**) (Kuzmic, 1996). The experimental data can be either reaction velocities dependent on the concentration of varied species (e.g., enzyme, substrate, and metal concentration vs. steady state velocity), or the reaction progress curves (e.g., in the global fit of single turnover data), or the equilibrium data (e.g., Ca(II) dependent enzyme titration). The established reaction scheme can be converted to scripts in DynaFit to represent the terms of symbolic, or stoichiometric, binding or chemical equations. The measured kinetic parameters are fixed in the global fits and the unknown kinetic parameters are given the initial values as estimate, which are varied and finally derived from the global fits. For global fits with Mg(II) dependence of *PvuII* single turnover and pre-steady state kinetics, the fixed kinetic parameters includes DNA association rates, DNA dissociation rates and metal dissociation rates. The floating kinetic parameters include metal association rates, turnover rates and product dissociation rates. A sample fit of Mg(II) dependence of single turnover progressive curves has been attached as **Appendix I** including the global fit script, fit curves and output.

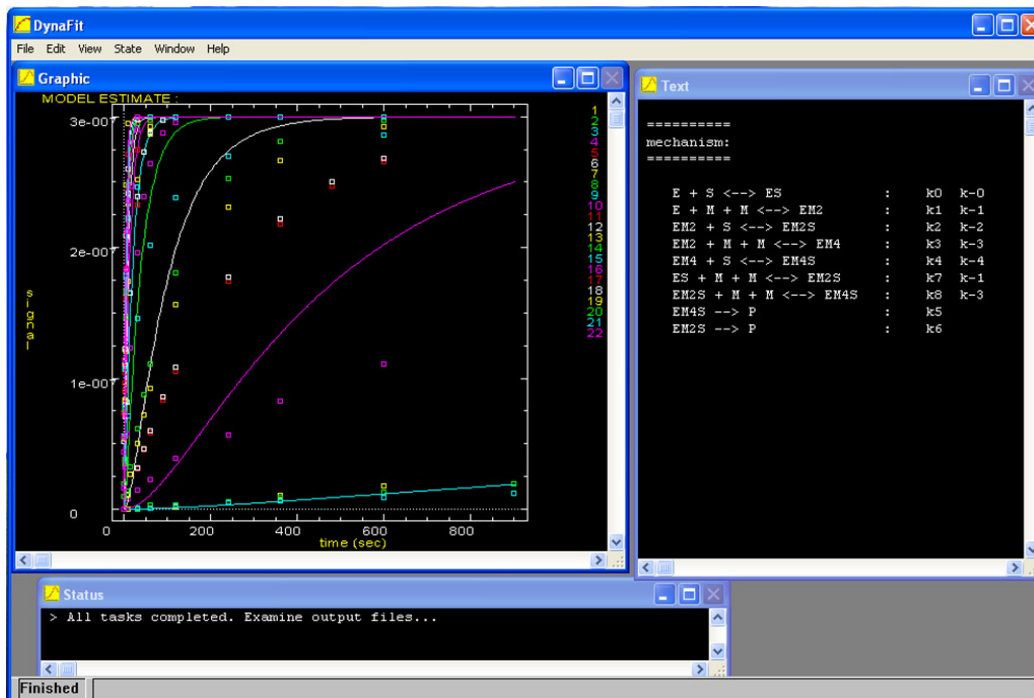


**Figure 2.5. The application of Dynafit in global fit.** It consists of three windows including such as data graphic, reaction mechanism and status. The graphic window shows the original data and generated fit curves marked with different colors. The text window shows the edit of reaction scheme and kinetic parameters for each step that is floating during the global fit. It partially shows the fit error status when fit is accomplished, which is indicated in status window.

---

The global fit quality can be evaluated by either overall standard deviation or the error of the derived unknown rate constants. In some cases, simulations based on the best fit unknown parameter sets to reproduce the metal dependent rate profiles are employed to facilitate the visualization and evaluation of various models.

---

## CHAPTER III. ELECTROSTATIC CONTRIBUTIONS TO WATER ACTIVATION IN PD...(D/E)<sub>x</sub>K METALLONUCLEASE

### INTRODUCTION

Most of the type II restriction endonucleases feature the conserved catalytic center motif PD...D/ExK. Two conserved carboxylate groups in the active sites ligate one or multiple divalent metal ions which are essential for catalysis. But Mg(II), Mn(II) and Co(II) are known to support the efficient catalysis while others like Ca(II) only drive the association of DNA (Bowen & Dupureur, 2003). The role of the Lys in the catalytic motif remains unclear. This Lys is not always conserved; in *Bgl*I and *Bam*HI, it is replaced with Gln and Glu, respectively (Newman, et al., 1998; Lukacs, et al., 2000).

The general mechanism of phosphodiester bond hydrolysis by type II restriction endonucleases starts with the activation of the nucleophile as a hydroxide ion, followed by attack on the scissile phosphate. The developed transition state is stabilized by the divalent metal ions in the active site. Another water molecule protonates the developed 3' oxyanion and facilitates its departure (Pingoud, et al., 2005).

The activation of the nucleophile and the roles of metal ions in catalysis remain controversial. Proposals are depicted in **Figure 3.1**. For the generation of the attacking nucleophile, the proposals include extrinsic mechanism, substrate assisted catalysis and general base catalysis. The extrinsic mechanism (**Figure 3.1A**) suggests penetration of the hydroxide from bulk solvent and is found to be the most favorable by quantum mechanical simulations and calculated energy barrier (Mones,

---

et al., 2007a). Substrate assisted catalysis and general base catalysis agrees with the formation of nucleophile by the deprotonation of metal ligated water molecules, but differs in which group abstracts a proton and assists its deprotonation (Jeltsch, et al., 1993; Horton & Cheng, 2000). In general base catalysis, the group that abstracts a proton from metal ligated water molecule is the conserved Lys or Glu (the substitution in *Bam*HI) (**Figure 3.1B**), and in substrate assisted catalysis it is the 3' neighboring phosphate (**Figure 3.1C**). Besides one metal ligated water molecule to form the nucleophile, the second metal ligated water molecule (**Figure 3.1D**) protonates the 3' oxyanion and facilitates the departure of the leaving group based on *Pvu*II-Ca(II)-cognate DNA crystal structure (Horton & Cheng, 2000). Solely based on the crystal structures, it appears that two metal ions are required to accomplish the formation of nucleophile and the following protonation of the leaving group since two metal ligated water molecules can serve as a general base and general acid, respectively. However, the number of metal ions essential for catalysis remains controversial and will be discussed in Chapter IV.

The significance of ionization of critical residues in binding and catalysis of nucleases has long been recognized. The measurements of pH dependence of metal binding, DNA binding and enzymatic activity has been conducted with many nucleases in order to disclose the ionizable groups involved (Zebala, et al., 1992; Sam & Perona, 1999a; Haq, et al., 2001; Tock, et al., 2003).

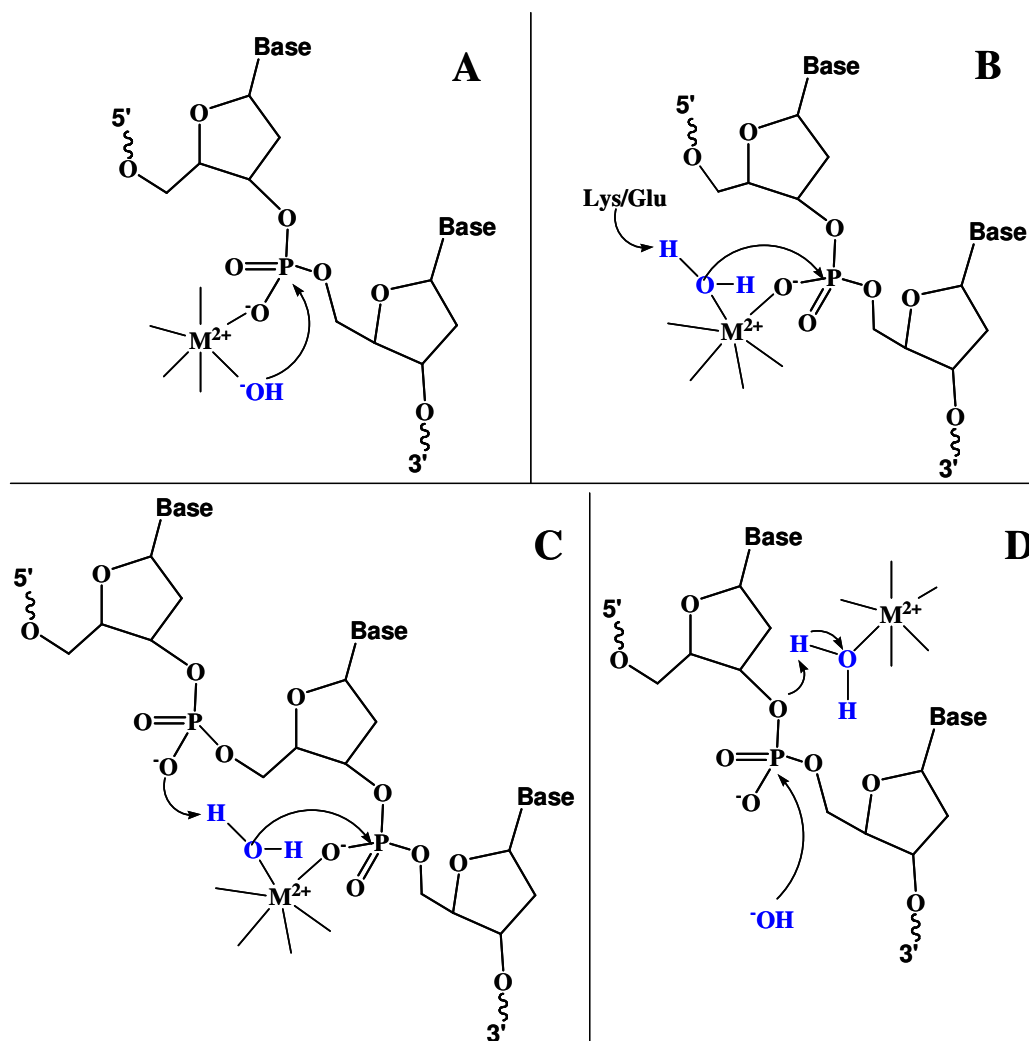


**Figure 3.1. Possible roles of metal ions and the activation of water molecule in the DNA hydrolysis by endonuclease.** The figure is adapted from the reference (Tock, et al., 2003). A. Penetration of the hydroxide ion from bulk solvent which is stabilized by the metal ions. Metal ions also stabilize the transition states in the DNA hydrolysis. B. The conserved Lys or Glu functions as a general base to abstract a proton from the metal ligated water molecule. C. Substrate assisted catalysis. The neighboring 3' phosphate abstracts a proton from the metal ligated water molecule. D. The nucleophilic attacking on the scissile phosphate by a hydroxide ion and the protonation of leaving group by a metal ligated water.

---

The steady state and single turnover kinetics of *TaqI* restriction endonuclease was characterized before the conserved catalytic center motif PD...D/ExK for type II restriction endonucleases was recognized (Zebala, et al., 1992). pH profiles of  $K_m$  and single turnover rate constant  $k_{st}$  (single turnover rate constant) both increased markedly with pH and showed sigmoidal curves, but  $k_{cat}$  did not. The pH dependence of  $K_m$  ( $pK_a=9$ ) and  $k_{st}$  ( $pK_a=7$ ) suggested a titration of Lys/Arg and His, respectively. Based on the fact that  $k_{cat}$  did not change much with pH, at least one step other than the chemical step ( $k_{st}$ ) is rate limiting step in the reaction pathway. Besides the pH study, initial velocities were studied as a function of  $Mg^{2+}$  concentration, and a  $K_d$  (2.5mM) for the cofactor binding was determined, although the experiments could not distinguish whether  $K_d$  was due to Mg(II) binding to the enzyme or the enzyme-substrate complex.

The single turnover rate constants for site specific DNA cleavage by *EcoRV* have been determined as a function of pH. A bell shaped pH-rate curve was determined in the presence of Mg(II), and log linear plot of pH-rate was consistent with general acid and general base catalysis (Sam & Perona, 1999a). Two equivalent  $pK_a$  values (8.54 and 8.52) derived from the pH-rate profiles agree well with a model in which the ionizations of two distinct metal-ligand waters generate the attacking hydroxide ion and the proton for donation to the leaving group. For Mg(II) a  $pK_a$  value of 11.4 for the inner sphere water molecule was commonly assumed. Compared with the  $pK_a$  (8.5) of the water molecules determined from the kinetic data, two pH units of the  $pK_a$  shift is speculated to be due to the proximity of Lys92.

---

pH dependence of specific DNA binding by *MunI* restriction endonuclease has been studied in the absence of Mg(II) (Haq, et al., 2001). The binding constant  $K_{\text{obs}}$  decreased with pH, and the curve showed two distinct inflections and was fit to a two-event model in which the same ionizable group in the free enzyme and substrate bound enzyme were distinguished with different  $\text{pK}_a$ 's. The free enzyme was assigned two ionizable groups ( $\text{pK}_a1=6.0$  and  $\text{pK}_a2=6.9$ ), which are interpreted as the  $\text{pK}_a$ 's of acidic residues in the active site such as D83 and E98. There is evidence that the analogous residues in *PvuII* (D58 and E68) have similar  $\text{pK}_{a,\text{app}}$  (Dupureur & Conlan, 2000). The upward shifts of those two  $\text{pK}_a$ 's in the DNA-bound form of enzyme have been speculated to be due to the negative charges of the bound DNA backbone. In addition to specific DNA recognition and binding studies, plasmid DNA cleavage by *MunI* restriction endonuclease has been investigated by single turnover and steady state kinetics (Sasnauskas, et al., 1999). The pH dependence of  $k_{\text{cat}}$  in steady state kinetics (measured at 1 mM  $\text{Mg}^{2+}$ ) gave a sigmoidal curve in the pH range (6-9). The apparent  $\text{pK}_a$  of 7.8 was derived from fitting to a single proton binding event; terminal phosphate and carboxylate groups might be responsible for this apparent  $\text{pK}_a$ . It is also found that the plots of plasmid cleavage rate against Mg(II) concentration were linear at low pH (<6.0) but hyperbolic at high pH (>6.0). Therefore, the unsaturated Mg(II) dependence at low pH indicates the competition binding between proton and Mg(II) ion to the active site.

The direct involvement of different divalent metal ions in nucleophile activation has been observed in flap endonuclease (Tock, et al., 2003). The single

---

turnover rate constant as a function of pH has been determined with Mg(II), Mn(II) and Co(II). The pH rate plots were fit with one ionization equation and the derived apparent  $pK_a$  shows a linear dependence on their metal ligated water  $pK_a$  (11.4 for Mg(II), 10.6 for Mn(II) and 9.6 for Co(II) ligated water molecule). Since the kinetic  $pK_a$ 's display good correlation with the acidity of the corresponding hexahydrated metal ions, this strongly suggests a role for metal bound hydroxide in catalysis.

The apparent  $pK_a$ 's near neutrality have been derived for *MunI*, *PvuII* and *EcoRV*, but typical  $pK_a$ 's of acidic groups (4.0 for Asp and 4.4 for Glu) and Lys (10.4) conserved in the active site obviously do not agree with it. From those pH dependence studies with nucleases, it is very challengeable to assign the apparent  $pK_a$ 's derived from pH profiles to the ionizable groups in the active site. But it is possible that the  $pK_a$  values of those active site residues shift in proteins and those  $pK_a$  shifts are not experimentally accessible by a normal titration experiment.  $pK_a$  prediction of protein residues by computational chemistry provide a tool to investigate the pH dependent properties of proteins since it can evaluate the  $pK_a$ 's for each titratable site in proteins. Although very precise  $pK_a$  predictions remain challenging, some programs such as UHBD and DelPhi have been developed based on solving the Poisson-Boltzman equation (Nielsen & Vriend, 2001). Those programs allow the application of X-ray crystal structures and NMR solution structures to predict the  $pK_a$  values of all the titratable groups in a protein and the results of calculations can be correlated with the pH dependence studies of protein stability and enzymatic activity. The apparent  $pK_a$ 's derived from pH profiles can generally reflect the ionizations of a

---

cluster of residues in the active site. By such correlations between those experimental determinations and the predicted  $pK_a$ 's of protein residues, the catalytic residues are expected to be identified.

The target protein we mainly work with in this chapter is *PvuII* restriction endonuclease. *PvuII* restriction endonuclease is a homodimeric enzyme of 18kDa. It recognizes DNA sequences 5'-CAG↓CTG-3' and cleaves DNA duplex in the presence of Mg(II) to produce 3'-hydroxyl and 5'-phosphate ends (Gingeras, et al., 1981). Applying isothermal titration calorimetry to *PvuII* restriction endonuclease, it is determined that two metal ions bind to its active site, which agrees well with crystal structure of *PvuII*-Ca(II)-DNA complex (Jose, et al., 1999; Horton & Cheng, 2000). Two acidic residues Asp58 and Glu68 and one basic Lys70 comprise its catalytic center and they are critical to enzymatic activity and specificity (Nastri, et al., 1997).

The pH dependence of Mg(II) binding was measured by  $^{25}\text{Mg}$  NMR experiments, and an abnormal apparent  $pK_a$  of 6.7 was determined for WT with a two ionizable group model (Dupureur & Conlan, 2000).  $pK_a$  predictions of acidic residues will be an appropriate approach to assign abnormal apparent  $pK_a$  to the specific ionizable groups.

*PvuII* endonuclease likely follows a two-metal ion mechanism in catalysis based on structural and biophysical characterization (**Figure 3.2**). The metal ions are responsible for lowering the  $pK_a$  of a neighboring water molecule, thereby facilitating its deprotonation to prepare the attacking nucleophile (Horton & Cheng, 2000). One metal ligated water molecule deprotonates to form the attacking

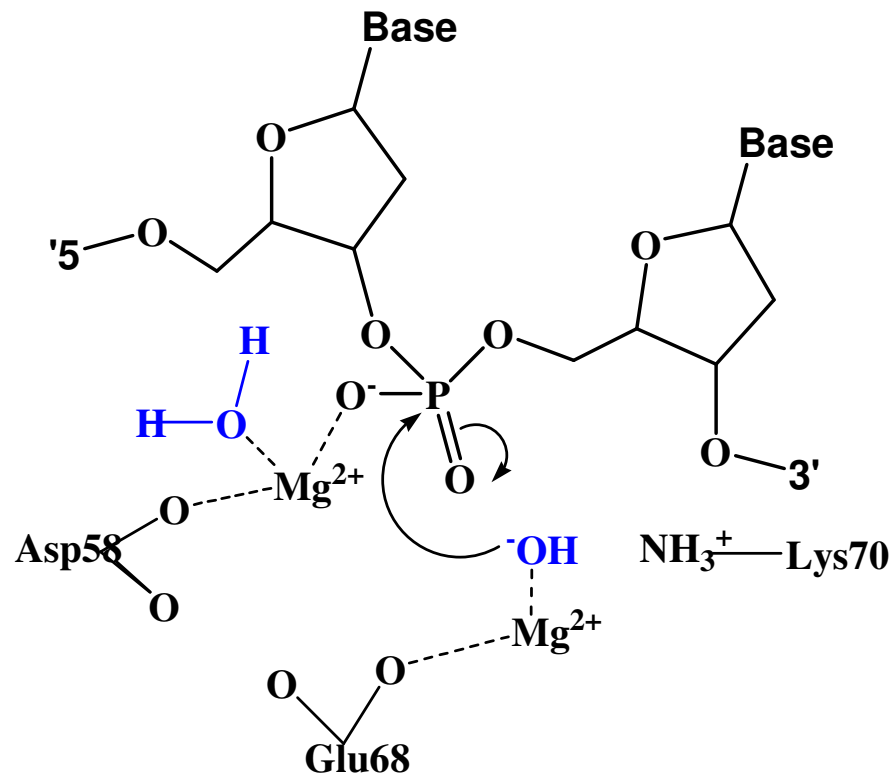


**Figure 3.2. The general mechanism of phosphodiester bond hydrolysis by type II restriction endonucleases.** The general catalytic mechanism for PvuII is adapted from crystal structure of *PvuII*-Ca(II)-DNA complex (Horton & Cheng, 2000). Two metal ligated water molecules are highlighted in the active site. One deprotonated to form the attacking nucleophile, with its deprotonation is assisted by a nearby Lys. The other protonates the hydroxyl group after the cleavage of phosphodiester bond.

---

nucleophile and a second metal ligated water molecule protonates the leaving group. The proximity of Lys70 may account for a magnitude of 2 pH units  $pK_a$  shift of metal ligated water molecule (Sam & Perona, 1999a).

In this work, I attempt to calculate the  $pK_a$  values of active site residues and crystallographic defined metal ligated water molecules in *PvuII* endonuclease using the implementation of protein ionization state prediction method embedded in the UHBD program (Antosiewicz, et al., 1994). The effect of local electrostatic environments on predicted  $pK_a$  value is also the focus of the  $pK_a$  calculations. The  $pK_a$  calculations are performed on several crystal structures of *PvuII* and finally are extended to other endonucleases featured with the motif PD...D/ExK to test a possible general trend that the  $pK_a$ 's of metal ligated water molecules are mediated by metal ions and conserved Lys.

---

## EXPERIMENTS AND METHODS

**pK<sub>a</sub> Predictions using UHBD.** The UHBD (University of Houston Brownian Dynamics) is a program capable calculating the electrostatic free energies in proteins on the basis of solving the Poisson-Boltzmann equation. pK<sub>a</sub> calculations were performed utilizing a methodology embedded in the UHBD package release 5.1. The detailed methodology of how to use the calculated electrostatic free energies to derive the apparent pK<sub>a</sub> has been described in Chapter II. The overall pK<sub>a</sub> predictions have been performed based on two stages. The first stage is to calculate the intrinsic pK<sub>a</sub> of each titratable site. The second stage is to determine the interaction energies among all the titratable sites. Monte Carlo simulations are performed to determine the ionization status for each titratable site, and the hybrid program predicts the apparent pK<sub>a</sub> with better precision. The charge distribution of one titratable site is simplified as a single site model which assumes that one unit positive or negative charge is added on a given atom of the ionizable group upon protonation or deprotonation. For example, atom CG in Asp, CD in Glu, CZ in Arg, NZ in Lys, OH in Tyr, NE2 in His and OW in H<sub>2</sub>O are the positions where the unit charge is added. To turn off a residue as a non titratable site in pK<sub>a</sub> calculations, the name of that titratable atom is changed so that it is not recognized in the program. Then no unit charge will be added on them and the whole site remains neutral in the pK<sub>a</sub> calculations.

**Parameters Applied In pK<sub>a</sub> Calculations.** Single-site approach was carried out with atomic charges and radii of CHARMM22 force field for amino acid residues, nucleic acids and metal ions (provided by Dr. Briggs in University of Houston). In the single

---

site approach, the ionization occurs to each titratable group as the addition of a single point charge of  $\pm 1$  electron to a single atom. The solvent and protein dielectric constants were set as 80 and 20, respectively. The ionic strength (150 mM) and temperature (293 K) were chosen to reflect the experimental conditions.

**Preparation of Protein Structures.** As described in Chapter II, PvuII and other endonuclease crystal structures in pdb form are downloaded from Protein Data Bank ([www.rcsb.org](http://www.rcsb.org)). To perform pKa calculation in apo enzyme, all the water molecules, metal ions and DNA molecules are removed from crystal structures prior to the calculations. The metal ions or DNA strand are kept when the inclusion of metal ions or DNA strand in pKa calculations is indicated. All the PvuII variants are created in SwissPdbviewer ([www.expasy.org/spdbv](http://www.expasy.org/spdbv)) by changing the target residues to Ala or turning them off (treat as untitratable site) and following up with energy minimization to refine the coordinates of variant structures.

#### **Single Turnover and Steady State Cleavage Assays as a Function of pH.**

Single turnover rate constants and steady state rate constants for specific DNA cleavage as a function of pH were measured using PAGE cleavage assay as described in Chapter II. The triple buffer system containing 10 mM Mg(II), 80 mM NaCl, 50 mM Tris, 25 mM NaAc and 25 mM MES was used to maintain the same ionic strength at various pH. pH values were adjusted at 37°C.

The steady state cleavage assay experiments measure the reaction velocity of the linear phase with 1 or 2 nM enzyme with at least 5 fold excess substrate concentrations as a function of pH. The reaction is slow enough to collect at different time points

---

manually. The reaction is usually terminated before 5% substrate cleavage is achieved. The amount of product vs time is plotted and the reaction velocity is calculated by normalization of linear phase slope using enzyme concentration. The plot of reaction velocity against substrate concentration is to fit the Michaelis-Menten equation to derive  $k_{\text{cat}}$  and  $K_M$ .

The single turnover reactions were performed in the same buffer with the same method of sample collection except for rapid reactions (pH 7~8.6), for which the instrument quench flow (BioLogic SFM-400) was used to monitor the reactions. The typical reaction concentration for single turnover reactions was 2  $\mu\text{M}$  enzyme and 300 nM DNA. As described in Chapter II quench flow section, the single turnover reactions were initiated by mixing metal-free enzyme from one syringe and DNA with pre-mixed Mg(II) containing buffer from another syringe. After the designated incubation time, the reactions were quenched by addition of 100 mM EDTA syringe from a third syringe. 200  $\mu\text{L}$  reaction samples were collected and 10-12  $\mu\text{L}$  of samples were loaded on a PAGE gel for further analysis. The amount of substrate and product both are quantitated from a gel image. For single turnover reactions, the amount of product was normalized and fit with a first order reaction equation to derive the apparent single turnover rate constant.

**Data Fit With *PvuII* pH Rate Profiles.** The pH dependence of *PvuII* activity regardless of single turnover and steady state reactions shows a typical bell shaped curve, which is similar to pH rate profiles of *EcoRV* (Sam & Perona, 1999a). It is generally interpreted that bell-shaped pH-rate profiles represents two ionizations

---

involved the catalytic activity with one deprotonation in the acidic pH serving as a general base and one protonation in the basic pH range serving as general acid. The two ionization equations below were used for *EcoRV* and can be used to fit the pH rate profiles of *PvuII* as well (Sam & Perona, 1999a).

The pH dependence of single turnover or steady state cleavage rate has been fitted to a classic **equation (1)** for bell shaped pH profiles, where  $k_{\max}$  represents the maximal enzymatic activity independent of pH, and  $pK_{a1}$  and  $pK_{a2}$  are the  $pK_a$  values of the deprotonated group in the acidic limb and the protonated group in the basic limb, respectively (Sam & Perona, 1999a). The ionizations of two groups are assumed to be independent and their apparent  $pK_a$  values should be separated by at least two pH units.

$$k_{\text{obs}}=k_{\text{max}}/(1+10^{(pka1-pH)}+10^{(pH-pka2)}) \quad \text{eq (1)}$$

A modified **equation (2)** deviated from classic equation (1) has also been applied to fit the pH-rate profile. **Equation (2)** gives two almost equivalent  $pK_a$  values for two ionizable groups, to address possibilities of reverse ionization ( $pK_{a1}$  is higher than  $pK_{a2}$ ). This allows a better estimation of real  $pK_a$  values when the difference of two  $pK_a$  values are less than two pH units.

$$k_{\text{obs}}=k_{\text{max}}/(1+10^{(pka1-pH)}+10^{(pH-pka2)}+10^{(pka1-pka2)}) \quad \text{eq (2)}$$

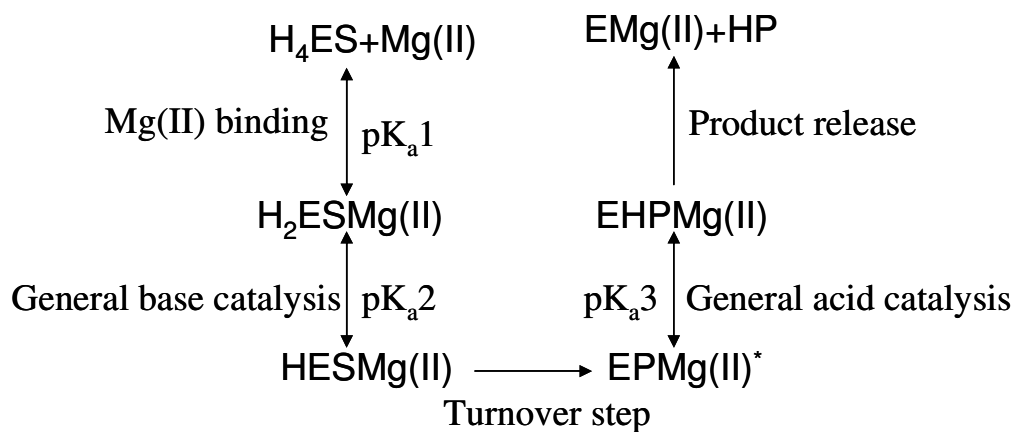
**Equation (3)** has also been applied to address the experimental data which deviated from a single ionization model in the acid limb. In the case of *PvuII*, multiple ionizable groups are involved in the acid limb, and competition binding between proton and Mg(II) ions occurs as well as a formation of a general base. In **equation**

---

(3), the additional  $pK_a1$  represents the apparent  $pK_a$  of two metal ion binding sites of *PvuII* which are essential and deprotonate prior to general base catalysis.  $pK_a2$  and  $pK_a3$  represent two ionizable groups for general base catalysis and general acid catalysis. The **Scheme 3.1** describes the speculated ionizations involved in catalysis. In the scheme, three ionizations involved in metal binding and chemistry steps are indicated.

$$k_{obs} = k_{max} / (1 + 10^{(2 * pKa1 + pKa2 - 3 * pH)} + 10^{(pKa2 - pH)} + 10^{(pH - pKa3)} + 10^{(pKa2 - pKa3)}) \quad \text{eq (3)}$$

$k_{max}$  is the maximum single turnover cleavage rate constant or steady state cleavage rate constant which is independent of pH.



**Scheme 3.1. The kinetic model scheme for equation 3.** Totally four ionizable groups involved in Mg(II) and catalysis includes two metal binding sites with equivalent  $pK_a1$ , a general base with  $pK_a2$  and a general acid with  $pK_a3$ . Two deprotonated metal binding ligands result in Mg(II) binding in the active site ( $H_4ES \rightarrow H_2ES$ ). The deprotonation of general base forms the pre-reactive complex  $HESMg(II)$ . After the turnover step, the post-reactive complex  $EPMg(II)^*$  is formed, which needs to be protonated by a general acid for product dissociation.

---

## RESULTS

Calculating  $pK_a$  values of titratable sites in *PvuII* endonuclease employs electrostatic interaction energies. Individual charged species like metal ions and DNA molecules contribute to the  $pK_a$  values of ionizable groups in *PvuII*. I assume that the inclusion of the metal ions and DNA molecules in the calculation procedure will make a significant difference on the predicted  $pK_a$  values of interesting ionizable groups. Therefore it is necessary to perform  $pK_a$  calculations on apo enzyme and binary E-M(II) and tertiary E-DNA-M(II) complexes, respectively. The various subsets of calculated  $pK_a$  values of interesting ionizable groups in *PvuII* are established based on WT or mutant apo enzyme and binary complex of E·Mg(II). Comparison of  $pK_a$  values of interesting ionizable groups in those subsets are important for understanding the perturbation of  $pK_a$  caused by metal ions and coupled electrostatic interaction between titratable sites. It is widely accepted that the deprotonation of metal ligated water molecules forms the attacking nucleophile to initiate the cleavage reaction. The rationale of  $pK_a$  perturbation is particularly helpful to understand the activation of water that is critical for the enzyme catalytic mechanism.

**Prediction of  $pK_a$  Values For Apo Enzyme.** Two acidic residues Asp58 and Glu68 in *PvuII* are regarded as metal binding ligands (Nastri, et al., 1997). X-ray crystal structures of Mg(II) or Ca(II) binding to *PvuII* indicates that the active site can coordinate with two Ca(II) ions in the presence of DNA and one Mg(II) ion in the absence of DNA by those two carboxylic groups. The two metal ions share the

---

similar metal binding ligands and geometry (Horton & Cheng, 2000; Spyridaki, et al., 2003). The metal binding studies on mutant D58A and E68A show that the roles of E68 and D58 in metal binding are probably not equivalent. E68 appears to dominate metal binding because Ala mutation on E68 causes a complete loss of metal binding ability of *PvuII*, but D58A retains the ability to bind Mg(II) (Dupureur & Conlan, 2000). Besides D58 and E68, a recent crystallographic study of *PvuII*-Mg(II) binary complex (1H56) unexpectedly revealed an active site Tyr94 as a metal ion ligand (Spyridaki, et al., 2003). Lysine residue is widely conserved in the active site motif of type II restriction endonucleases and probably assists the activation of metal ligated water molecules.

pK<sub>a</sub> calculations on the apo enzyme are performed on three X-ray crystal structures of *PvuII* which represent various conformers according to their crystallization conditions. 1NIO is apo form of *PvuII* mutant Y94F and in the pK<sub>a</sub> calculation it is mutated back to WT; 1H56 is binary complex of *PvuII* binding to Mg(II) with two different metal binding sites in each monomer; 1F00 is a ternary complex of *PvuII*-DNA-Ca(II) with two missing residues G53 and Q54 near to the active site (Horton & Cheng, 2000; Spyridaki, et al., 2003). The single Mg(II) ion coordinates with Asp58 and Glu68 in 1H56 subunit A which is consistent with Ca(II) binding sites in 1F00. Mg(II) ion coordinates with Tyr94 in 1H56 subunit B, but the mutant Y94F retains the metal binding capability and activity. This implies that Asp58 and E68 are still major metal binding ligands for *PvuII*. By removing metal ions in those structures (1H56 and 1F00), the pK<sub>a</sub> values of D58, E68, K70 and Y94

---

in apo enzyme are calculated and reported in **Table 3.1**.

The  $pK_a$  values of D58 and E68 are moderately shifted compared to their model  $pK_a$  values for all calculation sets in **Table 3.1**, regardless of the crystal structure used. The  $pK_a$  values of D58 and E68 vary among the structures, which indicates the quality of crystal structures and the conformations of proteins probably affect the  $pK_a$  calculation results. The similarity of  $pK_a$  values between 1NIO and 1H56 (expt 1 & 2 in **Table 3.1**) but their large differences compared with 1F00 (expt 1 & 2 compared with 3 & 4 in **Table 3.1**) is consistent with evidence that DNA binding induces the dramatic conformational change rather than metal ion binding (Dupureur, 2005). In spite of the differences caused by crystal structures for D58 and E68, one residue  $pK_a$  always shifts upward and the other shifts downwards compared to their model  $pK_a$  values. The  $pK_a$ 's of K70 and Y94 are much higher compared to their model  $pK_a$ 's, which are conserved for all three crystal structures.

The methodology of  $pK_a$  calculation is based on the Gibbs free energies difference between neutral state and ionized state. The Gibbs free energies calculated consists of desolvation energies and site-site electrostatic energies. The effect of site-site electrostatic energies on determination of  $pK_a$  values for a titratable site can be evaluated by electrostatic interaction potentials (personal communication with Dr. Briggs). Of course it is sensitive to the distance between two titratable sites. The high electrostatic interaction potentials imply a strong electrostatic interaction between D58 and E68 due to their proximity. The distance of titratable atoms

---

**Table 3.1. Summary of pK<sub>a</sub> predictions for apo enzyme.**

<b>Expt</b>	<b>Structure</b>	<b>D58</b>	<b>E68</b>	<b>K70</b>	<b>Y94</b>
1	1NIO(subunit A)	3.0	5.2	14.1	13.5
2	1H56(subunit A)	4.3	5.3	13.0	14.6
3	1F0O(subunit A)	5.2	2.2	13.0	12.4
4	1F0O(subunit B)	5.6	2.4	>15	11.8

For crystal structures 1F0O and 1H56, the crystallographic nucleic acids, water molecules and metal ions are deleted prior to the pK<sub>a</sub> calculations.

Model pK<sub>a</sub> of Asp, Glu, Tyr and Lys are 4.0, 4.4, 9.6 and 10.4, respectively.

---

between CG in D58 and CD in E68 is 4.25 Å in 1F0O structure, 4.68 Å in 1H56 structure and 4.22 Å in 1NIO structure, respectively. This strong electrostatic interaction between those two titratable sites (D58 and E68) probably is responsible for their pK<sub>a</sub> shift up and down in a coupled way. **Appendix II** lists the electrostatic potentials of some site-site interactions and can be used to rationalize the pK<sub>a</sub> shifts of those active site residues.

**Prediction of pK<sub>a</sub>'s for PvuII Variants.** The coupled pK<sub>a</sub> shifts of D58 and E68 upwards and downward is rationalized as the result of strong site-site interaction between them. Ala mutation or site neutralization is expected to disturb this kind of site-site interaction, resulting in large pK<sub>a</sub> shifts for those groups which exhibit strong site-site interactions in WT. The direction of pK<sub>a</sub> shifts can be predicted: Ala mutation on a nearby negatively charged residue will decrease the pK<sub>a</sub> of the target titratable residue, and Ala mutation on a positively charged residue will increase the pK<sub>a</sub> (Nielsen & Vriend, 2001).

Ala mutations are made at four positions (D58, E68, K70 and Y94) by Swisspdbviewer or charged residues are neutralized by altering the name of titratable atom as described in methods. The calculated pK<sub>a</sub>'s are summarized in **Table 3.2**.

For variant Y94F, the pK<sub>a</sub> shifts are not significant relative to WT. For the variant D58A (also the case D58 off), the pK<sub>a</sub> values of E68 and K70 both show a downward shift, which indicates D58 remains deprotonated. Therefore neutralization of D58 shifts the pK<sub>a</sub>'s of other residues in a predictable direction mentioned above. K70 has a high apparent pK<sub>a</sub> and can be interpreted as a titratable

---

**Table 3.2. Summary of pK<sub>a</sub> calculations for *PvuII* variants.**

<b>Structure</b>	<b>mutation</b>	<b>D58</b>	<b>E68</b>	<b>K70</b>	<b>Y94</b>
1NIO(subunit A)	WT	3.0	5.2	14.1	13.5
1NIO(subunit A)	Y94F	3.0	5.8	13.6	n/a
1NIO(subunit A)	D58A	n/a	3.6	13.1	13.2
1NIO(subunit A)	D58 off	n/a	3.4	13.0	13.1
1NIO(subunit A)	E68A	2.7	n/a	12.6	12.5
1NIO(subunit A)	E68 off	2.8	n/a	13.0	13.1
1NIO(subunit A)	K70A	4.0	6.2	n/a	13.6

pK<sub>a</sub> calculations were performed based on 1NIO structure which is switched back to WT by F94Y mutation. Model pK<sub>a</sub> of Asp, Glu, Tyr and Lys are 4.0, 4.4, 9.6 and 10.4, respectively. The mutation on one residue or neutralization on the same residue should have a very similar effect on calculated pK<sub>a</sub>'s. n/a means not available in the pH titration range from 0 to 15.

---

site with positive charge. So the neutralization on K70 increases the  $pK_a$  values of other residues in the active site.

**pH Titration With Metal Binding Sites.** pH titration of Mg(II) binding to WT and D58A were performed using  $^{25}\text{Mg(II)}$  NMR (Dupureur & Conlan, 2000). The apparent  $pK_a$ 's for WT (6.7) and D58A (7.1) obtained from data fit seems abnormally high compared with calculated  $pK_a$ 's of D58 and E68 in WT. However, considering the possible negative cooperativity for proton binding between D58 and E68, a two-site interacting model is used to fit the experimental pH titration of WT with calculated  $pK_a$  for D58 (3.0) and E68 (5.2) (expt 1 in **Table 3.1**). The two-site interacting model fits well with experimental data and generates the 5 kcal/mol interaction energies between two sites (**Figure 3.3**). Unfortunately, the  $pK_a$  calculation with D58A does not agree with pH titration of D58A by  $^{25}\text{Mg(II)}$  NMR spectroscopy (Dupureur & Conlan, 2000). The predicted  $pK_a$  of E68 decreases in D58A but the pH titration of D58A shifts to basic direction determined by  $^{25}\text{Mg(II)}$  NMR. The reasons for this discrepancy between  $pK_a$  calculation and experiments can be complex. The mutation may induce the conformational change in the active site which somehow compensates for the electrostatic effect.

## PvuII Mg(II) binding ionization behavior fitting to a two-site interacting model

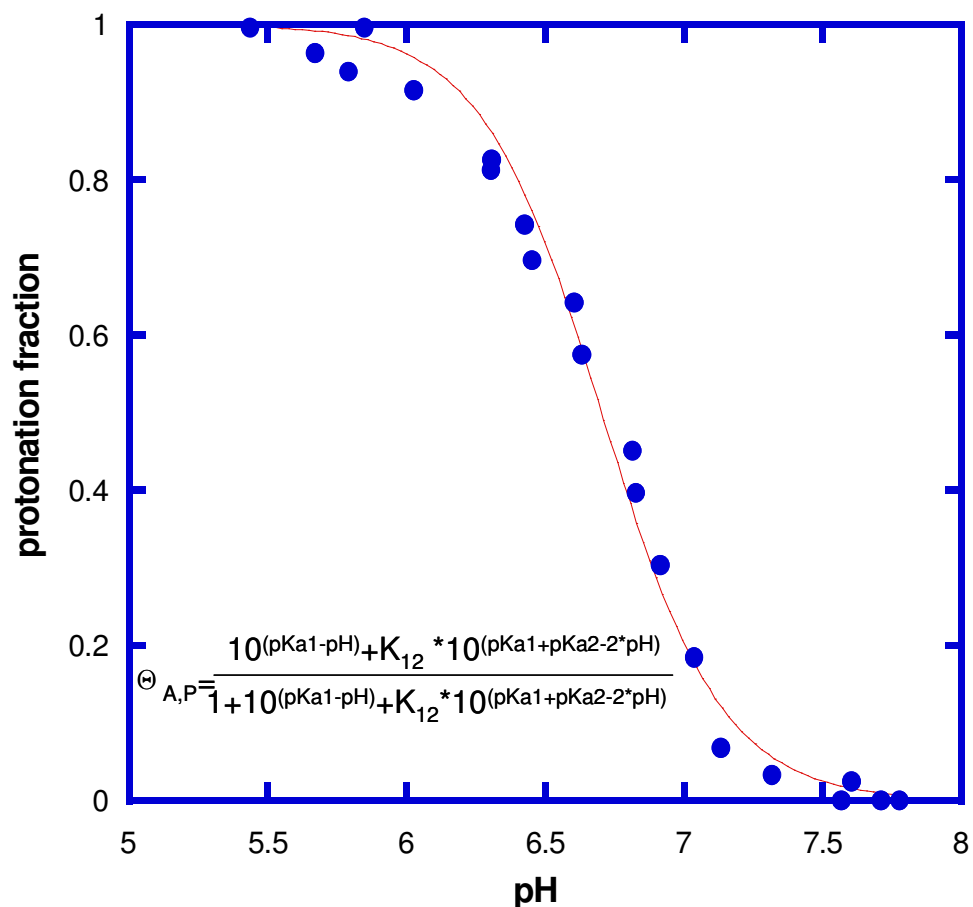


**Figure 3.3.** A two site interacting model fits well with experimental pH titration of WT using  $^{25}\text{Mg(II)}$  NMR. The D58 and E68 are considered as two Mg(II) binding sites. Their  $pK_a$ 's are fixed in the model as 3.0 ( $pK_{a1}$ ) and 5.2 ( $pK_{a2}$ ) obtained from  $pK_a$  calculation with apo enzyme (expt 1 in **Table 3.1**). The inset equation is adapted from reference (Dupureur & Conlan, 2000).

---

**pK<sub>a</sub> Calculation In the Presence of Mg(II).** Mg(II) ion is treated as background charge in the pK<sub>a</sub> calculation, which has a significant effect on the predicted pK<sub>a</sub>'s of active site residues. It is determined that *PvuII* contains two metal binding sites on each subunit (see Introduction). Their binding configurations observed in the *PvuII* crystal structures are illustrated in **Figure 3.4**. The influence of occupancy status of two metal binding sites is particularly of interest and investigated in the different calculation experiments.

The results are summarized in **Table 3.3**. In the pK<sub>a</sub> calculation expt 2, both metal binding sites are filled and the pH titration range is from 0 to 15. The apparent pK<sub>a</sub>'s of metal binding ligands (D58 and E68) are not detectable (their theoretical pK<sub>a</sub>'s must be negative). When Mg(II) ions occupy their metal binding sites, the strong electrostatic interaction between metal ions and side chain of carboxylic group causes the abnormal downward shift for pK<sub>a</sub> values of D58 and E68. Theoretically it is very unfavorable to protonate a metal binding ligand such as D58 and E68 when they coordinate with a metal ion. The pK<sub>a</sub> of K70 has a dramatic drop but it is still high enough to remain protonated at physiological pH.

The effect of occupancy of metal binding sites is also evaluated by performing pK<sub>a</sub> calculations on the crystal structures of *PvuII* when either metal binding site is filled. The pK<sub>a</sub> calculation (expt 3 in **Table 3.3**) is performed based on *PvuII* crystal structure 1H56 subunit A (**Figure 3.4B**), in which one Mg(II) coordinates with

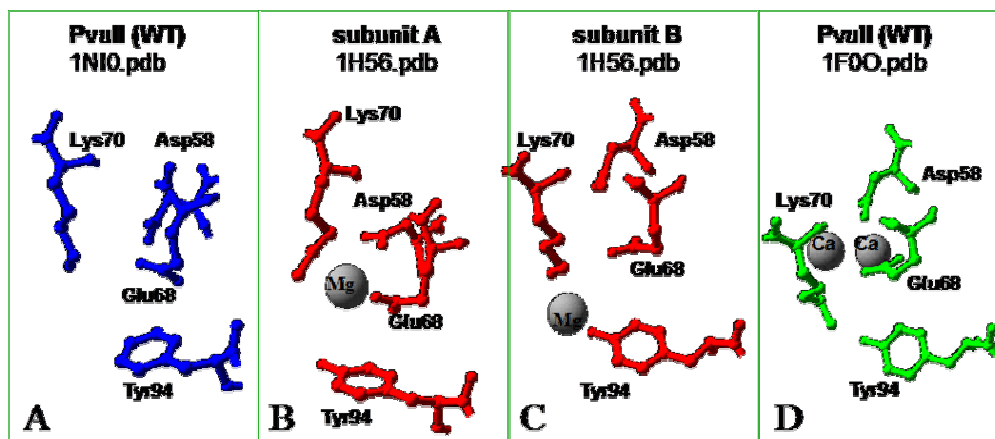


**Figure 3.4.** The metal ion occupancies in the *PvuII* active sites. (A) apo enzyme of *PvuII*(1NI0); (B) one Mg(II) bound in *PvuII* subunit A (1H56) (Spyridaki, et al., 2003); (C) one Mg(II) coordinates with Tyr94 in subunit B (1H56); (D) two Ca(II) ions in *PvuII* (1F00) (Horton & Cheng, 2000).

---

**Table 3.3. Summary of pK<sub>a</sub> calculations in the presence of Mg(II)**

<b>Expt</b>	<b>Structure</b>	<b>Metal Ions</b>	<b>D58</b>	<b>E68</b>	<b>K70</b>	<b>Y94</b>
1	1NIO(subunit A)	No	3.0	5.2	14.1	13.5
2	1F0O(subunit A)	2Ca(II)	n/a	n/a	10.3	8.7
3	1H56(subunit A)	Mg(II)	1.4	-1.9	9.9	10.8
4	1H56(subunit B)	Mg(II)	2.8	0.5	11.6	4.9

n/a means not available when the calculated pK<sub>a</sub> is out of pH titration range. pH titration range is from 0 to 15 for expt 1, 2 and 4. Expt 3 applies pH titration range from -5 to 15 due to an old version of executable file. The pK<sub>a</sub> calculation set 2, 3 and 4 are performed excluding all the solvent molecules in the crystal structures, and Ca(II) was replaced by Mg(II) without changing their positions in expt 2.

---

D58 and E68. The  $pK_a$  calculation (expt 4 in **Table 3.3**) is conducted on the *PvuII* crystal structure 1H56 subunit B (**Figure 3.4C**), where one Mg(II) ion coordinates with Y94. The electrostatic interaction energy between Mg(II) and binding site results in Mg(II)-ligand distance dependence on  $pK_a$  shift of metal binding ligands. In expt 3, D58 and E68 are the metal binding ligands and a dramatic downward  $pK_a$  shift is observed. In expt 4, Y94 is the metal binding site and the similar large downward  $pK_a$  shift for this residue. Among those three calculations (expt 2, 3 and 4) in the presence of metal ions, the  $pK_a$  of K70 is relatively stable and changes within a range from 9.9 to 11.5. The  $pK_a$  values of metal binding ligands D58, E68 and Y94 change dramatically upon changing metal ion positions in the crystal structures.

**$pK_a$  Calculations of Metal Ligated Water Molecules.** The metal ligated water molecule has a very important role in catalysis, and its ionization is of great interest in understanding the catalytic mechanism. The metal ligated water molecules (**Figure 3.5**) are well defined in crystal structures of *PvuII* (1H56 and 1F00) and are added as the additional titratable site in the  $pK_a$  calculations. The OW atom in the water molecule carries one unit negative charge when it is deprotonated, and its model  $pK_a$  in solution is regarded as 11.4 when it is ligated to the Mg(II) ion (model  $pK_a$  varies with ligated divalent metal ions) (Dahm, et al., 1993). The predicted  $pK_a$ 's of metal ligated water in various *PvuII* crystal structures are summarized in **Table 3.4**.

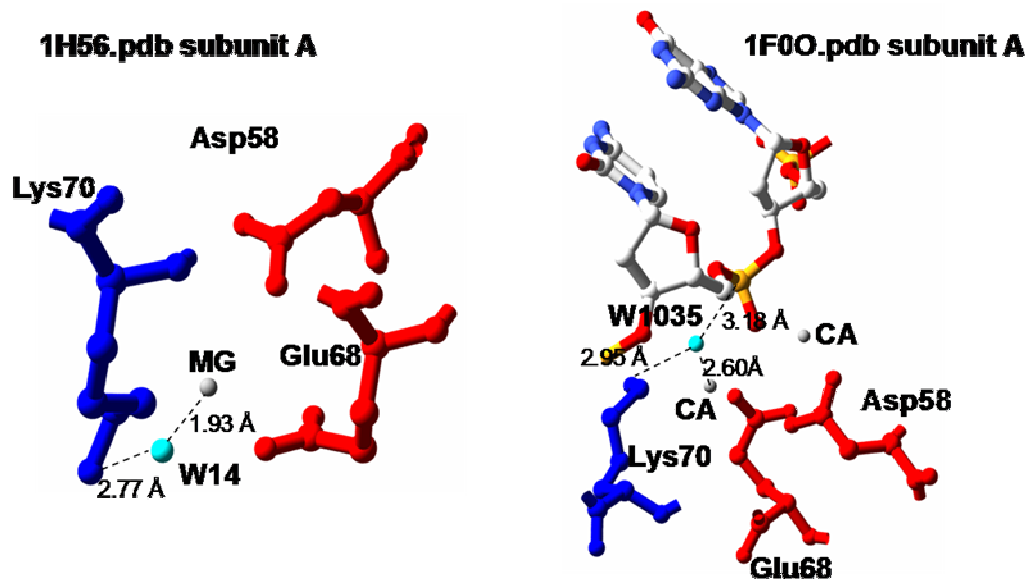


**Figure 3.5.** The defined metal ligated water molecules in *PvuII*. Left panel shows the Mg(II) ligated W14 in subunit A of 1H56 (Spyridaki, et al., 2003). Right panel shows a Ca(II) ligated water molecule in subunit A of 1F00. A similar W898 exists in subunit B of 1F00. W1035 in 1F00 subunit A actually is artificially added using SwissPdbviewer on the basis of geometry of W898 in subunit B (Horton & Cheng, 2000). Both highlighted water molecule are speculated to form the attacking nucleophile. The distances of those water molecules to metal ions and Lys70 are indicated.

**Table 3.4. Summary of pK<sub>a</sub> calculations of Mg(II) ligated water molecules.**

Structure	No. of Mg(II)	Model pK <sub>a</sub>	pK <sub>a</sub> of water	K70	Distance of Mg-O (Å)
1H56(subunit A)	0	11.4	>15	12.5	-
1F0O(subunit A) <sup>a</sup>	2	11.4	7.4	>15	2.6 Å
1F0O(subunit B) <sup>b</sup>	2	11.4	9.3	12.7	2.79 Å
1F0O(subunit B) Modified <sup>c</sup>	2	11.4	6.4	10.7	2.04 Å
1H56(subunit A) <sup>d</sup>	1	11.4	6.5	14.4	1.9 Å

a. pK<sub>a</sub> calculation is performed on subunit A with W1035 (**Figure 3.5**, right panel).

b. pK<sub>a</sub> calculation is performed on subunit B with W898.

c. The position of both metal ions are fixed and the W898 in 1F0O(subunit B) is shifted closer to metal ion CA761. The distance from OW in H<sub>2</sub>O to NE in K70 is 3.393 Å. The distance from OW in H<sub>2</sub>O to atom P of G8-p-C9 is 3.396 Å; in modified 1F0O(subunit B), the corresponding distance is 3.457 and 3.468 Å, respectively. So the water pK<sub>a</sub> shift between calculation b and c mainly comes from the extent of approaching Mg(II) ion.

d. pK<sub>a</sub> calculation is performed on subunit A with W14 as shown in **Figure 3.5** left panel.

All those pK<sub>a</sub> calculations are performed keeping the metal ions and specified water molecules, and all other water molecules are deleted. In 1F0O structure, Ca(II) is replaced by Mg(II) in the calculations.

---

The  $pK_a$  of metal bound waters in the 1F0O structure of *PvuII* are particularly interesting because 1F0O structure best reflects the pre-reactive *PvuII* conformation with Ca(II) ions and cognate DNA. One of the metal bound waters in subunit B of 1F0O structure is considered as the candidate carrying out the nucleophilic attack. In subunit A, a Ca(II) ligated water molecule (W1035) was built up artificially using SwissPdbviewer based on the geometry of metal ligated water (W898) complex in subunit B: the water molecule coordinates with Ca(II) ion, is within the hydrogen bound distance to Lys70 and is well positioned to attack the phosphorous atom on the DNA backbone. The distance between OW in water and metal ion are assigned to 2.60 Å, a default value for Ca(II) in Swisspdbviewer. The water molecule is incorporated at a position to avoid any clash with protein backbone or side chain. In **Table 3.4**, the distances between metal ion and OW atom in water molecule actually reflects the Ca(II)-ligand distance not Mg(II)-ligand distance, since the typical Mg(II)-H<sub>2</sub>O distance is around 2.0 Å. So W898 in subunit B (1F0O) is moved closer to the Ca(II) ion in order to reduce the metal-ligand distance (**Table 3.4** note c). When setting model  $pK_a$  of metal bound water as 11.4, the  $pK_a$  of metal ligated water is 7.4 in subunit A (W1035) and 9.3 in subunit B (W898). Considering the symmetry between subunit A and B, the difference of calculated  $pK_a$  may be partially due to the sensitivity of  $pK_a$  upon the distance between metal ion and water molecule because the distance of Mg(II)-OW in subunit A is 2.6 Å while that is 2.79 Å in subunit B (**Table 3.4**). In *PvuII* structure 1H56, the calculated  $pK_a$  of Mg(II) bound water is even lower (6.5) because the distance of Mg(II)-OW is closer than the

---

of Ca(II)-OW. To evaluate how well the Mg(II)-OW affects the predicted water pK<sub>a</sub>, in 1F00 structure subunit B the target water molecule was shifted close to metal ion (2.04 Å). So the modified 1F00 structure subunit B contains a very similar distance of Mg(II)-OW as observed in *PvuII* structure 1H56). It is not surprising that the pK<sub>a</sub> obtained in the modified 1F00 subunit B is similar to that obtained with 1H56 (6.4 vs. 6.5 in **Table 3.4**). Although the calculated pK<sub>a</sub> of metal ligated water varied due to the sensitivity of distance Mg(II)-OW, all those calculated pK<sub>a</sub> values support the deprotonation of metal ligated water and formation of hydroxide ion can be achieved at physiological pH according to the predicted pK<sub>a</sub>'s. As a control, when the pK<sub>a</sub> calculation with W14 in 1H56 structure is performed in the absence of Mg(II) ion; a very high pK<sub>a</sub> for W14 is generated (pK<sub>a</sub>>15 in **Table 3.4**). This strongly supports the involvement of metal ions in decreasing the pK<sub>a</sub> of ligated water in order to assist its deprotonation and form the attacking nucleophile.

**The pK<sub>a</sub> of Metal Ligated Water and Its Dependence on K70.** In the presence of metal ions, the pK<sub>a</sub> of K70 is still high enough to be protonated at physiological pH and carries a positive charge. Besides, the *PvuII* crystal structure (1F00) shows that Ca(II) ligated water molecule is within hydrogen bonding distance of K70. This suggests that K70 may also participate in the modulation of metal ligated water pK<sub>a</sub>. For each structure, the pK<sub>a</sub> of water is calculated in the presence of K70, and then the similar calculation is performed with K70 mutated to Ala or turned “off”. As summarized in **Table 3.5**, K70 does indeed influence the pK<sub>a</sub> of metal bound water. It is found that most of calculations show an upward pK<sub>a</sub>

**Table 3.5. Summary of water pK<sub>a</sub> calculations with WT and K70A variants.**

expt	Structure	Enzyme	No. of M(II)	$\Delta pK_a^a$	Water	Mg-OW
<b>Negative control in the absence of M(II)</b>						
1	1H56(subunit A)	WT	0	n/a	>15	n/a
<b>Comparison of water pK<sub>a</sub> between WT and K70A(K70 off)</b>						
2	1F00(subunit A)	WT	2		7.4	2.6
3	1F00(subunit A)	K70A	2	2.5	9.9	2.6
	1F00(subunit A)	K70 off	2	3.1	10.5	2.6
4	1F00(subunit B)	WT	2		9.3	2.79
5	1F00(subunit B)	K70A	2	1.2	10.5	2.79
	1F00(subunit B)	K70 off	2	1.2	10.5	2.79
6	1F00(subunit B)	WT	2		6.4	2.04
7	1F00(subunit B)	K70A	2	1.4	7.8	2.04
	1F00(subunit B)	K70 off	2	1.4	7.8	2.04
8	1H56(subunit A)	WT	1		6.5	1.9
9	1H56(subunit A)	K70A	1	3.3	9.8	1.9
	1H56(subunit A)	K70 off	1	3.3	9.8	1.9
<b>water pK<sub>a</sub> calculation with Arg substitution ----analog of Lys</b>						
10	1F00(subunit B)	K70R <sup>b</sup>	2		8.7	2.04
11	1F00(subunit B)	R70 off <sup>c</sup>	2	2.0	10.7	2.04

- a.  $\Delta pK_a$  is defined as  $pK_a$  of water in variant (Ala mutation or Lys off)- $pK_a$  of water in WT.
- b. Mutation was performed by Swisspdbviewer, the conformation of R70 after replacement was refined by energy minimization.
- c. To evaluate the contribution of R<sup>+</sup> (protonated state) to the water pK<sub>a</sub>, R70 was shut off by changing the name of titratable atom CZ in Arg70, thus during the pK<sub>a</sub> calculation, Arg70 remains neutral state and no charge will be added on CZ atom in any Arg70.

Model pK<sub>a</sub> of water molecules is assigned to 11.4 uniquely.

---

shift moderately beyond one pH unit after the neutralization of K70 (In **Table 3.5** expt 2 & 3, 4 & 5, 6 & 7 and 8 & 9).

The water  $pK_a$  of *PvuII* variant K70A shifts upward compared to WT and this  $pK_a$  shift is caused by the neutralization of positive charge of K70. Since the model  $pK_a$  of Arg (12.0) is higher than Lys and also can be protonated like Lys, it is expected that in *PvuII* mutant K70R should also have a similar  $pK_a$  shift compared with WT when R70 is turned “off”. The expt 10 & 11 in **Table 3.5** confirmed the predicted upward  $pK_a$  shift and a high water  $pK_a$  shift of 2.1 is obtained.

#### **The $pK_a$ Calculations on Other Nucleases Featured With Conserved Lys.**

To explore the possibility that such a contribution to lower water  $pK_a$  by conserved Lys generally exists in the PD...D/ExK endonuclease family, the same strategy was applied to the related enzymes *HincII*, *EcoRI*, *EcoRV*, NgoMIV, Tn7 transposase and T7 endonuclease I. In each structure, the metal ligated water is well positioned to attack the phosphodiester bond, and the side chain of conserved Lys is within hydrogen bonding distance with the attacking water molecule. **Table 3.6** lists the chosen crystal structures and the calculated water  $pK_a$  shift for lacking the positive charge on Lys in the catalytic center (**Appendix III** is the supplementary table showing all calculated  $pK_a$ 's). In each calculation set, the conserved Lys was shut off. Most of metal ligated waters have a  $pK_a$  shift beyond one pH unit (**Table 3.6**).

For *PvuII*, only crystal structures with Mg(II) and Ca(II) are available. In the

**Table 3.6. Summary of pK<sub>a</sub> calculations with other nucleases with conserved Lys.** pK<sub>a</sub> shifts caused by conserved Lys in restriction enzymes which share PD...D/ExK motif ( $\Delta pK_a = pK_a$  of water in variant (K off) - pK<sub>a</sub> of water in WT). This table only summarizes the pK<sub>a</sub> shift, and the calculated pK<sub>a</sub> values are listed in **Appendix III**.

Enzyme	pdb code	$\Delta pK_a$	Model pK <sub>a</sub>	Metal ion	Mutation position
<i>HincII</i>	1XHV.pdb	1.44	14	Two Mn <sup>2+</sup>	K129
		1.04	11.4	Two Mn <sup>2+</sup>	
		1.08	10.6	Two Mn <sup>2+</sup>	
<i>EcoRI</i>	1QPS.pdb	0.83	11.4	One Mn <sup>2+</sup>	K113
<i>EcoRV</i>	1EO4.pdb	1.15	10.6	Two Mn <sup>2+</sup>	K92
	1EON.pdb	2.11	11.4	Two Mg <sup>2+</sup>	
	1RVB.pdb	1.21	11.4	Two Mg <sup>2+</sup>	
	1SX5.pdb	2.08	14	Two Mn <sup>2+</sup>	
	1SX8.pdb	1.68	10.6	Two Mn <sup>2+</sup>	
<i>TnsA</i>	1F1Z.pdb	1.59	11.4	Two Mg <sup>2+</sup>	K132
T7 endonuclease I	1M0D.pdb	1.55	10.6	Two Mn <sup>2+</sup>	K67
<i>NgoMIV</i>	1FIU.pdb	1.57	11.4	Two Mg <sup>2+</sup>	K187

---

type II restriction endonucleases family, Mn(II) also supports the enzymatic activity (Bowen & Dupureur, 2003) and inner water of their metal complexes have a  $pK_a$  of 10.6 (Dahm, et al., 1993). In the  $pK_a$  calculation with crystal structures including Mg(II) and Mn(II), the model  $pK_a$  was assigned to various values to evaluate if the upward  $pK_a$  shifts caused by neutralization of conserved Lys is sensitive to the change of model  $pK_a$ . For the same crystal structure of *HincII*, although the different model  $pK_a$ 's of 10.6, 11.4 and 14 are applied, the  $pK_a$  shift caused by neutralizing conserved Lys did not change very much (**Table 3.6** *HincII*).

#### **The $pK_a$ Calculation of Metal Ligated Water In the Presence of Nucleotides.**

Since the  $pK_a$  of metal bound water is dominated by electrostatic interactions between water molecule and metal ions, the binding of highly charged DNA strand in the active site is expected to cause an upward  $pK_a$  shift of the metal bound water molecule. *PvuII* crystal structure (1F00) provides a description of *PvuII* binding to both metal ions and its cognate DNA strand. In the  $pK_a$  calculation, the DNA strand was modeled as non-titratable ligand with high charge density. The DNA contribution to the deprotonation of metal bound water molecule is tested by assigning its model  $pK_a$  as 11.4. **Table 3.7A** shows that the introduction of DNA strand not only compensates the  $pK_a$  shift caused by positively charged species such as metal ions and K70, but also elevates the  $pK_a$  of metal bound water molecule to the original value in bulk solvent. The same metal bound water  $pK_a$  was raised from 7.4 without the presence of DNA up to 14.1 in the presence of whole 14mer DNA strand (expt 4 **Table 3.7A**). These predicted results are not surprising because each phosphate has an overall -1.2 charge and a 14mer DNA strand

---

definitely can oppose the electrostatic contribution by metal ion with +2 charges and K70 with +1 charge. The elongation of DNA strand will bring more negative charges and cause a higher  $pK_a$  shift of metal bound water molecules. In **Table 3.7A** (expt 2), a water  $pK_a$  of 14.1 was obtained in the calculation including a 14mer DNA strand compared with 10.9 in the presence of two nucleotides.

The high density of negative charges on the DNA backbone is the main obstacle for us to get reasonable water  $pK_a$ 's when including DNA. Actually the DNA is bound to cationic ions in solution, so its high negative charge density on the phosphate backbone is speculated to be neutralized (Record, et al., 1976). To better simulate the electrostatic environment of DNA bound to salt ions, several ways to neutralize the negative charges of phosphate were explored. Assuming cations in salt buffer may directly bind to the phosphate backbone of DNA, the partial negative charge of the phosphorus or non-bridging oxygen in the DNA parameter sets are reduced by one or half unit charge and the reduced partial charge parameters for DNA backbone were applied in  $pK_a$  calculations (**Table 3.7B**). The calculation expt 1 is the original parameter set for DNA molecules (described in Experiments and Methods) we used in  $pK_a$  calculations shown in **Table 3.7A**. In expt 2, the partial charge on phosphorous atom is reduced by half unit. In expt 3, a relatively low water  $pK_a$  of 10.9 is obtained when a cation is directly bound to the phosphate and the overall charge on the phosphate are reduced by one unit positive charge (0.5 on each non bridging O atom). Other parameter sets such as Charmm27 and Amber force field are also applied to the  $pK_a$  calculations and the results are shown in

**Table 3.7. The pK<sub>a</sub> Calculation of Metal Ligated Water In the Presence of Nucleotides and Neutralization of DNA backbone.**

**A: The water pK<sub>a</sub> calculation in the presence of DNA strands.**

Expt	K70	W1035	Remark
1	12.60	7.4	No DNA
2	>15	10.9	CpG
3	>15	12.8	All bases removed
4	>15	14.1	DNA stand D 14mer fully reserved

All the calculations were conducted with crystal structure (1F00.pdb) subunit A. In expt 3, all bases on the DNA strand D have been removed.

**B: The application of neutralization of DNA strand in the pK<sub>a</sub> calculations**

Expt	pK <sub>a</sub> , Intrinsic	pK <sub>a</sub> , Apparent	Parameter set	Partial charge on atom P and O1P
1	13.7	>15	Charmm22 <sup>a</sup>	P = +1.5 and O1P=-0.8
2	10.9	14.6	Charmm22	P = +2 and O1P=-0.8
3	8.5	10.9	Charmm22	P = +2 and O1P=-0.3
4	13.6	>15	Charmm27 <sup>b</sup>	P = +1.5 and O1P=-0.8
5	15.0	>15	Amber force filed <sup>c</sup>	P=1.166 and O1P=-0.776

Water pKa calculations are conducted with crystal structure (pdb code:1F00) subunit B including the whole DNA strand C. Subunit A was deleted in the pKa calculation and all the reported pKa values are for W898 subunit B.

a. (MacKerell, et al., 1995)

b. (Follope & Alexander D. Mackerell, 1999)

c. (Cieplak, et al., 1994).

---

**Table 3.7B** expt 4 and 5. The water  $pK_a$  obtained by those parameter sets are not lowered.

**Substrate Assisted Catalysis.** The  $pK_a$  calculation is also used to examine the influence of phosphorothioate on the  $pK_a$  of attacking water molecule. The introduction of phosphorothioate is to test if 3' phosphate functions as a general base to activate the attacking water molecule in the proposal of substrate assisted catalysis (see **Figure 3.1C**) (Horton, et al., 1998). According to this mechanism, the  $R_P$  phosphorothioate carrying a negatively charged sulfur also can abstract the proton, whereas the  $S_P$ -phosphorothioate results in an uncharged double-bonded oxygen in the  $R_P$  position (Thorogood, et al., 1996). This uncharged oxygen cannot function as a base, resulting in  $S_P$  substitution catalytically inactive. It has been shown that substitution of the pro- $S_P$  oxygen of this phosphate with sulfur reduces  $V_{max}/K_M$  by at least 200-fold, whereas substitution of the pro- $R_P$  oxygen has little effect (Thorogood, et al., 1996). The effect of phosphorothioate on the attacking water  $pK_a$  would be abnormal, resulting in the reduced enzyme activity. Such simulations can be carried out once the charge parameterization of phosphorothioate is available (Bertrand, et al., 1999). The crystal structure of *EcoRV* (1BSS) has been selected to calculate the attacking water  $pK_a$  in the presence of phosphorothioate because that is the crystal structure used to support the substrate assisted catalysis (Horton, et al., 1998). Water 439 is ligated with one Ca(II) ion and is 4.2 Å to scissile phosphorus, and within 4 Å distance to O1P and O2P of 3' phosphate, which is considered as the ideal attacking water molecule. Upon substitution of S on either O1P or O2P of 3' phosphate, no dramatic changes on the  $pK_a$  of attacking water molecules was observed regardless of

---

whether the DNA backbone is neutralized by counter ions or not. All the calculated results are summarized in **Table 3.8**. From an insight of electrostatic interactions, the charge distributions do not make any difference between phosphate and phosphorothioate. So the electrostatic contributions to water  $pK_a$  caused by S substitution are very limited. In the presence of two nucleotides, the attacking water  $pK_a$  is determined to be within a range 9.3~10.5, depending on the neutralization of counter ions on the phosphate.

#### **Salt Concentration And Protein Dielectric Constant Dependence On $pK_a$**

**Calculation of Metal Ligated Water.** The ionic strength was usually assigned to 150 mM to simulate the real salt environment of experiments. The Debye-Huckel screening effect is incorporated into linear Poisson-Boltzmann equation and increasing salt concentration screens the charge-charge interaction, which may affect the predicted  $pK_a$ . Salt dependences of the  $pK_a$  values with amino acid residues and Mg(II) bound water molecules were examined. The increasing salt concentration slightly decreases the calculated  $pK_a$  of titratable sites (**Table 3.9A**).

The dielectric constant in proteins for the  $pK_a$  calculation package implemented in UHBD was calibrated to be 20 although 4 or less may better reflects the real dielectric value for proteins (Antosiewicz & McCammon, 1996). In **Table 3.9B**, the dielectric constant was assigned values from 4 to 30. The  $pK_a$ 's of amino acid residues are increasing along with dielectric constant increasing. The  $pK_a$  of metal bound water is not that sensitive to the change of dielectric constant, which achieves the minimum value at dielectric constant of 15 or 20.

**Table 3.8. The pK<sub>a</sub> calculation of attacking water molecules in *EcoRV* upon S substitution on non-bridging O of 3' phosphate.**

W439 pK <sub>a,apparent</sub>	Operations on DNA	Charge distributions on 3' phosphate <sup>a</sup>				
		P	O3	O5	O1P	O2P
No counter ion neutralization						
10.5	Phosphate	0.4561	-0.281	-0.278	-0.58	-0.58
10.3	S substitution on O1P	0.4419	-0.3227	-0.318	-0.561	-0.471
10.3	S substitution on O2P	0.4419	-0.3227	-0.318	-0.471	-0.561
Counter ion neutralization						
9.4	Phosphate	0.4561	-0.281	-0.278	-0.23	-0.23
9.3	S substitution on O1P	0.4419	-0.3227	-0.318	-0.307	-0.157
9.3	S substitution on O2P	0.4419	-0.3227	-0.318	-0.157	-0.307

The pK<sub>a</sub> calculation with W439 has been conducted with *EcoRV* mutant crystal structure (1BSS.pdb) subunit A (Horton, et al., 1998). During the calculation, two Ca(II) ions are replaced by two Mg(II) ions, and two nucleotides A907 and T908 are conserved with scissile phosphate and 3' phosphate. The charge parameters of phosphate and phosphorothioate are assigned according to reference (Bertrand, et al., 1999). The model pK<sub>a</sub> of water is 11.4.

**Table 3.9. The pK<sub>a</sub> of metal Ligated water dependence on salt concentration and protein dielectric constant.** All the pK<sub>a</sub> calculations were conducted based on 1F0O subunit A structure in the presence of two Mg(II) ions and water molecule W1035. Model pK<sub>a</sub> of Asp, Glu, Lys and metal ligated water are 4.0, 4.4, 10.4 and 11.4, respectively. pH titration range is from -5 to 15 in calculation.

**A: Salt dependence**

<b>Ionic strength (mM)</b>	<b>D58</b>	<b>E68</b>	<b>K70</b>	<b>Y94</b>	<b>W1035<sup>a</sup></b>
150	1.1	<0	>15	13.5	12.8
250	1.3	-2.1	>15	13.2	12.5

**B: Dielectric constant dependence**

<b>Dielectric constant</b>	<b>D58</b>	<b>E68</b>	<b>K70</b>	<b>Y94</b>	<b>W1035<sup>a</sup></b>
4	-3.3	<-5	-1.3	>15	14.6
10	-0.1	<-5	7.7	>15	13.6
15	0.7	-3.6	12.3	15.0	12.7
20	1.2	-2.3	>15	13.5	12.7
25	1.4	-1.4	>15	12.2	13.1
30	1.6	-0.7	>15	10.9	13.4

a. The same water molecule in 1F0O structure subunit A as in **Table 3.4**.

---

**pH Dependence of Single Turnover Cleavage Activity.** The pH dependence of *PvuII* single turnover cleavage rates shows a typical bell shaped curve (**Figure 3.6**), which have been also observed for pH rate profiles of *EcoRV* endonuclease (Sam & Perona, 1999a). It is generally interpreted that bell-shaped pH-rate profiles represents two ionizations involved in the catalytic activity, one deprotonation in the acidic pH range representing general base catalysis and one protonation in the basic pH range representing general acid catalysis. The enzymatic activity of *PvuII* reaches a maximum at pH 8.0. The plot of pH-rate on a logarithmic scale above pH 8.0 gives a classic linear phase with a slope of 0.78 (**Figure 3.6B**). Below pH 8.0 it is biphasic with two different slopes 1.3 and 2.8, and dramatic deviation from a linear dependence is observed in the very low pH region (5.5~6.5) (**Figure 3.6A**). This shows that at low pH multiple titratable groups might be involved. In addition to the deprotonation of a metal ligated water molecule to form the attacking nucleophile, the deprotonation of active groups to bind Mg(II) might be candidates for that. Sasnauskas proposed a competition between proton binding and Mg(II) binding at the active site from the investigation ns of the pH dependence of DNA binding and steady state plasmid cleavage by *MunI* endonuclease (Sasnauskas, et al., 1999). Since the binding of metal ions in the active site are critical for enzymatic activity, multiple ionizations are reflected in the pH-rate profiles at the low pH range, while the binding of metal ions gets saturated along with pH and single ionization is observed at high pH values. Based on two Mg(II) binding sites in *PvuII*, **Scheme 3.1** describes the kinetic model

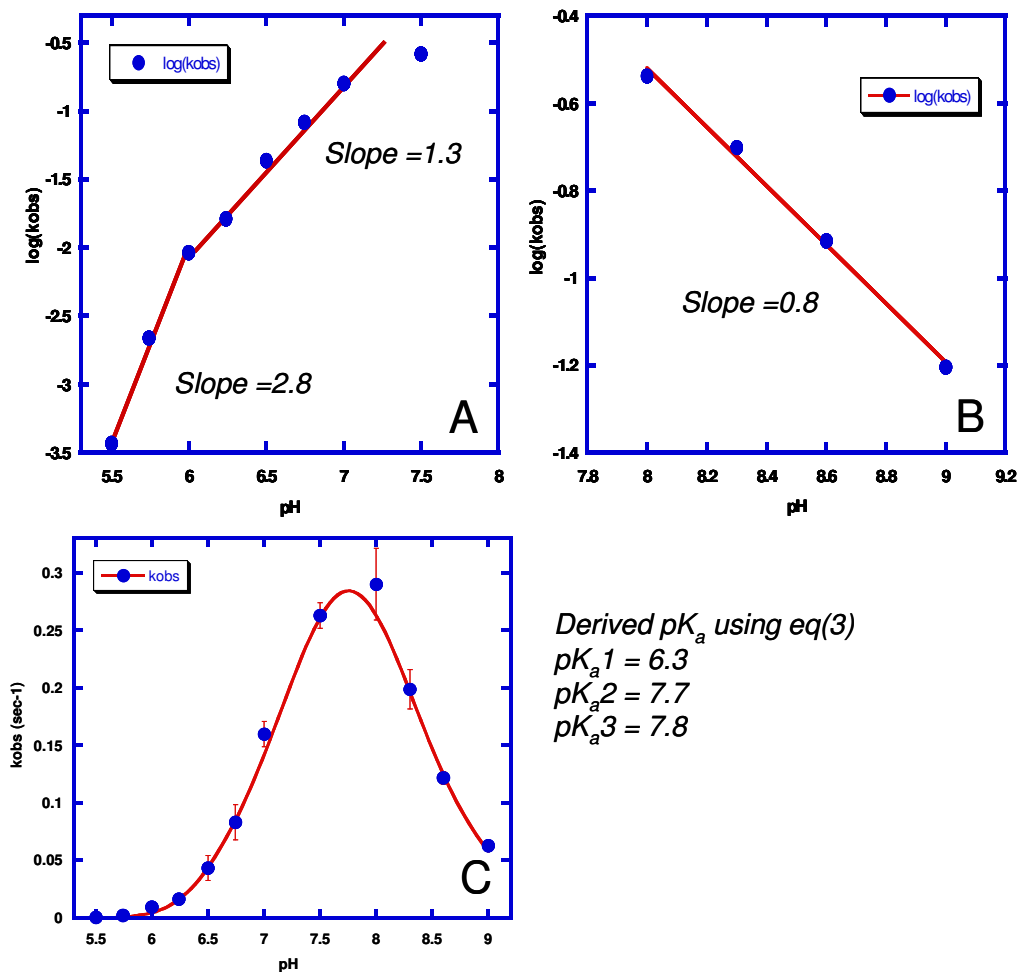


**Figure 3.6. pH dependence of single turnover rate constant.** pH- $\log(k_{\text{obs}})$  has been dissected into acid limb and basic limb. (A) Acid limb shows two phases with different slopes. (B) Basic limb shows a typical linear phase with slope of 0.8 representing general acid catalysis by one ionizable group. (C) Fit pH- $k_{\text{obs}}$  profile data with **equation 3** (described in Experiments and Methods), three apparent  $pK_a$ 's for metal binding site, general base and general acid are obtained.

---

for multiple ionizations involved in catalysis and **equation (3)** is derived (**Appendix IV** for details). pH rate profile data is fit with **equation (3)**, and the obtained  $pK_a1$  (6.3) for metal binding site is close to determined apparent  $pK_a$  in pH titration of Mg(II) binding experiments (Dupureur & Conlan, 2000).  $pK_a2$  (7.7) and  $pK_a3$  (7.8) are believed to reflect the metal ligated water  $pK_a$ 's, which can be correlated with calculated water  $pK_a$ 's in **Table 3.4**.

**pH Dependence of Steady State Cleavage Activity.** pH profiles of steady state kinetics has been determined with a fixed 10 mM Mg(II) concentration. In **Figure 3.7**, The plot of  $pH-k_{cat}$  shows a very similar bell shape as *EcoRV* and pH-rate plot of *PvuII* ((Sam & Perona, 1999a) and **Figure 3.6**). The maximum steady state activity appears at the pH range around 8.0, and the slope for the acid limb (6.0~8.0) in the log plot is 0.56 instead of two phases shown as in single turnover pH-rate profile (**Figure 3.6**). It could be interpreted that one ionizable group is involved in acid limb and basic limb, respectively. Due to the bell shaped pH profiles, a simple model assuming two ionization events are fit to  $pH-k_{cat}$  data using the **equations (1)** and **(2)** (see Experiment and Methods) (Sam & Perona, 1999a). **Equation (1)** showed a better fit quality and yielded two  $pK_a$ 's differing by just one pH unit. **Equation (2)** yielded two equivalent apparent  $pK_a$ 's, similar to that derived from single turnover pH-rate profile. The disappearance of two phases in the acid limb for steady state pH-profile can be attributed to a switch of rate-limiting step from turnover step in single turnover kinetics to physical release of product in steady state kinetics, and physical release of product probably is not sensitive to Mg(II) binding as catalytic step.

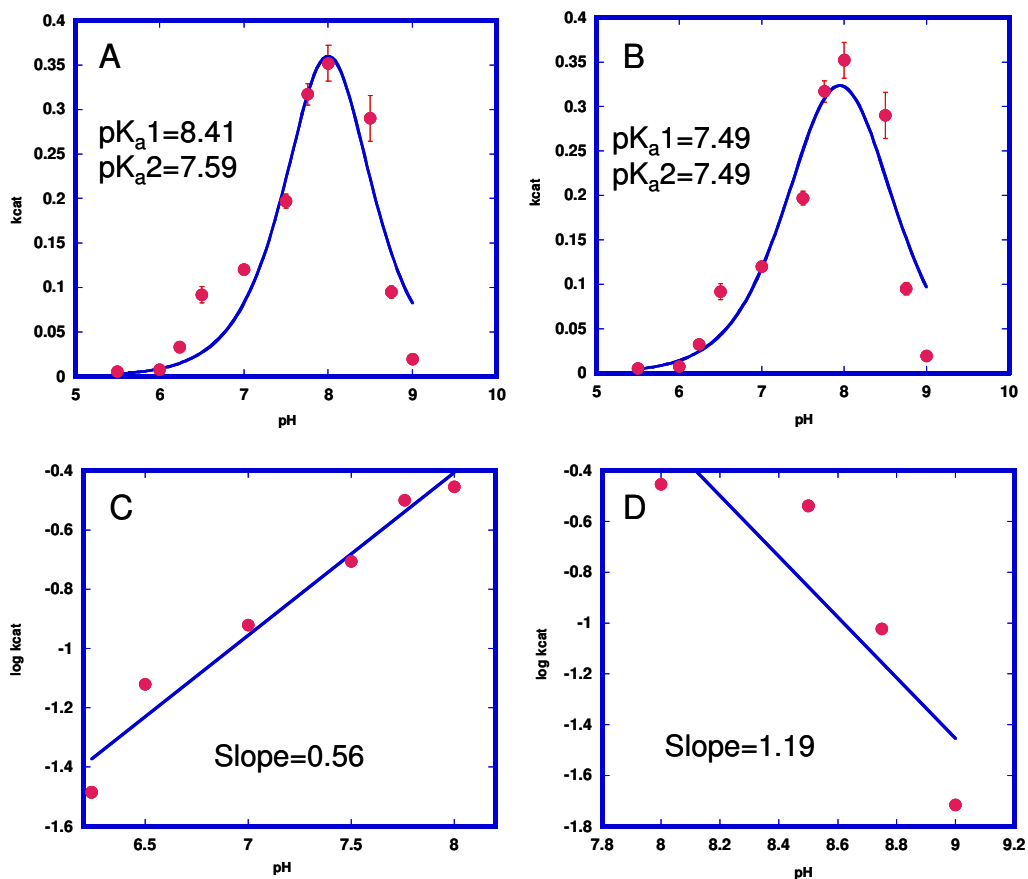


**Figure 3.7. pH dependence of steady state kinetics.** (A) pH- $k_{cat}$  fit to **equation 1** (for fit quality,  $R=0.948$  and  $\chi^2=0.017$ ). (B) pH- $k_{cat}$  fit to **equation 2** (for fit quality,  $R=0.938$  and  $\chi^2=0.020$ ). Derived  $pK_a$ 's are indicated in the plots. (C) Acidic limb plotted as pH- $\log(k_{cat})$ . (D) Basic limb plotted as pH- $\log(k_{cat})$ . The slopes are shown in the plots.

---

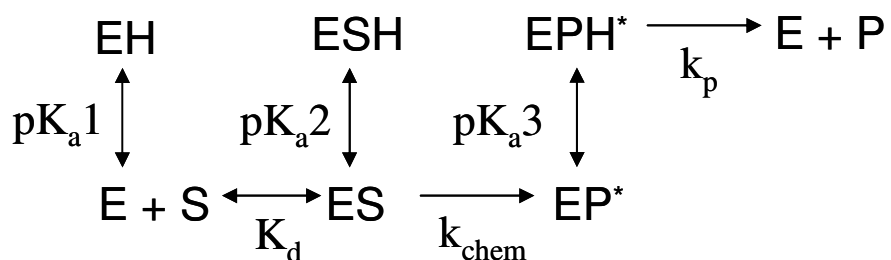
### An Optional Approach For Kinetic Analysis of pH Dependence Using

**DynaFit.** The equations used to derive the apparent  $pK_a$ 's are based on the binding equilibrium equations among different ionizable forms of *PvuII*. Assuming some specific ionizable forms of *PvuII* are active, the binding equilibrium equations can be easily converted to fractional activity equations. In other words, the apparent observed enzymatic activity is the maximal activity of those species multiplied by its fraction in the ionization equilibrium. If the overall reaction scheme is depicted by binding, catalytic turnover and product release, the different ionizations occurs at different stages during the reaction. For example, the ionizations of metal binding sites are coupled with metal binding, and the deprotonation of the metal ligated water molecule is directly related to catalytic turnover step after substrate binding. The application of DynaFit in global fits allows incorporation of ionizations into different kinetic steps in the reaction scheme.

In **Scheme 3.2**, a general kinetic model for single turnover kinetics and steady state kinetics has been constructed to fit the pH dependent rate profiles. Actually **Scheme 3.2** should be considered as an extension version of **Scheme 3.1** with the addition of new binding and turnover step kinetic parameters. Starting with EH, metal binding sites in *PvuII* (Asp58 and Glu68) are deprotonated to form E, then E can bind metal ions. The DNA binding affinities of metal bound form of *PvuII* have been characterized in the presence of 10 mM Ca(II) (about 125 pM) and Mg(II) (5 nM according to Shabir's unpublished steady state kinetic data, see details in Chapter IV **Table 4.3**) (Conlan & Dupureur, 2002a).  $k_{chem}$  is the conversion of ES to a transition

---

The general kinetic model fit to single turnover and steady state kinetics data using DynaFit



**Scheme 3.2. The general kinetic model for single turnover and steady state reaction.** Each ionization is described by proton association rate and dissociation rate constants in the reaction scheme and all the proton dissociation rate constants were fixed as  $1 \text{ sec}^{-1}$  and proton association rate constants are floating.  $\text{pK}_a$  for each ionization can be calculated from proton association rate constant and dissociation rate constant.  $K_d$  varies in two trials corresponding to determined DNA binding affinities in the presence Ca(II) and Mg(II), respectively.  $k_{\text{chem}}$  represents chemistry step and  $k_p$  represents product dissociation step.  $k_p$  is the rate limiting step in steady state kinetics and  $k_{\text{chem}}$  is the rate limiting step in single turnover kinetics.

---

state EP\* after the cleavage of scissile phosphate bond, and EP\* forms the final product EPH\* through the protonation to form the 3' hydroxyl group.  $k_p$  represents the product dissociation step and is rate limiting step in steady state kinetics. For single turnover kinetics,  $k_{chem}$  would be rate limiting step, since both EPH\* and P account for the amount of final product.

Global fit has been performed with single turnover reaction courses at various pH, and local fit has been performed with reaction velocities with 100 nM substrate against pH. Several kinetic parameters have been fixed to reduce the number of unknown parameters and improve fit qualities including DNA association rate constant ( $8 \cdot 10^6 \text{ M}^{-1} \text{ s}^{-1}$  for Ca(II) and  $2 \cdot 10^5 \text{ M}^{-1} \text{ s}^{-1}$  for Mg(II)), DNA dissociation rate constant ( $0.001 \text{ s}^{-1}$ ) and proton dissociation rate constant ( $1 \text{ s}^{-1}$ ). The floating kinetic parameters include proton association rate constant,  $k_{chem}$  (floating in global fit to single turnover data and derived value fixed for local fit to steady state data) and  $k_p$ . So the  $\text{pK}_a$  values can be calculated from proton association rate constant and dissociation rate constants. The global fit results using DynaFit are summarized in **Table 3.10**. The global fits to single turnover data generate simulated reaction courses with apparent  $k_{obs}$  against pH, which are plotted with determined experimental pH-rate profiles. The simulated pH- $k_{obs}$  plot and local fit to pH dependent steady state velocities are shown in **Figure 3.8**.

As shown in **Figure 3.8**, there are large deviations between simulated pH profiles and experimental pH profiles particularly for single turnover data. This indicates that the developed unique kinetic model and global fits using DynaFit are not successful, although the derived  $\text{pK}_a$  values have low percentage errors (**Table 3.10**). Those efforts can not

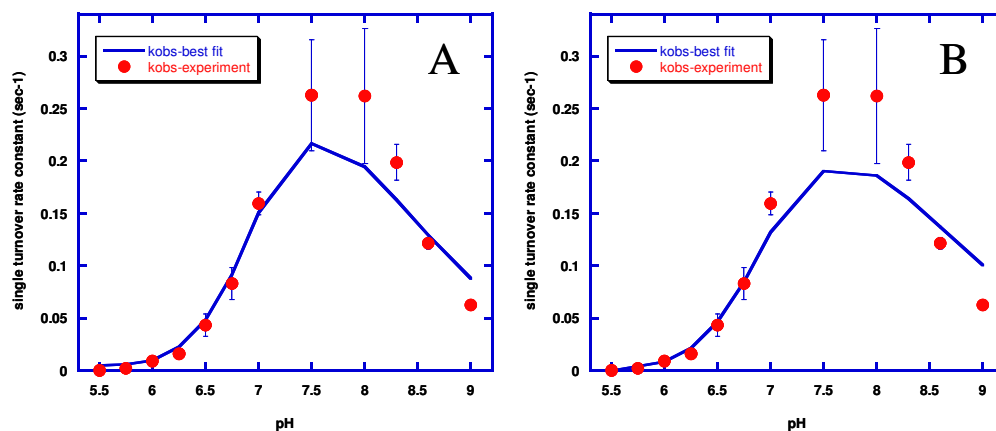
**Table 3.10. The summary of global fits and local fits with pH profiles of single turnover and steady state kinetics.**

	Single turnover kinetics		Steady state kinetics	
	Trial 1	Trial 2	Trial 1	Trial 2
k1	3.6e6 (13%)	2.7e6 (13%)	5.7e7 (>100%)	4.6e7 (>100%)
k2	2.4e8 (9.9%)	4.2e8 (14%)	2.2e9 (68%)	4.5e9 (70%)
k3	1.9e9 (13%)	2.3e9 (15%)	2.1e7 (>100%)	4.9e7 (>100%)
k <sub>chem</sub> (s <sup>-1</sup> )	0.31 (5%)	0.70 (12%)	0.31*	0.70*
k <sub>p</sub> (s <sup>-1</sup> )	1e8 (>100%)	6.9e7 (>100%)	0.062 (>100%)	0.028 (>100%)
<b>Calculated pK<sub>a</sub> values according to proton association rate constant k</b>				
pK <sub>a</sub> 1	6.6	6.6	7.8	7.7
pK <sub>a</sub> 2	8.4	8.6	9.3	9.7
pK <sub>a</sub> 3	9.3	9.4	7.3	7.7

The difference of trial 1 and trial 2 lies on DNA binding affinities ( $K_d = 125$  pM in trial 1 and 10 nM in trial 2). The DNA dissociation rate constant is  $0.001$  s<sup>-1</sup> in both trials. The corresponding DNA association rate constants are  $8 \cdot 10^6$  M<sup>-1</sup>s<sup>-1</sup> in trial 1 and  $2 \cdot 10^5$  M<sup>-1</sup>s<sup>-1</sup> in trial 2. Proton dissociation rate constant is fixed as  $1$  s<sup>-1</sup>.

\* k<sub>chem</sub> in local fit is assigned to the derived value from global fit to single turnover data. The % errors of derived parameters are indicated in bracket.

## Single turnover pH rate profiles



## Steady state pH rate profiles

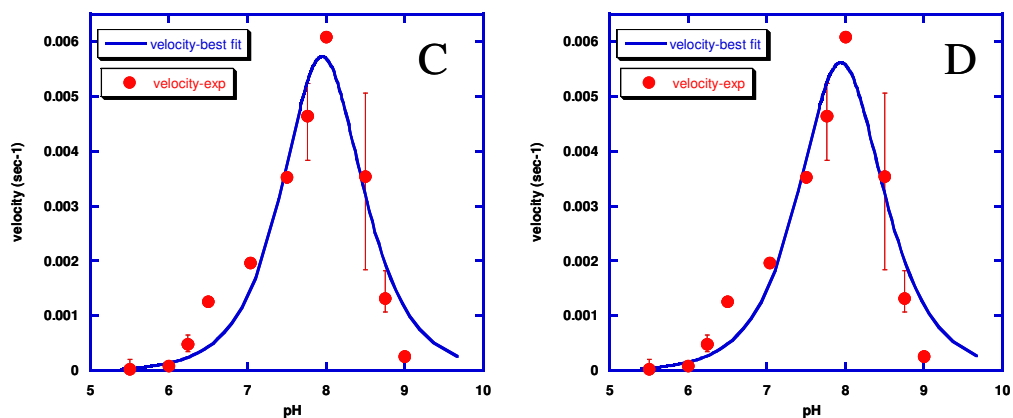


**Figure 3.8. Simulated pH-rate profiles for single turnover and steady state reaction by derived  $pK_a$  and kinetic parameters in corresponding global fits and local fits.** Single turnover reactions were conducted with 2  $\mu\text{M}$  WT *PvuII*, 300 nM DNA with cognate sequence. Steady state reaction was conducted with 1 or 2 nM WT *PvuII* and 100 nM DNA 14 mer with cognate sequence. Both pH dependent single turnover reaction courses and steady state velocity profiles have been fitted to the kinetic model shown in **Scheme 3.2** using DynaFit. The single turnover progress curve is the amount of product over time, which is calculated by determined  $k_{\text{obs}}$  from 0 to 100 seconds with interval of 2 seconds. Experimental steady state velocity is calculated as the slope of linear phase and normalized by enzyme concentration. Panel A and B represent simulated single turnover pH profiles from trial 1 and trial 2. Panel C and D represent local fits with steady state velocities from trial 1 and trial 2.

---

effectively improve the fit qualities compared with **Figure 3.6** and **Figure 3.7**. The derived  $pK_a$  values from single turnover and steady state kinetics are still dramatically different, which implies that different ionizable groups may be involved in those two kinetic processes.

## DISCUSSION

***BamHI* vs. *PvuII*.** *BamHI* has to be discussed here because published computational studies on *BamHI* seems to contradict with what we propose based on our  $pK_a$  calculations (Fuxreiter & Osman, 2001; Mones, et al., 2007a). We propose that metal ions in the active site dramatically lower the  $pK_a$  value of water and promote its deprotonation in order to form the nucleophile. Conserved Lys in the active site aids this process. The extrinsic mechanism (**Figure 3.1**) has been shown to be feasible as well as the general base catalysis by E113, based on calculations of activation energy barrier using quantum mechanical/molecular mechanical simulation on *BamHI*. Here the hydroxide ion can penetrate from solvent to reach the active site and probably is stabilized by metal ions. If this is true, there is no need for metal ions to lower the  $pK_a$  of its ligated water molecules since hydroxide is available from the bulk solvent. Secondly, among the type II restriction endonucleases family, *BamHI* is a structural exception since it has a Glu residue instead conserved Lys in its active site. Based on computer simulations using the semiempirical protein dipoles Langevin dipoles (PDL/D/S) method, general base catalysis involving Glu and substrate assisted catalysis have been ruled out due to a much higher energy barrier compared with the pathway a proton transferring from the attacking water molecule to

---

bulk solvent (Fuxreiter & Osman, 2001). However, in a recent study, the same group reevaluated the pK<sub>a</sub>'s of attacking water molecule (5.7) and Glu (6.7) by using a new force field (AMBER vs. ENZY MIX) and the treatment of negatively charged phosphate groups, and concluded that a general base catalysis by Glu113 is feasible (Mones, et al., 2007a).

The contribution of this Glu113 in *Bam*HI is expected to elevate the water pK<sub>a</sub>, since Lys in *Pvu*II lowers the water pK<sub>a</sub>. This is verified by our calculations (7.2 in *Bam*HI WT and 8.3 when E113 is off). Due to the opposite electrostatic contributions to metal ligated water pK<sub>a</sub> by Glu113 in *Bam*HI and Lys70 in *Pvu*II, it seems unlikely that *Bam*HI and *Pvu*II follow the same water activation mechanism or that Glu and Lys have a similar structural or functional role. However, the superposition of *Bam*HI vs. *Pvu*II crystal structures (**Figure 3.9**) shows a very similar active site configuration except the position of the second metal ion. Considering diversity among type II restriction endonucleases, it is quite possible that one theory or mechanism can not be generalized for the whole family without any exceptions. Although an extrinsic mechanism is proved valid for *Bam*HI (**Figure 3.1 A**), it is still not widely accepted for type II restriction endonucleases (Mones, et al., 2007a). If metal ions just stabilize the transition state but are not involved in the activation of nucleophile, all divalent metal ions should be able to support catalysis since they all carry the same positive charges (Pingoud, et al., 2005). pH studies of flap endonucleases provide evidence that divalent metal ions are directly involved in the activation of nucleophile (Tock, et al., 2003).

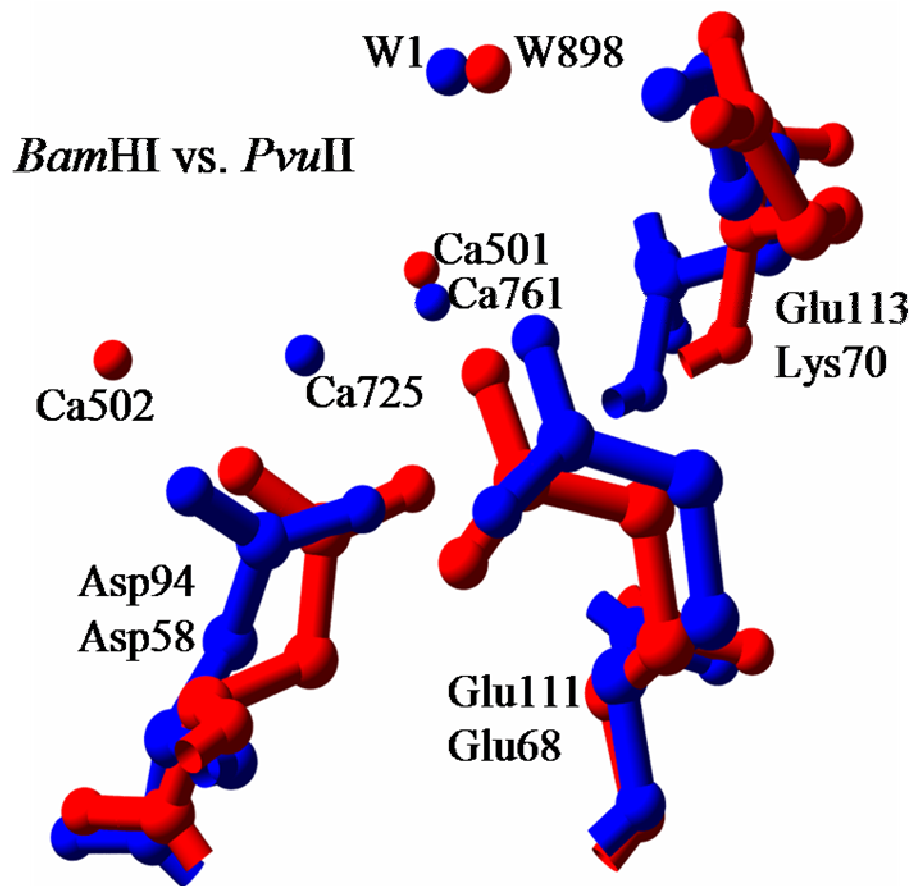


**Figure 3.9. Superposition of *Bam*HI and *Pvu*II active site.** The active sites of *Bam*HI and *Pvu*II are labeled in red and blue, respectively. The active site of *Bam*HI in subunit A includes Asp94, Glu111, Glu113, CA502, CA501 and W1. The active site of *Pvu*II in subunit B includes Asp58, Glu68, Lys70, CA725, CA761 and W898. Both highlighted water molecules are proposed to form the attack nucleophiles. pdb code is 1F00 for *Pvu*II and is 2BAM for *Bam*HI.

---

**pH Dependence Studies and Correlations With Predicted  $pK_a$ 's.** The general mechanism for hydrolysis of the phosphodiester bond can be clearly described when those ionizable groups such as nucleophile, general base and general acid are identified. So the primary question will be whether we can identify those ionizable groups by correlating the calculated  $pK_a$  of those candidates (metal binding sites and metal ligated water) with the derived apparent  $pK_a$  from experimental pH profiles. The improvement of correlations will greatly depend on the accuracy of  $pK_a$  calculations and in many cases the calculated  $pK_a$  are not accurate enough to match the apparent  $pK_a$  determined kinetically.

There are some examples using a  $pK_a$  calculation program based on the Poisson-Boltzmann equation to examine such kind of possibilities (Lamotte-Brasseur, et al., 1999; Noble, et al., 2000; Tolbert, et al., 2005). Lamotte-Brasseur applied such  $pK_a$  calculations to wild type class C  $\beta$ -lactamases and mutants (Lamotte-Brasseur, et al., 1999). Mutation of charged residues in the active site cause moderate  $pK_a$  shifts of Tyr150, which is in good agreement with relative measured  $k_{cat}$  values. This indicates that Tyr150 is directly involved in the activation of nucleophilic serine. The  $pK_a$  of active site residue Asp158 in papain has been experimentally determined (2.8) and predicted by UHBD program (2.0) (Noble, et al., 2000). A slightly lower  $pK_a$  than 2.8 has been predicted when hydrogen bond network of Asp158 has been considered. The pH dependent stopped flow kinetic study combined with  $pK_a$  calculations proposed that Asp158 was one of the electrostatic modulator mediating the enzymatic activities. The  $pK_a$  of Cys in

---

ubiquitin-conjugating enzymes has been predicted to elevate about 2 pH units compared with its model  $pK_a$ , which is in good agreement with experimental determinations and is speculated to be due to the proximity of carboxyl terminus (Tolbert, et al., 2005). Water molecules have been treated as titratable sites in  $pK_a$  calculations on bacteriorhodopsin. It was found that the overall predicted protonation curves within a wide pH range assuming a water dimer coupled with two Glu residues matched perfectly with the concept of proton storage in the active site (Spassov, et al., 2001).

Another challenge in the study of the pH dependence of protein-DNA interactions is to predict the influence of the substrate. For *MunI*, the apparent  $pK_a$  of the same moiety shifts upward to one pH unit upon DNA association (Haq, et al., 2001). Unfortunately, the  $pK_a$  calculation using UHBD can not provide the reliable solution to address this question (**Table 3.7**). It is known that the linear Poisson-Boltzmann equation has been mostly used in proteins and non linear Poisson-Boltzmann equation is more appropriate for systems with high charge density (Tang, et al., 2007).

For *PvuII*, the apparent  $pK_a$  for metal binding sites are determined to be 6.7 by the pH titration of Mg(II) binding, but the calculated  $pK_a$  of metal binding sites (D58 and E68) is 5.2 maximally (**Table 3.1**) (Dupureur & Conlan, 2000). The extremely low  $pK_a$  of metal binding sites calculated from *PvuII* structure (**Table 3.2**) with one Mg(II) ion bound in the active site also preclude the protonation of those sites in the presence of Mg(II). This indicates that ionizations of metal binding sites with the

---

apparent  $pK_a$  actually reflect a cluster of ionizable groups rather than a single residue as metal binding ligand. The application of those calculated  $pK_a$  with two sites interacting model (**Figure 3.3**) shows good agreement with experimental titration curve for WT, which confirmed the coupled ionizations of two nearby residues actually is responsible for this unusual apparent  $pK_a$ . This reminds us the complexity of interpreting experimental pH profiles.

The pH dependence of cleavage kinetics is more complex than the ligand binding behaviors, since additional titratable sites involved in the catalysis may not belong to protein residues. For hydrolysis of phosphodiester bonds by metallonucleases, the metal-ligated water serves as the attacking nucleophile, and its  $pK_a$  is speculated to be more correlative with apparent  $pK_a$  from pH dependence of single turnover cleavage rate than active site residues (Sam & Perona, 1999a; Tock, et al., 2003). pH dependence studies with *EcoRV* endonuclease and flap endonuclease were performed with carefully selected Mg(II) concentrations to assure the Mg(II) binding saturation at physiological pH and very similar apparent  $pK_a$ 's are derived (8.5 in *EcoRV* and 8.3 for flap endonuclease) (Sam & Perona, 1999a; Tock, et al., 2003). For *PvuII*, the biphasic acidic limb of pH- $\log(k_{obs})$  plot indicates competition between proton and metal ions binding to metal binding sites at low pH. This allows the application of **Scheme 3.1** to fit the pH- $k_{obs}$ , and derived apparent  $pK_a$  for metal binding sites agrees well with experimental apparent  $pK_a$  for metal binding sites obtained via  $^{25}\text{Mg}$  NMR (Dupureur & Conlan, 2000). The derived apparent  $pK_a$ 's of general base and general acid fall within the range of the calculated  $pK_a$  of

---

water molecules (**Table 3.4**).

Steady state parameters rely on a multitude of pH dependent processes extending to metal ion and DNA binding and product release (Sasnauskas, et al., 1999; Bastock, et al., 2007). The kinetic parameters of *PvuII* demonstrate that product dissociation is the rate limiting step in the steady state kinetics since the cleavage rates differ by almost 2 orders of magnitude between single turnover and steady state conditions at the same Mg(II) concentrations. Surprisingly, the pH dependence of steady state  $k_{\text{cat}}$  shows a very similar bell shape as single turnover rate constants, and the derived  $\text{pK}_a$  (7.59) for the general base and acid well reproduces the apparent  $\text{pK}_a$ 's in single turnover kinetics. The similar phenomenon has been observed in the Mg(II) dependence studies since derived Hill coefficients and apparent  $K_d$ 's are similar to both kinetics (Chapter IV). One possible explanation for this similarity would be that the steady state rate in *PvuII* actually is proportional to the turnover rate within the experimental pH range, which means turnover rate actually determines the product dissociation rate. Or it might be just a coincidence that different moieties occur to have the same macroscopic effect. Therefore it is not clear if the apparent  $\text{pK}_a$ 's in steady state kinetics should be assigned to the same moieties as in single turnover kinetics. A further kinetic analysis with same assignments on ionizable groups using DynaFit (**Scheme 3.2**) actually generates quite different apparent  $\text{pK}_a$ 's for single turnover and steady state kinetics, which seems that the involvements of ionizable groups somehow are different. In the kinetics study it has been proposed that the terminal phosphate might strengthen the product enzyme interaction and

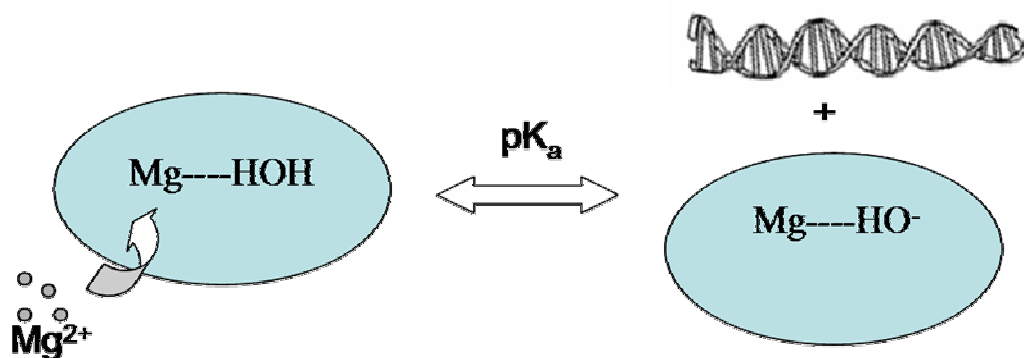
---

retard the product dissociation of *MunI*. So this group may be a candidate as well (Sasnauskas, et al., 1999).

Since our  $pK_a$  calculations do not include DNA, objections can be raised that the influence of DNA on  $pK_a$ 's of metal binding sites or metal ligated water is not evaluated and this influence could be large enough to change the overall conclusion. The influence of DNA on predicted  $pK_a$  depends on reaction scheme (**Figure 3.10**). If metal ion binds to active site prior to DNA, then with assistance of metal ions and Lys, in the active site hydroxide might be formed and populated soon after metal ion binding. Then scissile phosphate would be attacked by the hydroxide ion as soon as it's bound in the active site. So when does the nucleophile form? If nucleophile formation is prior to DNA binding, then influence from DNA is very limited on the  $pK_a$  shift because the irreversible cleavage step will go on, which makes it less likely that the hydroxide will get protonated back to water even if water's  $pK_a$  is shifted to higher extent by phosphate. If nucleophile formation occurs after DNA is bound in the active site, it makes more sense to discuss the DNA influence on the activation of water.

**The Role of Conserved Lys in Metallonucleases.** The  $pK_a$  of Lys70 in *PvuII* has been predicted to be high in any case and its protonation seems very reasonable in physiological pH. With the assistance of the positive charged Lys nearby, it is quite possible that the attacking water's  $pK_a$  can be further lowered by more than two pH units if Lys is close enough to the attacking water molecule. In conformational behavior accessible in solution, such flexibility on distance criteria

### A. Water activation without the presence of DNA



### B. Water activation in the presence of DNA

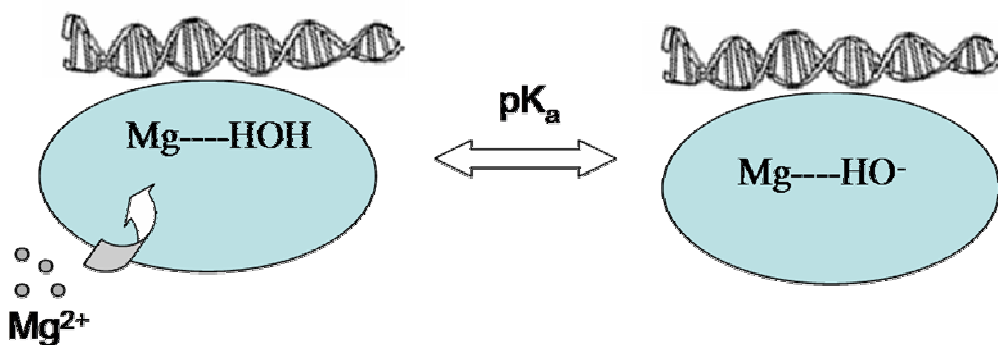


**Figure 3.10. The water activation in the presence and without the presence of substrate.** A. The Mg(II) ions is bound to the active site of enzyme prior to DNA binding, and Mg ligated water is deprotonated without the presence of DNA molecules. B. Mg(II) ligated water is deprotonated after the formation of ternary complex E-M(II)-DNA. The calculated water pK<sub>a</sub>'s in scheme A and B are largely different due to the high negative charge density of DNA molecules.

---

can easily be met.

The role of conserved Lys as a general base can not be concluded from any  $pK_a$  calculations shown in this chapter. Actually even in apo form of *PvuII*, the Lys70 remains a high  $pK_a$  and is supposed to be charged if it is fully hydrated. But its protonation status can be compromised depending on how easily the water molecules penetrates into the active site; and it is still possible that Lys is available as a proton acceptor when it is buried and not hydrated. At least a general base catalysis by E113 is proved to be feasible in *BamHI* (Mones, et al., 2007b).

## CONCLUSIONS

pH profiles of *PvuII* activity have been characterized and the derived apparent  $pK_a$ 's are assigned to metal binding sites and metal ligated water molecules. Both the  $pK_a$ 's of metal binding sites and metal ligated water molecules have been studied with computational approach using the UHBD suite program on a series of active site configurations. It is concluded that the  $pK_a$  of attacking water molecule is modulated by the metal ions and the nearby conserved Lys for the PD...D/ExK motif enzymes. The calculated  $pK_a$  can be correlated with experimental  $pK_a$ 's. Applying this approach to a number of metallonucleases with similar active site configurations confirmed that the water  $pK_a$  is lowered by the conserved Lys, which provides a general nucleophile activation mechanism for the PD...D/ExK motif enzymes.

---

## CHAPTER IV. METAL DEPENDENCE STUDY AND KINETIC MODELING

### INTRODUCTION

Type II restriction endonucleases are members of a restriction modification system that protect the bacteria and archaea against invading DNA. They protect their host by cleaving the invading phage DNAs at specific sites of 4-8 bp in length and require Mg(II) as the cofactor for catalysis (Horton & Perona, 2004). *PvuII* restriction endonuclease belongs to the family of type II restriction endonucleases and shares the catalytic motif PD...D/ExK (Anderson, 1993). Metal cofactors play a very critical role in the mechanism of nuclease activity and their binding properties and functions are to be addressed by kinetic analysis in this chapter.

The most common metal cofactor supporting DNA hydrolysis by restriction enzymes is Mg(II) and its physiological concentration in cells is about 0.5 mM (Cowan, 1998). In addition, Mn(II) and Co(II) support the detectable cleavage activity (Bowen & Dupureur, 2003). Ca(II) promotes DNA association to *PvuII* endonuclease (Conlan & Dupureur, 2002b; Bowen & Dupureur, 2003), but it also supports the hydrolytic cleavage of DNA in a few cases (e.g. *staphylococcal* nuclease). The stoichiometry of the metal cofactor and metal binding sites of *PvuII* restriction endonucleases has been characterized by X-ray crystallography structures (Horton & Cheng, 2000; Spyridaki, et al., 2003). **Figure 4.1** shows all the active site configurations resolved for metal bound *PvuII*. In the presence of Ca(II) and cognate DNA sequence (Horton & Cheng, 2000), *PvuII* binds two metal ions at each subunit (**Figure 4.1A**). However when soaked solely with high Mg(II)

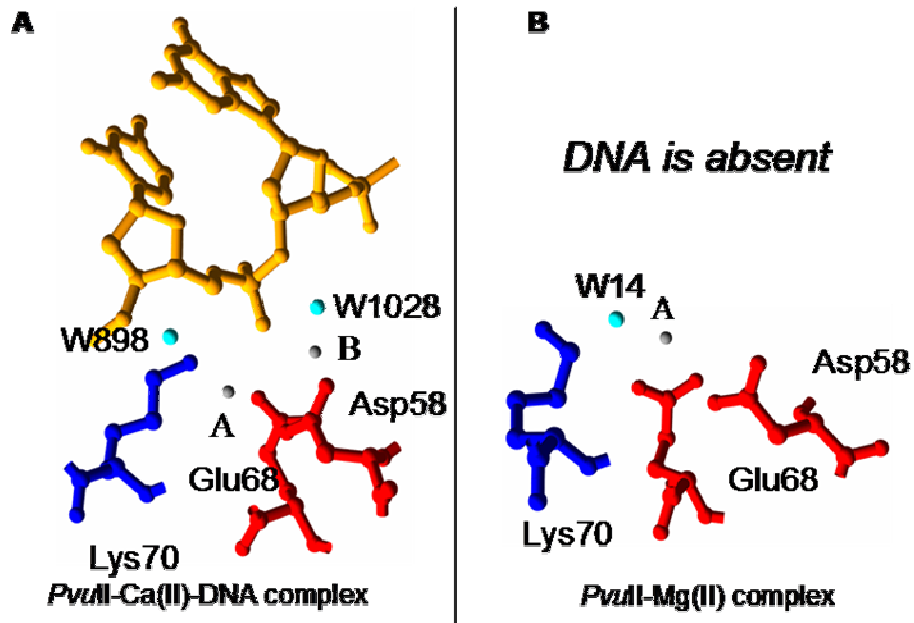


**Figure 4.1. The resolved metal binding sites in *PvuII*.** A. Subunit B of *PvuII* structure (1F00) with two Ca(II) ions and cognate DNA (Horton & Cheng, 2000). The two water molecules bound to Ca(II) ions are labeled and are speculated to be the general base (the one near to Lys residue) and general acid in catalysis. The two Ca(II) ions are distinguished as site A and B. B. Subunit A of *PvuII* structure (1H56) with one Mg(II) ion, and DNA is absent in such a binary complex (Spyridaki, et al., 2003). The Mg(II) ion only binds the active site at site A. The water molecule positioned as nucleophile bound to Mg(II) is highlighted.

---

concentrations, the enzyme binds one Mg(II) ion with each subunit (**Figure 4.1B**) (Spyridaki, et al., 2003). It has been determined via isothermal titration calorimetry and  $^{25}\text{Mg}$  NMR that two metal ions bind to each *PvuII* active site with mM binding affinity (Dupureur & Hallman, 1999; Jose, et al., 1999). The Hill analysis of Ca(II) dependence of DNA binding also supports two metal ions involved in the DNA association for each subunit (Conlan & Dupureur, 2002b).

The general mechanism of DNA hydrolysis by type II restriction endonuclease has been described in Chapter I including proposed three catalytic mechanisms on the basis of crystal structures. The number of metal ions involved in catalysis is still the controversial problem for type II restriction endonucleases (Pingoud, et al., 2005).

**Kinetic Evidence Of A Two-Metal Ion Mechanism?** Besides the supporting evidence from crystallographic data, the mutagenesis and kinetic approach has been applied to address the number of metal ions required in catalysis. By mixing two different metal ions, the bell shaped metal dependent cleavage rates appears to support the two-metal ion mechanism. In the cleavage reaction of *EcoRV* at low Mn(II) concentration, addition of small amounts of Ca(II) which does not support catalysis stimulates DNA cleavage; however large amounts of Ca(II) inhibit catalysis (Vipond, et al., 1995a). Titration with La(III) ions of the hammerhead ribozyme catalyzed RNA cleavage against a fixed Mg(II) background concentration also yielded a bell-shaped curve of cleavage rate against La(III) concentration, with activation at low concentration and inhibition at high concentration (Lott, et al., 1998). Both experimental results can not be explained by one-metal ion mechanism,

---

therefore a two-metal ion mechanism is proposed based on the distinct roles of two metal ions in catalysis. However, Mn(II) is used to conduct those mixing metal experiments for *EcoRV* instead of Mg(II) discussed in this chapter. So it does not provide the direct support evidence for two-metal ion mechanism with Mg(II). Mn(II) is known to have the additional inhibitory sites on *EcoRV*, and it also binds to DNA efficiently in mM concentrations (Reid & Cowan, 1990; Groll, et al., 1997). The two-metal ion mechanism suggested from bell shaped Ca(II) effect on cleavage rate can be compromised with respect to the different binding behavior between Mg(II) and Mn(II).

The sigmoidal dependence of cleavage rate as a function of Mg(II) concentration has been observed in both *EcoRV* and *PvuII*, and derived Hill coefficients indicate the multiple metal ions involved in binding and catalysis (Groll, et al., 1997; Spyridaki, et al., 2003). It should be noted that sigmoidal dependence only indicates the multiple metal ions influence the cleavage rate but does not prove that two metal ions participate the catalytic steps. The Hill coefficient actually depends on the cooperativity of sites, which remains unclear for the metal binding to *PvuII* or *EcoRV*.

Besides deriving the number of metal ions in catalysis from macroscopic binding data, mutagenesis on the candidate metal binding sites is a more direct approach to determine if two metal ions are essential for the detectable enzymatic activity. Mutations on metal binding sites have been performed on both *EcoRV* and *PvuII*. *EcoRV* have two candidate metal binding sites the D74/D90 site and the

---

E45/D74 site (Kostrewa & Winkler, 1995). D74A and D90A mutants are catalytically inactive, but the activity of E45A is only 1.8 fold reduced compared with WT (Groll, et al., 1997). Therefore one metal binding site (E45) is ruled out as a catalytic residue in *EcoRV*.

In *PvuII*, alanine mutations of metal binding ligands such as D58 and E68 give the residual activity of about 1000 fold and 50 fold lower compared with WT, respectively (Dupureur & Conlan, 2000). It was known structurally that both residues are the ligands for two Ca(II) ions for the interactions of *PvuII* and DNA (Horton & Cheng, 2000). While in the  $^{25}\text{Mg(II)}$  NMR titration experiments it seems that D58A binds one Mg(II) ion with similar affinity to WT, Mg(II) binding in the active site is clearly disrupted in E68A (Dupureur & Conlan, 2000). From those observations, it is plausible that E68 is the bridging ligand essential for two metal ions binding and D58 is the ligand that enhances the binding affinity for the second metal ion. Besides bound to the active site, the metal ions are required to be positioned in the right place to support efficient catalysis, which could be a reasonable explanation for the 1000 fold reduced activity for D58A.

Here, on the basis of two metal binding sites in the *PvuII* restriction endonucleases, we establish the two-site kinetic models to fit Mg(II) concentration dependence of *PvuII* cleavage kinetics. The two-site kinetic models are divided into two groups which differ in the number of metal ions directly required for the catalysis. In group A, the catalysis requires two metal ions bound per active site. In group B, the catalysis occurs no matter how many metal ions in the active site; two distinct

---

catalytic activities are dependent on one and two metal ions bound in the active site, respectively. The binding equilibrium and kinetics of catalytic steps and product release steps are globally fit to the candidate models separately so that the metal dependence of apparent cleavage activity are analyzed with respect to the whole reaction scheme. The qualities of global fits with candidate models have been compared to determine the most kinetically favorable reaction pathway or parameters for metal participation in binding and catalysis.

## **EXPERIMENTS AND METHODS**

**The Determination of Single Turnover Rate Constants.** A series of single turnover experiments were conducted with 2  $\mu\text{M}$  enzyme and 300 nM DNA duplex which is a 14 mer hybridized from strand sq3121-1 and sq3121-2 (see CHAPTER II **Table 2.1**, all the DNA cleavage assay use the same oligonucleotides). Reaction conditions were determined at low Mg(II) concentration (below 1 mM) to assure the measured single turnover rate constants are independent of enzyme and DNA concentrations. The reaction buffer contains 50 mM Tris, NaCl (adjusted to keep ionic strength constant) and desirable  $\text{MgCl}_2$ . The concentration of NaCl was adjusted with Mg(II) concentration to keep the same ionic strength as a buffer solution containing 100 mM NaCl and 10 mM Mg(II). The pH of buffer is 7.5 at 37  $^\circ\text{C}$ . DNA consisted of a small amount of radiolabeled probe added to cold DNA 14 mer. At Mg(II) concentrations below 3 mM, reactions were initiated by addition of metal-free enzyme and reaction samples were collected manually at different time

---

points. The reactions were quenched by stop dye containing 100 mM EDTA. At 2 mM Mg(II), a different mixing order procedure with the same reaction conditions was examined to prove that the mixing orders did not have any dramatic effect on the measured single turnover rate constants. The samples were loaded on 20% PAGE gel with 8 M urea. PAGE gel was scanned with Storm Imager and gel image was quantitated using ImageQuant. The cleavage extent was normalized and fit to the first order exponential equation to derive the single turnover rate constants.

**Quench Flow Experiments.** At Mg(II) concentration above 3 mM, the reaction progress was so fast that an SFM4/Q quenched-flow device (Bio-Logic) was used to mix equivalent volume of solutions containing 600 nM DNA and 4  $\mu$ M enzyme. Both DNA or enzyme were incubated with the same reaction buffer containing Mg(II) described in the single turnover experiments. At Mg(II) concentration of 10 mM, mixing the metal free enzyme and DNA containing 20 mM Mg(II) gave the similar apparent single turnover rate constants as mixing the enzyme and DNA both containing 10 mM Mg(II). At appropriate time intervals (250 ms-30 s) the reaction was quenched by mixing with 140  $\mu$ L of 100 mM EDTA solution. The collected samples were loaded on a PAGE gel and gel image was obtained and processed as described above.

**The Characterization of Mg(II) Dependent Steady State Kinetics.** Cleavage experiments were performed at 37 °C in the same reaction buffer containing various Mg(II) concentrations. Reaction mixtures typically contained 2 nM enzyme and at least 5 times higher DNA concentrations. The reaction was initiated by the

---

addition of metal free enzyme and quenched by stop dye containing 100 mM EDTA. The reaction was quenched by adding stop dye at the appropriate time so that less than 10% substrate was cleaved during the reaction. The product and substrate in the collected reaction samples were separated and analyzed by PAGE gel. The reaction rates were determined from the linear parts of the reaction progress curves by linear regression and were normalized to enzyme concentrations.

**Pre-Steady State Experiments Against Various Mg(II).** Pre-steady state experiments were performed at 37 °C in the same reaction buffer containing various Mg(II) concentrations. The reaction samples were collected manually at Mg(II) concentration below 2.5 mM and conditions was the same as the steady state rate measurements. The reaction progress was monitored by quench flow at higher Mg(II) concentrations. The equivalent volume of enzyme and DNA incubated with the same buffer with Mg(II) were mixed and reactions were quenched by EDTA. Reaction mixtures typically contained 20 nM enzyme and at least 5 times higher DNA concentrations. Within 30 seconds, reaction were monitored by quench flow while reaction sample with longer time intervals was monitored by a manually sample collection. All the samples were loaded on a PAGE gel for further processing and data quantitation.

**Global Fit Using DynaFit And Model Analysis.** To quantitatively understand the Ca(II) dependence of DNA association equilibrium and Mg(II) dependence of DNA cleavage kinetics, the candidate models have been developed to determine the most favorable reaction scheme and derive those parameters not

---

measured experimentally. Since *PvuII* has two metal binding sites per active site, the two-site model is the basis of all the candidate models in this chapter, and the first and the second metal binding events are assumed to occur in a sequential way. The global fits using DynaFit have been applied to Ca(II) dependent DNA binding titration curves (equilibrium), Mg(II) dependent single turnover and pre-steady state reaction courses (progress) and Mg(II) dependent steady state velocity (velocity) in order to determine the kinetically favorable reaction pathways and metal binding affinities. In the global fits, DNA bound fraction, amount of product and normalized reaction velocity as a function of Ca(II)/Mg(II) concentrations, enzyme concentrations and DNA concentrations are treated as original data sets, which are fit with possible reaction schemes to examine the standard deviations and percentage errors for the unknown kinetic parameters.

---

## RESULTS

### Dissection of Ca(II) Dependence Of Specific DNA Association.

*Experiments.* The DNA binding equilibrium constants were measured by nitrocellulose filter binding or fluorescence anisotropy (Conlan & Dupureur, 2002b). In **Figure 4.2**, the plot of equilibrium association constants as a function of Ca(II) concentration appears to be sigmoidal and yields a Hill coefficient of 3.5 per enzyme dimer, consistent with two metal binding sites for each monomer (Horton & Cheng, 2000). The apparent DNA association constants is the average value of several titrations, in which the enzyme is being titrated to some amount of DNA and signal is monitored by nitrocellulose filter binding or fluorescence anisotropy. The data is normalized as DNA bound fractions at a series of Ca(II) concentrations.

*Reaction Scheme.* The unique model of Ca(II) participation in the DNA binding equilibrium is shown in **Scheme 4.1**. This is the only case in this chapter that the model has been decided uniquely and the goal of global fit is to simply derive the apparent DNA binding affinity for EM<sub>2</sub> (which is not accessible experimentally) and apparent Ca(II) binding affinities for two sequential binding steps. Assuming the same metal ion occupancy in each subunit for a homodimeric enzyme, the species of *PvuII*-Ca(II) complex are restricted to EM<sub>2</sub> and EM<sub>4</sub>. Therefore, the substrate the cognate DNA duplex potentially can bind to three species: apoE, EM<sub>2</sub> and EM<sub>4</sub>, and the distribution among those three species can be dictated by Ca(II) binding affinities and Ca(II) concentrations.

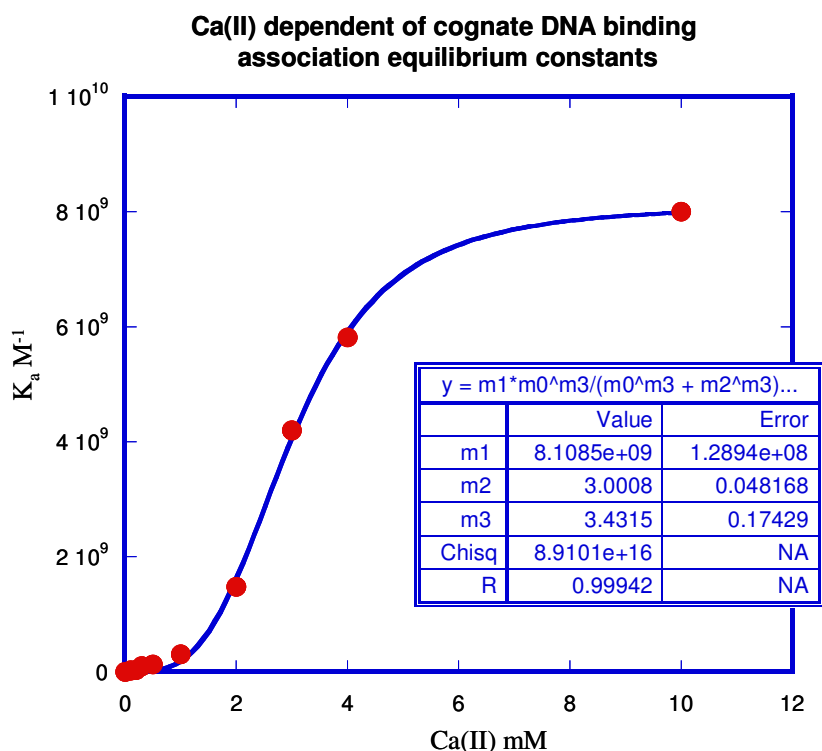
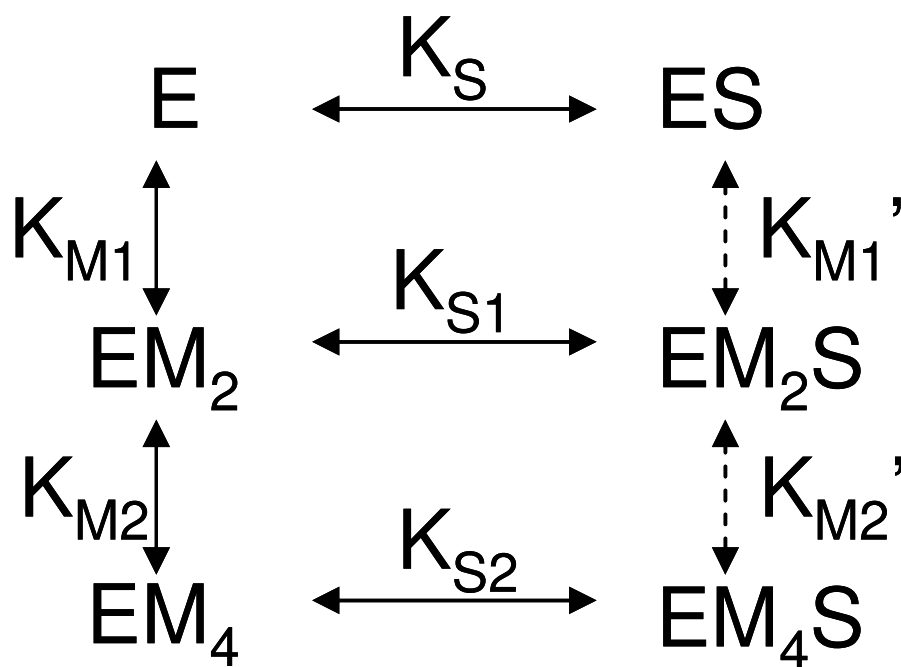


**Figure 4.2. DNA binding affinity is dependent on Ca(II) concentration.** The buffer contained 50 mM Tris, NaCl and desirable Ca(II) concentration, pH 7.5 at 25 °C. The NaCl concentration was adjusted to assure a constant buffer ionic strength of 107.5 mM. Below 1 mM CaCl<sub>2</sub>, binding constants were collected by fluorescence anisotropy assay with 2.5 nM Hex-labeled 14-mer duplex. At higher Ca(II) concentrations (>1 mM), binding constants were measured using nitrocellulose filter binding with 9 pM DNA duplex titrated with enzyme (Conlan & Dupureur, 2002b).



**Scheme 4.1. Model of metal ion participation in metal dependence of DNA binding equilibrium.** E: homodimeric enzyme, S: cognate DNA duplex, M: metal ion. All the K's are dissociation constants. The scheme presents all the  $K_d$ 's involved in the global fit of Ca(II) dependent DNA binding equilibrium constants. Dashed lines indicate the possible equilibrium among ES,  $EM_2S$  and  $EM_4S$  but those equilibria are not included in the global fit. Reasons for that are explained in the results.

---

*Global Fits.* The raw *PvuII* titration curves (DNA bound fractions against titrated enzyme concentrations at a series of Ca(II) concentrations) were fit globally to the unique binding model (**Scheme 4.1**). The metal binding equilibria among ES, EM<sub>2</sub>S and EM<sub>4</sub>S (the binding steps involve K<sub>M1</sub>' and K<sub>M2</sub>') have not been included in DynaFit script for global fit since they have been proven incapable to affect any global fit results; however they were shown in **Scheme 4.1** as possible binding pathways. In such a simplified scheme, three DNA disassociation constants (K<sub>S</sub>, K<sub>S1</sub> and K<sub>S2</sub>) and two metal disassociation constants (K<sub>M1</sub> and K<sub>M2</sub>) dictate Ca(II) dependence on DNA association. Two trials of global fits have been conducted with respect to available experimental evidence. Since there is no direct measurement for K<sub>S1</sub>, K<sub>S1</sub> is floating in both trials. Trial 1 makes full use of the measured DNA binding affinities and attempts to derive all the metal binding affinities, but trial 2 does the opposite. In trial 1, DNA binding affinity for apo E and EM<sub>4</sub> is assigned to 300 nM and 125 pM, respectively, according to DNA binding assays at metal free condition and 10 mM Ca(II) (Conlan & Dupureur, 2002b). In trial 2, Ca(II) binding affinities are assigned to 0.12 mM and 2.1 mM according to ITC experiments (Jose, et al., 1999). **Table 4.1** listed the derived constants with percentage error, fixed parameters (without error) for both trials and corresponding experimental measurements in order to compare.

*Comments.* In **Table 4.1**, global fits trial 1 and trial 2 give the same K<sub>S1</sub> value about 10 nM in both trials, which indicates this value should be reliable with neglect of variations on Ca(II) binding affinities applied to both trials. According to the

**Table 4.1. Experimental measurements and corresponding global fits on the equilibrium constants in Scheme 4.1.**

Species	DNA binding affinity (nM)			Metal binding affinity(mM)	
	Apo E	EM <sub>2</sub>	EM <sub>4</sub>	Apo E	EM <sub>2</sub>
Experiments	K <sub>S</sub>	K <sub>S1</sub>	K <sub>S2</sub>	K <sub>M1</sub>	K <sub>M2</sub>
Gel shift assay <sup>a</sup>	n/a	n/a	0.11 <sup>a</sup>	n/a	n/a
Fluorescence anisotropy <sup>b</sup>	307± 146	n/a	0.056 ±0.02	n/a	n/a
Nitrocellulose filter binding <sup>b</sup>	n/a	n/a	0.053 ±0.01	n/a	n/a
ITC <sup>c</sup>	n/a	n/a	n/a	0.12±0.08	2.1±0.14
Global fit Trial 1	300*	10.6 (31%)	0.125*	0.087 (88%)	4.3 (22%)
Global fit Trial 2	300*	10.9 (17%)	0.22 (14%)	0.12*	2.1*

a. (Nastri, et al., 1997)

b. (Conlan & Dupureur, 2002b)

c. (Jose, et al., 1999)

Kinetic parameters labeled with \* are assigned to experimental measurements and the rest are derived by global fit with error status inside the bracket.

---

experimental methods applied to quantitate Ca(II) binding and DNA binding affinities, it is easier and more precise to measure the latter. So fixing  $K_S$ 's and floating  $K_M$ 's in trial 1 probably is more reasonable than fixing  $K_M$ 's to guess  $K_S$ 's in trial 2. The derived metal binding affinities from global fit trial 1 is acceptable compared with measurements by ITC experiments (Jose, et al., 1999). In the subsequent global fits, it is noticeable that metal binding association rate constants or dissociation rate constants will be floating in the most of cases rather than those parameters for DNA binding due to the difficulty in achieving accurate metal ion binding equilibrium parameters.

In **Scheme 4.1**, the net equilibrium among ES, EM<sub>2</sub>S and EM<sub>4</sub>S has been indicated in dashed line. ES complex can form EM<sub>2</sub>S and EM<sub>4</sub>S respectively by two sequential metal binding steps, in which the  $K_d$  for metal ion binding ( $K_{M1}'$  and  $K_{M2}'$ ) remains unknown for the ES and EM<sub>2</sub>S complex. There is no experimental evidence to address the metal binding affinity of ES complex. Surprisingly, floating  $K_{M1}'$  and  $K_{M2}'$  with any initial values in the global fits always generate the same best fit values as the initial values, which means  $K_{M1}'$  and  $K_{M2}'$  are not critical to the scheme.

$K_{M1}'$  and  $K_{M2}'$  are not affecting the net equilibrium in **Scheme 4.1** because in the global fit the signal (substrate bound fraction) is counted as the sum of ES, EM<sub>2</sub>S and EM<sub>4</sub>S, and equilibrium among those three species only change the distributions among them but not the sum of their amount. To obtain reliable  $K_{M1}'$  and  $K_{M2}'$  from global fit, binding experiments have to be conducted in a way that distinguishes the signals of ES, EM<sub>2</sub>S and EM<sub>4</sub>S, respectively. For example, those three species

---

might display the different anisotropy values and global fit could to be conducted using original data. The other way to derive  $K_{M1}'$  and  $K_{M2}'$  is from perspective of thermodynamic cycles.  $K_{M1}'$  and  $K_{M2}'$  can be calculated if all other equilibrium constants are known in **Scheme 4.1**. Such a strategy will be applied and discussed in the kinetic modeling section.

### **Mg(II) dependence on DNA Association.**

*Experiments.* Since the goal is to develop the kinetic model of *PvuII* on the basis of reaction courses, it is essential to know the association and dissociation rate constants for Mg(II) binding and DNA binding. The direct measurements of the association and dissociation rate constants for DNA binding by *PvuII* endonuclease have been reported (**Table 4.2**) (Conlan & Dupureur, 2002a). At 10 mM Ca(II),  $k_{on}$  reaches the maximal value of  $2.7 \cdot 10^7 \text{ M}^{-1} \text{ s}^{-1}$  as determined using a nitrocellulose filter binding assay.  $k_{on}$  is 100 fold slower at 0.2 mM Ca(II). The dissociation rate constants range from  $10^{-3}$  to  $10^{-4} \text{ s}^{-1}$  at various metal concentrations and Ca(II) does not make a dramatic difference relative to Mg(II). Therefore, for E, EM<sub>2</sub> and EM<sub>4</sub> in the future global fits,  $k_{off}$  was assigned to  $10^{-3} \text{ s}^{-1}$  uniquely. Their association rate constants  $k_{on}$  can be calculated from  $k_{off}$  according to DNA binding affinity  $K_d$ .

The remaining question would be if we can use  $K_S$ 's in **Table 4.1** as corresponding DNA binding affinities in the presence of Mg(II). The hydrolyzable DNA binding affinity in the presence of Mg(II) is not measurable since Mg(II) supports catalysis; but it can be evaluated by measurement of  $K_M$  in the steady state

---

**Table 4.2. Measured dissociation rate constants for DNA binding equilibrium of PvuII.<sup>a</sup>**

Metal ion concentration	Rate constants (s <sup>-1</sup> )	Experiments
Metal free	3.42*10 <sup>-3</sup>	Fluorescence anisotropy
10 mM Ca(II)	3.87*10 <sup>-4</sup>	Fluorescence anisotropy
0.3 mM Ca(II)	1.13*10 <sup>-3</sup>	Fluorescence anisotropy
1 mM Mg(II)	1.8*10 <sup>-3</sup>	DNA trap experiments
0.3 mM Mg(II)	4.0*10 <sup>-4</sup>	DNA trap experiments

a. (Conlan & Dupureur, 2002a)

---

kinetics. In Michaelis-Menten kinetics,  $K_M$  is a function of substrate association rate constant ( $k_1$ ), dissociation rate constant ( $k_{-1}$ ) and catalytic rate constant ( $k_{cat}$ ). If  $k_{cat}$  and  $k_{-1}$  are known,  $k_1$  can be calculated from  $K_M$ . In steady state kinetics, both  $K_M$  and  $k_{cat}$  are derived by fitting reaction velocity as a function of DNA concentration to the Michaelis-Menten equation at a series of Mg(II) concentrations. If DNA dissociation rate constants are assigned to  $10^{-3} \text{ s}^{-1}$ , the DNA dissociation rate constants and DNA binding affinities can be derived from  $K_M$  as shown in **Table 4.3**.

The plot of the Mg(II) dependent DNA association rate constants shows a typically sigmoidal shape and can be fitted to Hill equation to yield a Hill coefficient of 3.4, which exhibits the same pattern as Ca(II) (shown in **Figure 4.3**). The derived association rate constant ( $k_1$ ) in the presence of 10 mM Mg(II) is about  $2 \cdot 10^5 \text{ M}^{-1} \text{ s}^{-1}$ , 100 fold lower compared with measured DNA association rate constant ( $2.7 \cdot 10^7 \text{ M}^{-1} \text{ s}^{-1}$ ) at the same concentration of Ca(II) (Conlan & Dupureur, 2002a). This is consistent with the 100 or 50 fold difference in DNA binding affinities for non hydrolysable DNAs at the same concentration of Ca(II) and Mg(II) (Engler, et al., 1997; Martin, et al., 1999a; King, et al., 2004).

The difference in association rate constant on this kind of scale may have a dramatic effect on the kinetics. So instead of using measured Ca(II) dependent DNA association rate constants, the calculated association rate constants from steady state kinetics will be regarded as the best approximation for Mg(II) supported DNA binding and will be used in the global fit of kinetics.

---

**Table 4.3. Estimate Mg(II) dependent DNA association rate.** Measured  $K_M$  and  $k_{cat}$  in the steady state kinetics and estimated  $K_d$  and DNA association rate constants ( $k_{on}$ ) at various Mg(II) concentrations.

Mg(mM)	$K_M$ (nM)	$k_{cat}$ ( $s^{-1}$ )	$k_1$ ( $M^{-1}s^{-1}$ ) estimate	$K_d$ (nM) estimate
10	27	0.0045	2e5	4.9
6.5	65	0.0068	1.2e5	8.3
3	50	0.0035	9e4	11.1
2.5	94	0.0033	4.6e4	21.6
2.25	136	0.0028	2.8e4	35.5
2	170	0.0017	1.6e4	63.8
1.25	74	0.00088	2.6e4	39.3
1	71	0.00022	1.7e4	58.4
0.5	110	3.7E-05	9.4e3	106.1
Metal free	n/a	n/a	3.3e3	300

The  $k_{-1}$  was assumed to be  $0.001 s^{-1}$  and  $k_1$  was estimated from equation  $K_M=(k_{-1}+k_{cat})/k_1$ . All the data in this table were collected by Dr. Qureshi as a former post-doc in the lab.

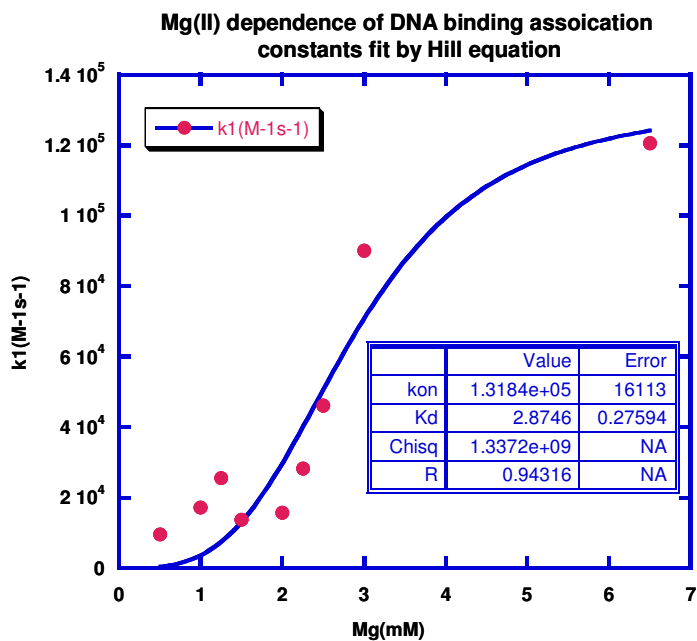


**Figure 4.3.** The Hill analysis of Mg(II) dependence of DNA association rate constants.  $k_1$  in Table 4.3 can be fit to the Hill equation yielding the similar coefficient of 3.4 as presented in Ca(II) binding data (see Figure 4.2).

---

### One vs. Two Chemistry Step

*Experiments.* The Mg(II) dependence of single turnover rate constants shows a typical sigmoidal shape with Hill coefficient of 3.9 (**Figure 4.4**), which indicates that multiple metal ions are involved in specific DNA binding and cleavage by homodimeric *PvuII* endonucleases. However, this is not the direct experimental evidence that *PvuII* really requires two metal binding sites occupied for catalysis to occur (see Introduction of this chapter). In the investigation of Ca(II) dependent DNA association, the pre-reactive complex is described as a mixture of EM<sub>2</sub>S and EM<sub>4</sub>S (**Scheme 4.1**). If both species are catalytically active, it is believed that they might have different turnover rates and involve a reaction scheme with two chemistry steps. If EM<sub>4</sub> is the only active species, the reaction scheme with one chemistry step is suggested, and *PvuII* does requires two metal ions for catalysis. Here we will address the number of metal ions required in *PvuII* active site for catalysis by proposing the following new reaction scheme.

*Reaction Scheme.* **Scheme 4.2** describes all the possible reaction pathways in Mg(II) dependent single turnover kinetics. The preference of apo enzyme binding to cognate DNA or metal ions is given serious consideration among those candidate models. Besides the examination of binding order preference, one turnover step supported by EM<sub>4</sub>S or two turnover steps supported by EM<sub>2</sub>S and EM<sub>4</sub>S are distinguished into groups A and B. Each candidate model is named after the reaction pathway and its turnover steps belonging to group A or B. Reaction

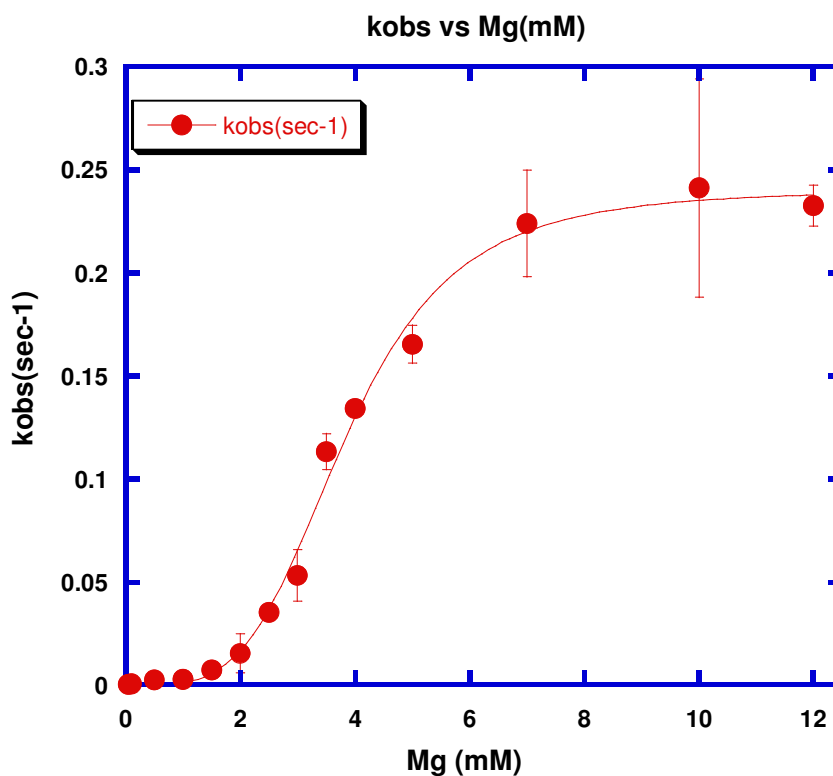
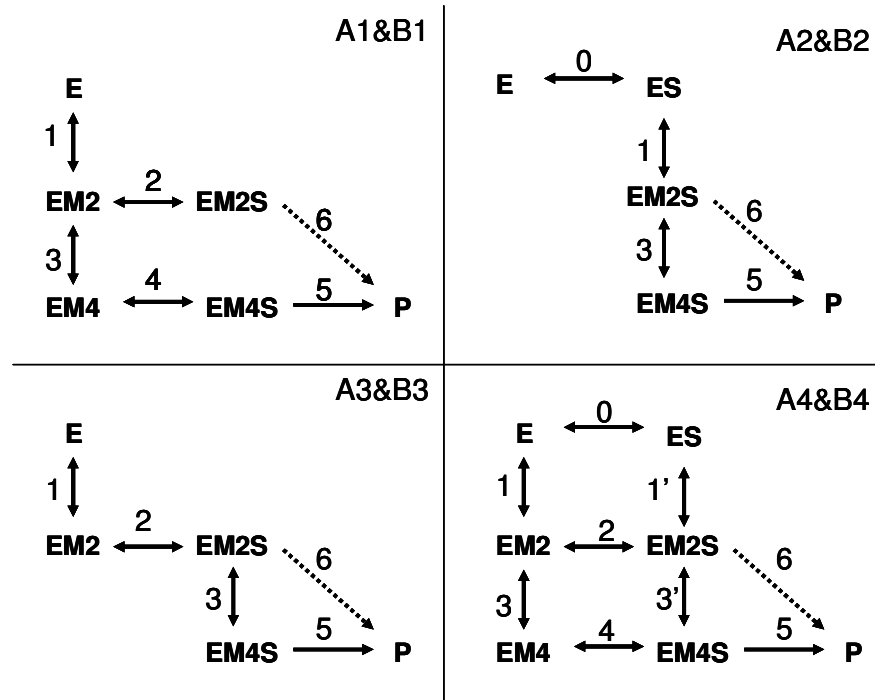


**Figure 4.4. Dependence of single turnover rate constants on metal ion concentrations.** The conditions were 50 mM Tris, pH 7.5 at 37 °C. The NaCl concentration was adjusted to a constant ionic strength of 125 mM according to Mg(II) concentration. Below 3.5 mM MgCl<sub>2</sub>, reaction courses were monitored manually at 37 °C with 2 μM enzyme and 300 nM 14-mer duplex (The rate constants were provided by Greg Papadakos). Above 3.5 mM MgCl<sub>2</sub>, rate constants were measured by quench flow using the same reaction conditions. The Hill coefficient of 4 is yielded by the fit shown in the plot.



**Scheme 4.2. Proposed candidate kinetic models for global fits to Mg(II) dependent single turnover progressive courses.** Eight candidate models from A1 to A4 with one turnover step ( $k_5$ ) and B1 to B4 with two turnover steps ( $k_5$  &  $k_6$ ) depending on four reaction pathways. Note: double arrow represents equilibrium in the scheme including two kinetic parameters (e.g.  $k_1$  and  $k_{-1}$ ) and single arrow represents turnover step ( $k_5$  or  $k_6$ ). The units of those rate constants are given in results. The dashed line indicate the chemistry step ( $k_6$ ) only exist in group B candidate models.

---

pathway 4 is the most comprehensive one including all possibilities. In reaction pathway 1, metal binding is obligated to occur prior to DNA binding and the binding order is the opposite in reaction pathway 2. Pathway 3 obligates DNA binding prior to the second metal ion binding event. **Scheme 4.2A** shows all the eight candidate models. In candidate model A1, it appears that EM<sub>2</sub>S become a dead end complex due to its inactivity. In model B1, it looks unnecessary for this modification since the presence of model B4. Finally eight candidate models are examined in global fits to single turnover reactions courses as a function Mg(II) concentrations.

*Global fits.* In **Scheme 4.2**, it is obvious that each kinetic model contains at least two metal ion association rate constants (k1 and k3) and two DNA association rate constants (k2 and k4) plus their corresponding dissociation rate constants. The measurements of DNA association rate constants are easier and more reliable than measurements of metal ions dissociation rate constants. To reduce the unknown kinetic parameters in the global fits, DNA association rate constants (k2 and k4), dissociation rate constants (k-2 and k-4) and metal ion dissociation rate constants (k-1 and k-3) are fixed in the global fits while metal ion association rate (k1 and k3) and turnover rates (k5 and k6) were floating to derive the best fit results. The DNA dissociation rate constants (k-2 and k-4) are measured experimentally (see **Table 4.2**) and assigned to 10<sup>-3</sup> s<sup>-1</sup> (Conlan & Dupureur, 2002a). The association rate constant for each species can be calculated if the DNA binding affinity is known, which is estimated from the K<sub>M</sub> of Mg(II) dependent steady state velocities (see **Table 4.3**). The DNA binding association rate constants are calculated from K<sub>d</sub> (around 300 nM)

---

for apo enzyme under metal free conditions and  $K_M$  (**Table 4.3**) of steady state kinetics for  $EM_4$  when the metal ions were saturated. Theoretically the DNA association rate constant ( $k_2$ ) for  $EM_2$  could take any values between estimated binding rates under metal free and 10 mM Mg(II) in **Table 4.3**. DNA association rate constants of  $EM_2$  is particularly important in deriving the second turnover step and might have a dramatic effect on discriminating one vs. two chemistry step models. Two separate global fit trials have been conducted to address this rate constant. Therefore,  $k_2$  as the DNA association rate constant for  $EM_2$  is assigned to be  $1 \cdot 10^4 \text{ M}^{-1}\text{sec}^{-1}$  in trial 1 (lowest limit under metal free conditions) and  $1 \cdot 10^5 \text{ M}^{-1}\text{sec}^{-1}$  in trial 2 (highest limit under saturated Mg(II) conditions). And  $k_4$  for  $EM_4$  is assigned as  $2 \cdot 10^5 \text{ M}^{-1}\text{sec}^{-1}$ , which is the apparent DNA binding rates estimated at 10 mM Mg(II).

The dissociation rate constants ( $k_{-1}$  and  $k_{-3}$ ) for metal ion binding (see **Table 4.4**) ranges from several hundred  $\text{s}^{-1}$  to a few thousand  $\text{s}^{-1}$  with various enzymes and metal species (Ca(II) and Mg(II)). To simplify our kinetic models, the dissociation rate constants for metal binding are fixed at  $1000 \text{ s}^{-1}$ . The floating kinetic parameters include turnover steps and Mg(II) binding association rate constants ( $k_1$  and  $k_3$ ) for species apo E, ES,  $EM_2$  and  $EM_2S$ .

In global fit with candidate models A4 and B4, apo E and ES are assigned to the same metal binding association constant to simplify the model, as well as  $EM_2$  and

---

**Table 4.4. The dissociation rate constants for metal ion binding.**

<b>Enzyme</b>	<b>Metal ion</b>	<b>Rate constants (sec<sup>-1</sup>)</b>
Calmodulin <sup>a</sup>	Mg(II)	k <sub>off</sub> =2700 for strong site k <sub>off</sub> =6600 for weak site
Enolase <sup>b</sup>	Mg(II)	1/T <sub>2</sub> =4000
Pyruvate kinase <sup>b</sup>	Mg(II)	1/T <sub>2</sub> =2200
Phospholipase A <sub>2</sub> <sup>c</sup>	Ca(II)	k <sub>off</sub> =1000
PPLA <sub>2</sub> <sup>c</sup>	Ca(II)	k <sub>off</sub> =3000
Troponin C <sup>d</sup>	Ca(II)	k <sub>off</sub> =600
Troponin C <sup>e</sup>	Mg(II)	k <sub>off</sub> =4000
Parvalbumin <sup>f</sup>	Ca(II)	k <sub>off</sub> >3*10 <sup>5</sup>

a. (Tsai, et al., 1987)

b. (Lee & Nowak, 1992)

c. (Andersson, et al., 1981; Drakenberg, et al., 1984)

d. (Braunlin, et al., 1985)

e. (Forsen, et al., 1983)

f. (Andersson, et al., 1982)

---

EM<sub>2</sub>S. However, there is evidence that substrate can potentially influence the metal binding affinity due to direct metal-phosphate contact observed in *PvuII* crystal structures and possible active site conformational changes caused by substrate binding (Jose, et al., 1999; Horton & Cheng, 2000; Dupureur, 2005). Special care has been taken in handling metal binding affinities of apo E and ES since they are probably different and are yet not characterized quantitatively. Candidate models A4 and B4 in **Scheme 4.2** contain the closed thermodynamic box for the formation of EM<sub>n</sub>S (E->ES->EM<sub>n</sub>S or E->EM<sub>n</sub>->EM<sub>n</sub>S, n=2 or 4). In such a closed thermodynamic cycle, the overall change of binding free energies regardless of the binding pathway should be the same and therefore the following equation is expected:  $K_1 * K_2 = K_0 * K_1'$ ,  $K_3 * K_4 = K_2 * K_3'$ . As mentioned above, in the global fits with model A4 and B4, the same metal association rate constants are floating for apo E/ES (k<sub>1</sub>) and EM<sub>n</sub>/EM<sub>n</sub>S (k<sub>3</sub>) species. To fulfill the binding constants relations based on thermodynamic equations described above, the metal dissociation rate constants (k<sub>1</sub>' and k<sub>3</sub>') for ES and EM<sub>n</sub>S are adjusted from 1000 s<sup>-1</sup> by multiplying by the factor K<sub>2</sub>/K<sub>0</sub> and K<sub>4</sub>/K<sub>2</sub>. As described above, K<sub>0</sub> and K<sub>4</sub> are fixed as 300 nM and 5 nM, respectively. K<sub>2</sub> is assigned to 100 nM in trial 1 and 10 nM in trial 2. The detailed assignments for all those kinetic parameters are listed in the notes of **Table 4.5**.

In the global fit, the data sets are original single turnover reaction time courses at various Mg(II) concentrations. They were selected to best reflect the determined average single turnover constants. The data have been collected by rapid quench

**Table 4.5. Global fit results with single turnover reaction courses as a function of Mg(II) concentrations.**

A. Comparison of standard deviation and error status of floating rate constants for all the kinetic models

Model	Trial 1 error status					Trial 2 error status				
	Standard deviation *10 <sup>-8</sup>	k1 (%)	k3 (%)	k5 (%)	k6 (%)	Standard deviation *10 <sup>-8</sup>	k1 (%)	k3 (%)	k5 (%)	k6 (%)
A1	2.78	31	22	13	n/a	2.88	62	57	9.4	n/a
A2	11.5	>500	>500	>500	n/a	11.5	>500	>500	>500	n/a
A3	8.36	23	>500	>500	n/a	3.30	5.3	>500	>500	n/a
A4	2.83	350	340	12	n/a	2.86	150	140	12	n/a
B1	2.19	16	8.3	20	34	2.11	9.6	10	13	22
B2	11.5	>500	>500	>500	>500	11.5	>500	>500	>500	>500
B3	8.36	20	>500	>500	>500	3.3	5.2	>500	>500	>500
B4	2.87	170	160	14	>500	2.85	150	140	13	>500

B. Comparison of best fit for model A1, A4, B1 and B4.

Model	A1	A4	B1	B4
<b>Kinetic parameters floating in global fits in trial 1</b>				
<b>k1 (M<sup>-2</sup>s<sup>-1</sup>)</b>	6.2e7	2.4e6	1.4e8	5.9e6
<b>K<sub>d</sub> 1(mM)</b>	4.0	20.6	2.72	13.0
<b>k3 (M<sup>-2</sup>s<sup>-1</sup>)</b>	1.2e8	8.0e8	5.0e7	3.6e8
<b>K<sub>d</sub> 3(mM)</b>	2.9	1.1	4.5	1.7
<b>k5 (s<sup>-1</sup>)</b>	0.74	0.62	1.9	0.66
<b>k6 (s<sup>-1</sup>)</b>	n/a	n/a	0.0095	1e-7
<b>Kinetic parameters floating in global fits in trial 2</b>				
<b>k1 (M<sup>-2</sup>s<sup>-1</sup>)</b>	2.0e6	2e6	1.6e7	1.7e6
<b>K<sub>d</sub> 1(mM)</b>	22	22.3	7.9	24.1
<b>k3 (M<sup>-2</sup>s<sup>-1</sup>)</b>	2.8e9	1e9	2.3e8	1.1e9
<b>K<sub>d</sub> 3(mM)</b>	0.59	1.0	2.1	1
<b>k5 (s<sup>-1</sup>)</b>	0.53	0.6	1.1	0.65
<b>k6 (s<sup>-1</sup>)</b>	n/a	n/a	0.02	1e-7

Error status about floating rate constants is shown in table A.

Note: in the global fits, fixed parameters include:

DNA binding dissociation rates k-0, k-2, and k-4 are all assigned to be 0.001 s<sup>-1</sup>.

Metal ion binding dissociation rates k-1, k-3 are all assigned to be 1000 s<sup>-1</sup> in all trials;

For model A4 and B4 which involved k1' & k3' and k-1' & k-3', k1 equals to k1' and k3 equals to k3'; k'-1 and k'-3 are assigned to be 333.3 s<sup>-1</sup> and 50 s<sup>-1</sup> in trial 1, 33.33 s<sup>-1</sup> and 500 s<sup>-1</sup> in trial 2, respectively.

---

methods and conducting reactions manually. For those data sets collected manually, a mixing time of 1.5 seconds as delay time is used in the global fit using Dynafit.

The **Table 4.5** listed all the results including error status. In addition to evaluating errors, the best fits were used to derive the single turnover constants, which are plotted as a function of Mg(II) concentrations (**Figure 4.5A**). At low Mg(II) concentrations of 0.1 and 0.5 mM Mg(II), the single turnover rate constants can not be derived since time course only cover 900 seconds and during this short time range the reaction is not completed yet. The global fits of reaction time courses are directly plotted to visualize the fit quality (**Figure 4.5B**).

*Conclusion.* According to error status listed in **Table 4.5A**, obviously model A2, A3, B2 and B3 can be ruled out as the kinetically favorable models since their error status is far higher than others. This indicates that apo-enzyme prefers binding metal ions prior to DNA (model A2 and B2) and proceeds via the EM<sub>2</sub> (model A3 and B3). Although it can not be completely ruled out, the ES complex binding metal ions to form the active species is at least not the major pathway. The smaller deviations from model A1 and B1 also confirm the postulated reaction pathway of enzyme binding metal ions as prior to the DNA association. Results with models A4 and B4 can determine if a random binding mechanism will improve the fit quality. Theoretically, fitting quality generally can be improved by increasing model complexity by introducing more reaction pathways and more kinetic parameters. In this case, the fitting quality of models A4 and B4 did not improve compared with models A1 and B1 (see deviations of those models in **Table 4.5A**). In **Table 4.5A**,

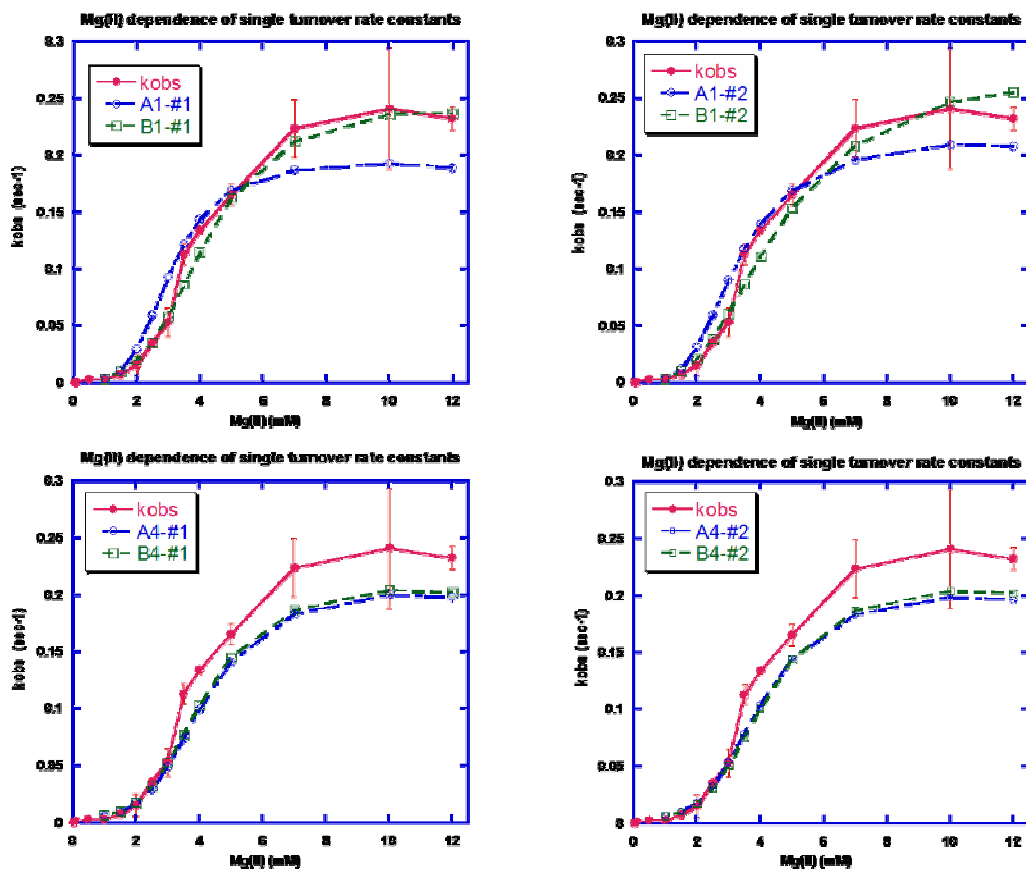


**Figure 4.5 A.** Simulated  $Mg(II)$ - $k_{obs}$  profiles from the best fit based on model A and B are plotted with experimental  $Mg(II)$  - $k_{obs}$  profile. The compared models are indicated at the right corner of each plot. The experimental  $k_{obs}$  against  $Mg(II)$  concentrations are shown in solid line and solid circle, the simulated  $k_{obs}$  against  $Mg(II)$  concentrations are indicated in dashed line, models in group A and B are shown in empty circle and square, respectively. All the simulated  $k_{obs}$  are derived from the progress curves in the same global fit as shown in **Table 4.5**.

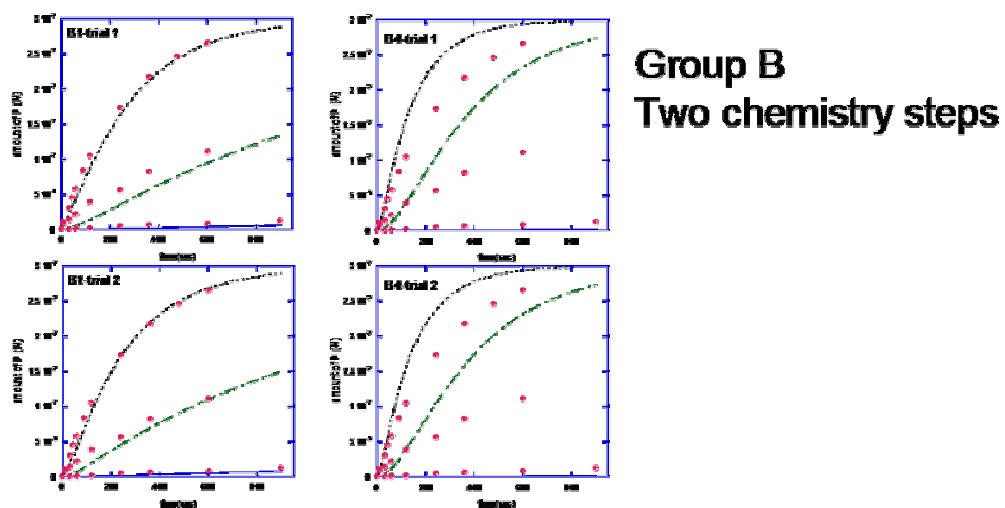
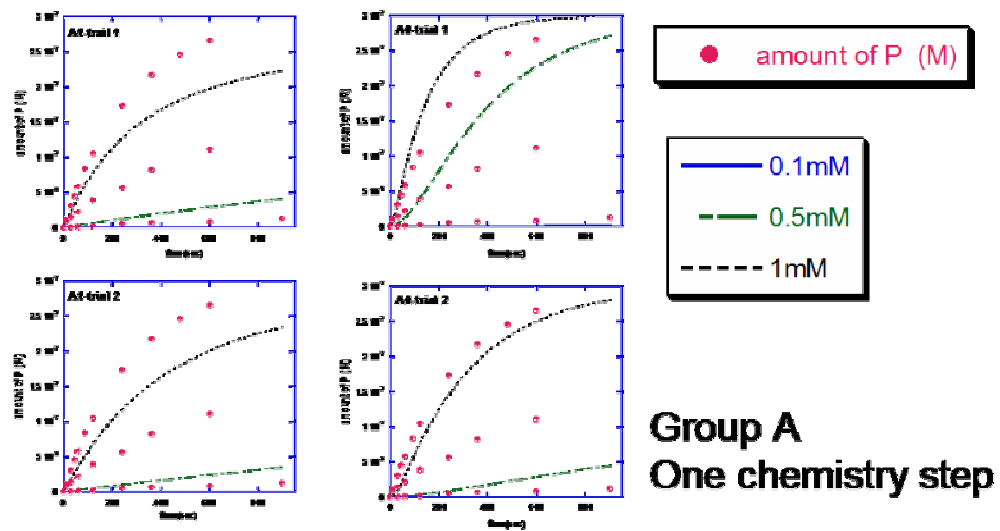


**Figure 4.5 B.** Global fits of single turnover time courses at 0.1, 0.5 and 1 mM Mg(II). Partial single turnover progress curves at 0.1, 0.5 and 10 mM Mg(II) are shown to examine the fit qualities of candidate models in group A and B. The simulated progress curves are from the same global fit as shown in **Table 4.5**.

---

standard deviation of model B1 is the smallest but is at the similar to models A1, A4 and B4. The errors status of floating kinetic parameters shows that B1 generates the smallest error. Besides model B1, Model A1 and A4 mostly give errors for unknown kinetic parameters below 50%.

In **Table 4.5B**, some best fit metal ion binding affinities of models A1, A4 and B4 reach as high as 20 or 50 mM, which is not reasonable. The derived metal ion binding affinity of model B1 is always below 10 mM, regardless of the trials. This can be demonstrated by the introduction of alternative reaction pathways. The metal ion binding affinities basically is dictated by the portion of apo E and its metal bound form. In models A4 and B4, the  $EM_nS$  complex can be formed by the alternative path not including  $EM_n$  so that the derived apparent portion of  $EM_n$  is less than that derived from model B1. Therefore, the apparent metal ion binding affinities increase as a result of that. In **Table 4.5**, it could be concluded that model B1 is the best model. It is also noteworthy that the metal binding affinities below 10 mM are consistent with that obtained from the Hill equation (**Figure 4.9**).

The quality of the global fits can also be visualized in the fits of reaction time courses and reproduced  $Mg(II)-k_{obs}$  plots. **Figure 4.10A** compares the reproduced  $Mg(II)-k_{obs}$  plots by global fits with two groups of models A and B in trial 1 and trial 2. First of all, although DNA binding rates of  $EM_2$  ( $k_2$ ) differ by 10 fold in trial 1 and trial 2, two chemistry models (group B) always show a better agreement than one chemistry step models (group A). While models A4 and B4 appear similar, the difference between A1 and B1 in both trials is dramatic. B1 shows a better

---

agreement at both high and low Mg(II) compared with A1. Except in the transition region near 3.5 and 4 mM Mg(II), the predicted  $k_{\text{obs}}$  are slower than determined experimentally; others fits reproduced experimental single turnover rate constants quite well. Models A1 in the plot shows an obvious shift towards the left at low metal concentrations and a lower plateau at high metal concentrations related to experimental data. This indicates that for one chemistry step model, it is hard to find a turnover rate which satisfies both apparent enzymatic activities at high and low metal concentrations. The model B1 introducing with two chemistry steps solves this problem easily. In **Figure 4.5B**, the global fits of time courses for 0.1, 0.5 and 1 mM Mg(II) were directly plotted and divided by group A (one chemistry step) and group B (two chemistry steps). Obviously the group B global fits are dramatically better than group A since all models in group A show large deviations from experimental data. In particular, model B1 shows an even better fitting quality than model B4. It can be concluded from this analysis that model B1 is the best model.

**Table 4.5B** gives the turnover rate for EM<sub>2</sub>S (for model B1,  $k_6$  is 0.009 s<sup>-1</sup> in trial 1 and 0.02 s<sup>-1</sup> in trial 2). Compared with first turnover step by EM<sub>4</sub>S ( $k_5$ ), this is almost 2 orders of magnitude slower. However, the difference between trial 1 and trial 2 is not enough to change the final conclusion that model B1 is the best model. The DNA association rate constant ( $k_2$ ) did make quite some difference on the turnover rate constant. With a 10 folder slower DNA association rate constant ( $k_2$ ) in trial 1 ( $1 \cdot 10^4 \text{ M}^{-1}\text{s}^{-1}$ ) compared with trial 2 ( $1 \cdot 10^5 \text{ M}^{-1}\text{s}^{-1}$ ), a 2 fold faster turnover rate constant are obtained and appears to impact  $k_5$  and  $k_6$  similarly. It is interesting

---

that the ratio of  $k_5/k_6$  is about 100 and remains unchanged while DNA association rate constants change. In an attempt to apply Ca(II) dependent DNA association rate constants (derived from DNA binding constants in **Table 4.1** and 100 fold faster than Mg(II)) to the same kinetic model B1, a much lower turnover rate of  $0.28 \text{ s}^{-1}$  ( $k_5$ ) was obtained (data not shown). This is consistent with what is observed in **Table 4.5B**. The DNA association rate constant does affect the turnover rate constant in the global fit until it is fast enough to be ignored. Reaction conditions such as enzyme and substrate concentrations should be elevated to achieve the rapid binding, although this may not affect Mg(II) dependence on the apparent activity. It seems that our reaction conditions are not the optimal to reach maximal activity. With  $5 \text{ }\mu\text{M}$  enzyme and unchanged DNA concentration, a single turnover rate constant ( $0.47 \text{ s}^{-1}$ ) at  $10 \text{ mM}$  Mg(II) has been determined, which is higher than  $0.24 \text{ s}^{-1}$  measured with  $2 \text{ }\mu\text{M}$  enzyme at  $10 \text{ mM}$  Mg(II).

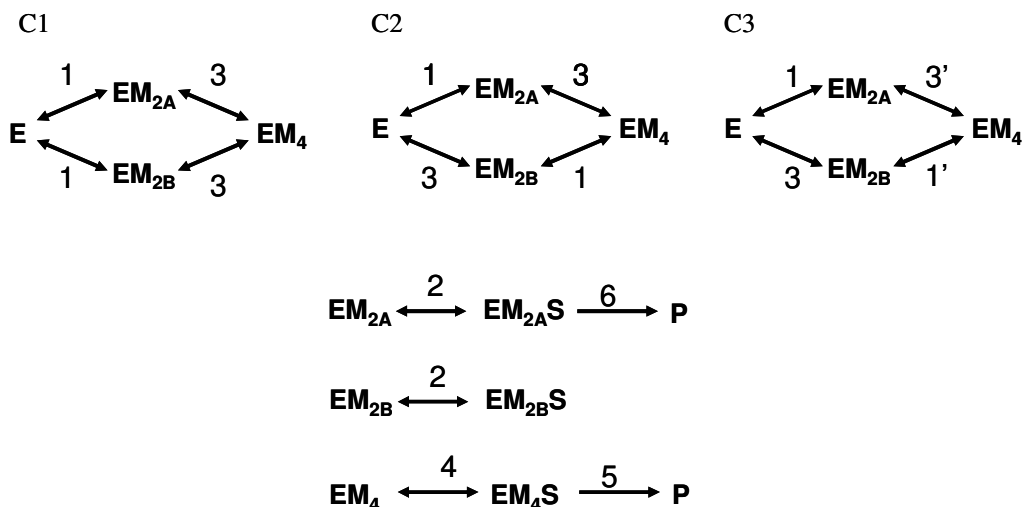
#### **Dissection of Two Metal Binding Sites (A and B).**

As shown in last section, the global fits with **Scheme 4.2** finally suggest one-metal ion catalysis is possible but slow and that a sequential binding model in which metal ions bind prior to DNA. Two metal binding sites are identified distinctively in the *PvuII* crystal structure bound to cognate DNA (Horton & Cheng, 2000). Those two sites probably are not functionally equivalent in DNA binding and cleavage, which has been discussed in the introduction of this chapter. Since there are few experiments to characterize two sites distinctively, it would be interesting to model two distinct sites in global fits and derive their metal ion binding affinities and

---

cooperativity between those sites.

*Reaction Scheme.* All the candidate kinetic models shown in **Scheme 4.2** assume that metal binding occurs in a sequential way without distinguishing two metal binding sites A and B. Site A and site B can only be distinguished if the first metal binding results in two different binary complexes ( $EM_{2A}$  and  $EM_{2B}$ ) as shown in **Scheme 4.3** but the second metal binding step results in the same  $EM_4$  complex as in **Scheme 4.2**. The computational studies on *BamHI* indicate that site A seems more catalytically critical than site B (Mones, et al., 2007c). So in **Scheme 4.3**, the complex  $EM_{2A}S$  is regarded catalytically active but  $EM_{2B}S$  inactive. Since the kinetic model B1 with two chemistry steps has been accepted to be the best (concluded from last section), replacing  $EM_2$  with  $EM_{2A}$  and  $EM_{2B}$  generates new kinetic models which examine the cooperativity between site A and B. All  $EM_2$  related steps and parameters are unchanged and diverted to  $EM_{2A}$  and  $EM_{2B}$  except turnover step 6 which is specified for  $EM_{2A}S$ . Depending on properties of site A and B (equivalent or non equivalent) and their interactions (independent or interacting), three candidate models C1 (equivalent and interacting), C2 (non equivalent and independent) and C3 (non equivalent and interacting) are examined, and each contains two trials. The assignments are the same as in **Table 4.5**: 100 nM in trial 1 and 10 nM in trial 2 for DNA binding affinity of  $EM_2$ .



**Scheme 4.3. Proposed candidate models to dissect two metal binding site A and site B.** Model C1, C2 and C3 have the same DNA binding and turnover steps indicated by lower panel but are different in the properties of two sites. Two sites are equivalent or not depending on the binding constants of site A and B with E. Two sites are interacting or independent depending on the binding constants with E and  $\text{EM}_2$  at the same site. According to the assignments of  $k_1$  and  $k_3$ , C1 is two site equivalent and interacting model, C2 is two site non equivalent and independent model, C3 is two site no equivalent and interacting model. In model C1 and C2,  $k_1$  and  $k_3$  are metal association rate constants and floating in the global fits. In model C3, metal association rate constants  $k_1$  and  $k_3$  are equal to  $k_1'$  and  $k_3'$ , respectively, but the dissociation rate constants for step 1' and 3' ( $k_{\text{off}}$ ) are treated as unknown parameters in the global fits, unlike  $k_{-1}$  and  $k_{-3}$  given as  $1000 \text{ s}^{-1}$ .

---

*Global Fits.* Mg(II) dependent single turnover reaction courses are globally fit to three kinetic model candidates, and each contains two trials assuming the DNA binding affinity of EM<sub>2A</sub> and EM<sub>2B</sub> (they have the same binding affinities) are 10 nM in trial 1 and 100 nM in trial 2. The error status and derived kinetic parameters are summarized in **Table 4.6A** to demonstrate the qualities of those global fits. **Table 4.6B** summarizes the derived metal binding affinities of two distinctive sites and their cooperativity. The interaction factor (**Table 4.6B**) is introduced in order to discuss the cooperativity of two metal binding sites. The interaction factor is defined as  $K_{BA}/K_A$  or  $K_{AB}/K_B$ , and  $K_A$  is the metal binding affinity of site A in apo enzyme and  $K_{BA}$  is still the site A metal binding affinity when site B is pre-occupied. The same applies for site B. According to **Scheme 4.3**, the interaction factor is  $K_{d3}/K_{d1}$  in model C1 and 1 in model C2. For model C3, the interaction factor actually is determined by comparing the derived  $k_{off}$  (dissociation rate constant for step 1' and 3') and  $1000 \text{ s}^{-1}$  (dissociation rate constant for step 1 and 3) since those steps have the same metal association rate constants ( $k_1$  and  $k_3$ ). The interaction factor value larger than 1 reflects the negative cooperativity between two sites; a value below 1 reflects positive cooperativity. The criteria to evaluate those models focus on the standard deviations for the global fits and the obtained metal binding affinities.

**Table 4.6. The investigations of two distinct sites on metal binding properties and cooperativity.** Fixed kinetic parameters are the same as in **Table 4.5**, please refer to its note for detailed information.

A. The derived kinetic parameters with % error from global fits.

Model	Trial	k1 (M <sup>-2</sup> s <sup>-1</sup> )	k3 (M <sup>-2</sup> s <sup>-1</sup> )	k5 (s <sup>-1</sup> )	k6 (s <sup>-1</sup> )	k <sub>off</sub> (s <sup>-1</sup> )
C1	1	8.41e7 (19%)	1.00e8 (9.6%)	1.48 (19%)	0.02 (96%)	n/a
	2	8.58e5 (16%)	5.85e8 (15%)	0.79 (12%)	0.049 (94%)	n/a
C2	1	1.63e8 (17%)	5.19e7 (11%)	4.6 (41%)	0.01 (47%)	n/a
	2	3.40e8 (26%)	1.89e8 (15%)	0.79 (17%)	0.01 (36%)	n/a
C3	1	1.41e8 (16%)	2.27e7 (71%)	3.48 (32%)	0.01 (47%)	446 (64%)
	2	1.63e7 (10%)	2.78e6 (37%)	1.06 (13%)	0.03 (29%)	11.27 (38%)

B. Calculated metal binding affinities for two sites and interaction factor.

Model	Trial	Stand deviation *10 <sup>8</sup>	K <sub>A</sub> (mM)	K <sub>B</sub> (mM)	K <sub>BA</sub> (mM)	K <sub>AB</sub> (mM)	Interaction factor
C1	1	2.35	3.45	3.45	3.14	3.14	0.91
	2	2.49	10.79	10.79	1.31	1.31	0.12
C2	1	2.21	2.48	4.40	2.48	4.40	1
	2	3.68	1.71	2.30	1.71	2.30	1
C3	1	2.18	2.67	6.64	1.78	4.43	0.67
	2	2.10	7.84	18.90	0.83	2.01	0.11

The interaction factor is defined as  $K_{BA}/K_A$  or  $K_{AB}/K_B$ .  $K_A$  is the metal binding affinity of site A in apo enzyme and  $K_{BA}$  is still the site A metal binding affinity when site B is pre-occupied. The same rule works with site B.  $K_A$ ,  $K_B$ ,  $K_{AB}$  and  $K_{BA}$  are defined according to **Scheme 4.3** and definitions vary depending on models.

---

Like **Figure 4.5**, the derived apparent single turnover rate constants from those global fits are also plotted together with experimental data (**Figure 4.6**). Since global fits never generate a negative cooperativity scenario for **Scheme 4.3**,  $k_{\text{off}}$  of  $3000 \text{ s}^{-1}$  is obligated so that the interaction factor of model C3 will be above 1 and C3 became a two site non equivalent model with negative cooperativity. The global fit with such a model generates the simulated Mg(II)-rate plot which is also shown in **Figure 4.6** and does not agree well with experimental data.

*Comments.* Model C1 assumes two metal binding sites to have the same metal binding affinities which is supported by the shared metal binding ligands and the very similar geometries of Ca(II) binding sites (Horton & Cheng, 2000). In both trials, model C1 gave the reasonable metal binding affinities (**Table 4.6B**) as well as the turnover steps ( $k_5$  and  $k_6$  in **Table 4.6A**). Model C2 is constructed based on two independent sites. According to standard deviation shown in **Table 4.6B**, trial 1 improves a little bit compared with model C1 but with a much higher turnover step for EM<sub>4</sub>, which is in doubt since no kinetic experiments show such a high apparent turnover rate ( $k_5$  **Table 4.6A**). Trial 2 actually is a bad fit since its standard deviation is the highest in **Table 4.6B**. Therefore, model C2 seems to be unlikely to be selected as the most favorable model. Model C3 is another reasonable model which fits well according to standard deviations in both trials; however, the metal binding affinities derived from trial 2 seems to be out of the range ( $>10 \text{ mM}$ ).

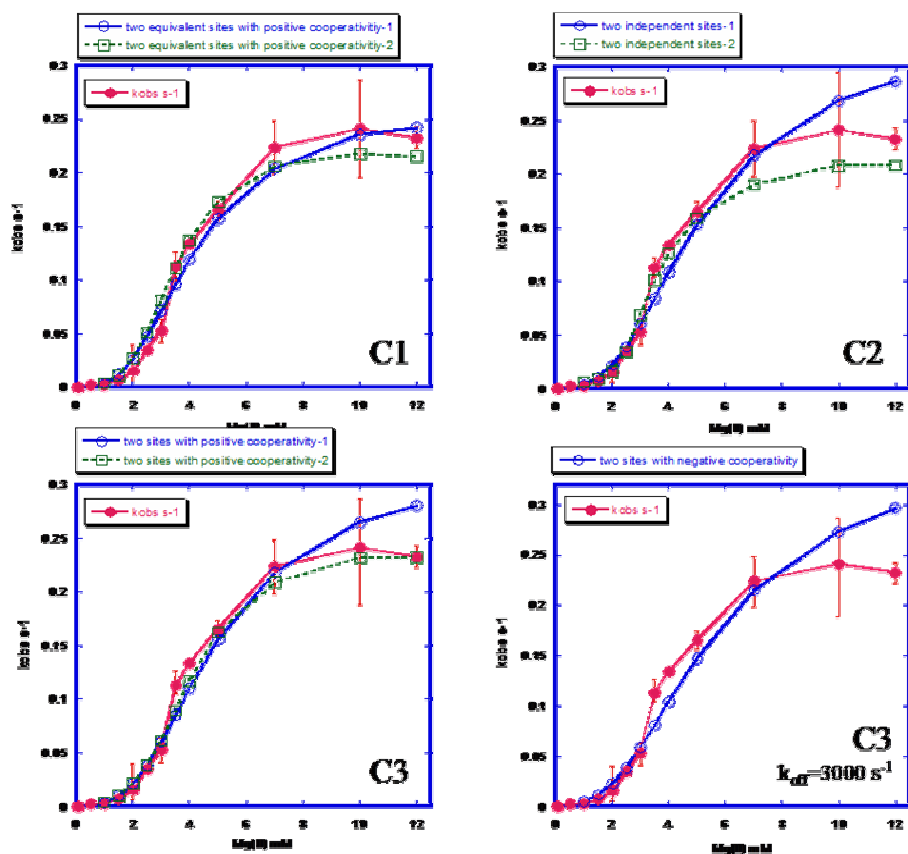


**Figure 4.6.** Simulated Mg(II)- $k_{\text{obs}}$  profiles from the best fit based on model C1, C2 and C3 are plotted with experimental Mg(II)- $k_{\text{obs}}$  profile. The models are indicated at the right corner of each plot. The experimental  $k_{\text{obs}}$  against Mg(II) concentrations are shown in solid line and solid circle, the simulated  $k_{\text{obs}}$  against Mg(II) concentrations are indicated in dashed line, models in two trials are shown in empty circle and square, respectively. The first three panels are corresponding to model C1, C2 and C3 shown in **Table 4.6**. The global fit of last panel is not shown here and the  $k_{\text{off}}$  is obligated to be  $3000 \text{ s}^{-1}$  and other parameters are set the same as model C3 trial 2.

---

Except model C2 (non interactions between two sites), the best global fits to model C1 and C3 both gave positive cooperativity.

The simulated Mg(II)-rate (**Figure 4.6**) also shows both trials with model C2 do not agree well with experimental Mg(II) dependence. Both trials of model C1 and trial 2 of model C3 agree with experimental data quite well. And obviously model C3 with an obligated negative cooperativity does not look good since it lacks a plateau at high Mg(II) concentration region. The analysis about error status and metal binding affinities based on **Table 4.6** also concludes that model C2 is unlikely to be the best. Since trial 2 of model C3 does not generate the reasonable Mg(II) binding affinities (>10 mM), it seems that model C1 is the best model being tested.

#### **Dissection Mg(II) Dependence On Product Release.**

*Experiments.* Product release steps were investigated by Mg(II) concentration dependence study of steady state kinetic and pre-steady state kinetic parameters. The steady state kinetics data including  $K_M$  and  $k_{cat}$  are shown in **Table 4.3**, which was used to derive the Mg(II) dependent DNA association rate constants. Pre-steady state kinetic time courses show a burst phase at high Mg(II) concentrations (>2 mM) (**Figure 4.7**), which indicates that product release becomes rate-limiting (Sam & Perona, 1999b). At 10 mM Mg(II), the measured single turnover rate ( $0.24 \text{ s}^{-1}$ ) is nearly 2 orders of magnitude faster than the measured steady state rate constant ( $0.0035 \text{ s}^{-1}$ ), which also confirms the product release as the rate limiting step.

It has been proposed from the steady state kinetics study of *MunI* that Mg(II) ions might still remain bound to the enzyme-product complexes after DNA cleavage,

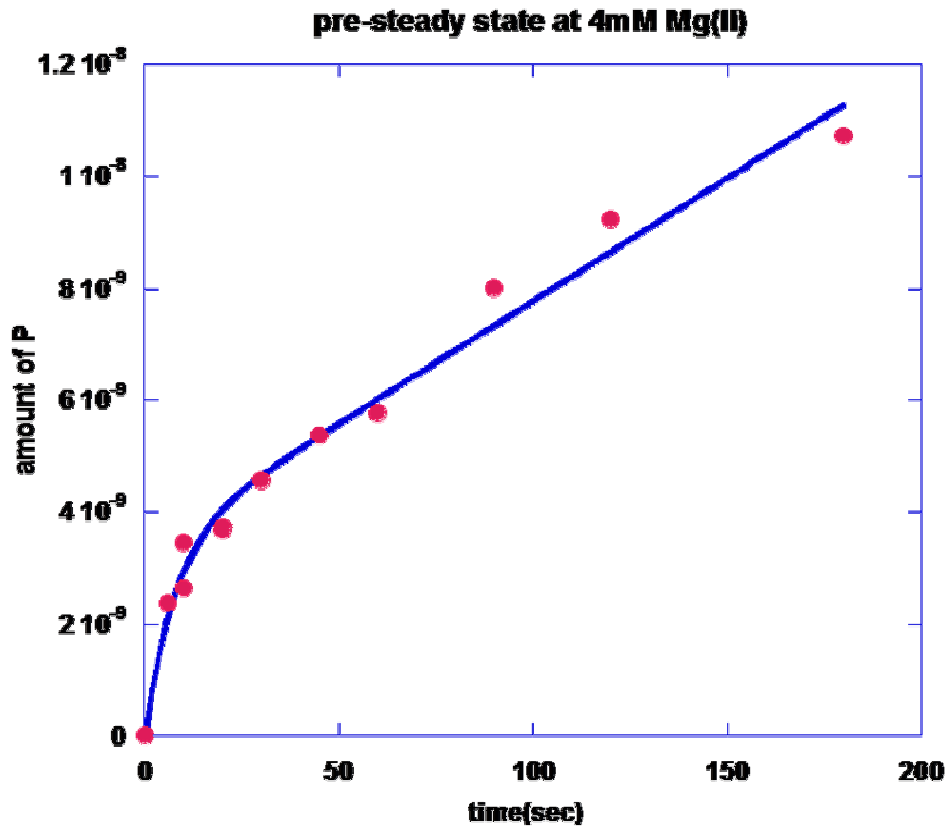


**Figure 4.7. A Typical Burst Phase Observed In Specific DNA Cleavage by *PvuII* Under Pre-Steady State Kinetics Conditions.** 20 nM enzyme and 100 nM cognate 14mer with 4 mM Mg(II), pH 7.5. The ionic strength was adjusted to the same as 100 mM NaCl, 50 mM Tris and 10mM Mg(II). The experimental data were fitted to the typical burst phase equation  $P = A(1 - e^{-k_1 t}) + k_2 t$ ; A is burst phase amplitude, k1 is assigned as  $0.136 \text{ sec}^{-1}$  according to measured single turnover rate constants (average) at 4 mM Mg(II) and k2 is the slope of linear phase.

---

and this probably retards product dissociation (Sasnauskas, et al., 1999). To investigate the possible effects of Mg(II) on product dissociation, the fluorescence anisotropy assay using dansyl labeled 11mer was conducted to monitor the weak interactions between enzyme and product under the metal free conditions or in the presence of high Mg(II) concentrations. The simulated product (a 11mer duplex) is hybridized from complementary oligo strands fx09101 containing CAG-3' hydroxyl group and fx09102 containing 5'phosphate CTG (**Table 2.1**), which reflects the cleavage site configuration of a 14mer used in the cleavage assay. Considering the 5' phosphate as a potential Mg(II) ligand in the post-reactive complex, the non specific 11mer with the same sequence (no phosphate at 5' terminus) was also tested using the same assay. For this non specific 11mer without 5' phosphate, the fluorescence anisotropy increased similarly due to enzyme binding to DNA, regardless the presence and absence of Mg(II) (**Figure 4.8**). For the simulated product 11mer with 5' phosphate it is surprised to observe the weak binding equilibrium ( $K_d > 10 \mu\text{M}$ ) under metal free conditions but obviously this weak binding equilibrium has been perturbed at high Mg(II) concentrations (10 mM). **Figure 4.8** shows the typical enzyme titration curves with 11mer product duplex and non specific 11mer duplex. Except that titration with simulated 11mer product at 10 mM Mg(II) does not show a obvious trend on anisotropy values, the obtained isotherms are used to yield  $K_d$ 's for enzyme binding to product.

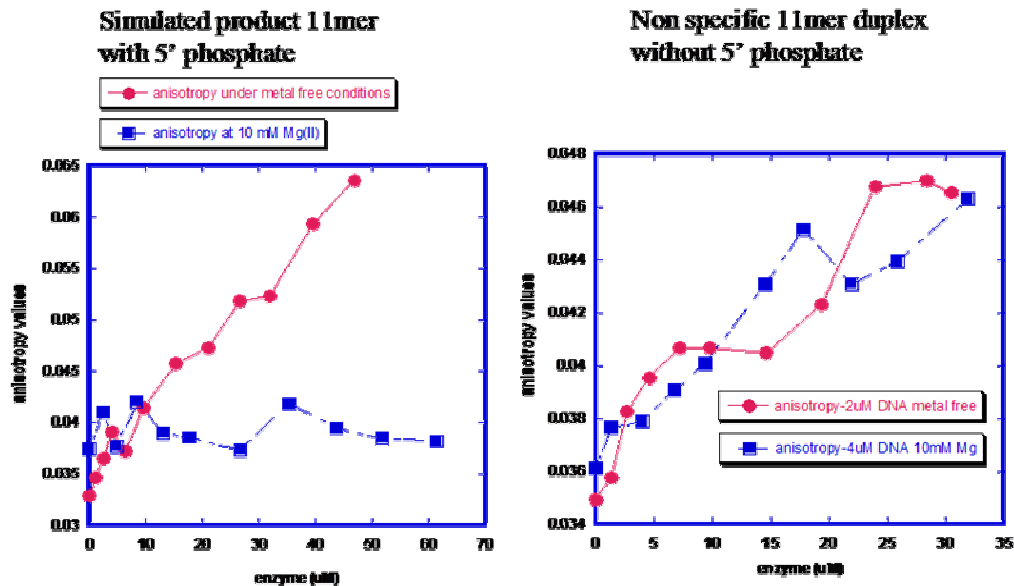


**Figure 4.8. Mg(II) effect on the weak interactions between protein and product using fluorescence anisotropy binding assays.** All the oligos are dansyl labeled. The product 11mer duplex is hybridized from complementary oligo strands fx09101 with CAG-3' hydroxyl group and fx09102 with 5' phosphate CTG. The nonspecific 11mer duplex has the exactly same sequence as product 11mer except without a 5' phosphate. Duplex concentration is 2  $\mu$ M under metal free conditions and 4  $\mu$ M at 10 mM Mg(II). The buffer consists of 125 mM NaCl, 50 mM Tris without Mg(II) or 100 mM NaCl, 50 mM Tris with 10 mM Mg(II). The buffer pH was adjusted to 7.5 at 25  $^{\circ}$ C. Except for the titration with simulated 11mer product at 10 mM Mg(II) (no trend), the obtained isotherms are used to yield  $K_d$ 's for enzyme binding to product. The averaged apparent  $K_d$ 's are about 15  $\mu$ M.

---

*Reaction Scheme.* **Scheme 4.4** features candidate kinetic models to address the product release pathway. Model B1 in **Scheme 4.2** is in good agreement with experimental data and has the least error (see Section One vs. Two chemistry step). Therefore this model with obtained turnover rate constants ( $k_5$  &  $k_6$  in **Table 4.5B**) is selected to generate the new models for the dissection of the product release pathway. Starting with the post-reactive complex  $EM_nP$ , the release of P can occur through  $EM_nP$  (B1-1) or indirectly through an intermediate EP (B1-2) or both. If either B1-1 or B1-2 fits well with experimental data, in theory B1-3 should also fit well as long as one pathway dominates in B1-3.

In the global fits, the metal binding association rate constants ( $k_1$  ad  $k_3$ ) are floating plus introduced product dissociation rate constants ( $k_7$  &  $k_8$ ). In the model B1-2 and B1-3, the product bound enzyme is involved in the metal binding equilibrium, and the corresponding parameters have to be addressed. In order to reduce the number of unknown kinetic parameters, EP ( $EM_2P$ ) are assigned to the same floating metal binding association rate constants as E ( $EM_2$ ) in the global fit. The anisotropy binding experiments (**Figure 4.8**) with simulated product duplex (11mer duplex hybridized from strands fx09101 and fx09102, see Chapter II) shows a weak binding equilibrium between enzyme and product with micromolar binding affinity under metal free conditions. In order to simplify the model, the dissociation of product from EP complex is regarded as an irreversible step with one rate constant ( $k_8$ ) in most of the global fits. Subsequently, trials to replace this step with an



---

equilibrium step (highlighted in dash line in **Scheme 4.4**) including  $k_8$  and  $k_{-8}$  are found to make no difference in the global fit output.

*Global Fits With Steady State Kinetic Data.* Using DynaFit, a single plot of the reaction rates as a function of Mg(II) under steady state conditions has been fitted to two models B1-1 and B1-2, respectively. In the global fit of model B1, two separate trials were conducted regarding DNA binding affinity of EM<sub>2</sub> specie. Those two trials differ in the selection of  $k_2$  value ( $k_2=1*10^4 \text{ M}^{-1}\text{s}^{-1}$  in trial 1 and  $1*10^5 \text{ M}^{-1}\text{s}^{-1}$  in trial 2). The same two trials have been conducted for model B1-1 and B1-2. In model B1-2, the EP (EM<sub>2</sub>P) complex is assumed to have the same metal binding affinity as apo-E (EM<sub>2</sub>), and the same binding rate constants  $k_1$  ( $k_3$ ) are assigned as shown in **Scheme 4.4**. The best fits of model B1-1 and B1-2 in both trials are plotted in **Figure 4.9**.

*Comment on Steady State Kinetics.* In both trials, it is clear that model B1-1 fits much better than model B1-2. The Mg(II)-rate curve generated by the best fit of model B1-1 shows a plateau at Mg(II) concentrations above 5 mM in good agreement with experimental data. The plot of model B1-2 appears to be bell shaped, deviating dramatically from the experimental plot. In the case of model B1-2, the increase of metal concentration increases the amount of active species and speeds up the chemistry step. However, the product release is limited by EP, and the amount of EP is reduced at high metal concentrations in a metal binding equilibrium. Therefore, a bell shaped metal dependence on reaction velocity is expected. It can be concluded

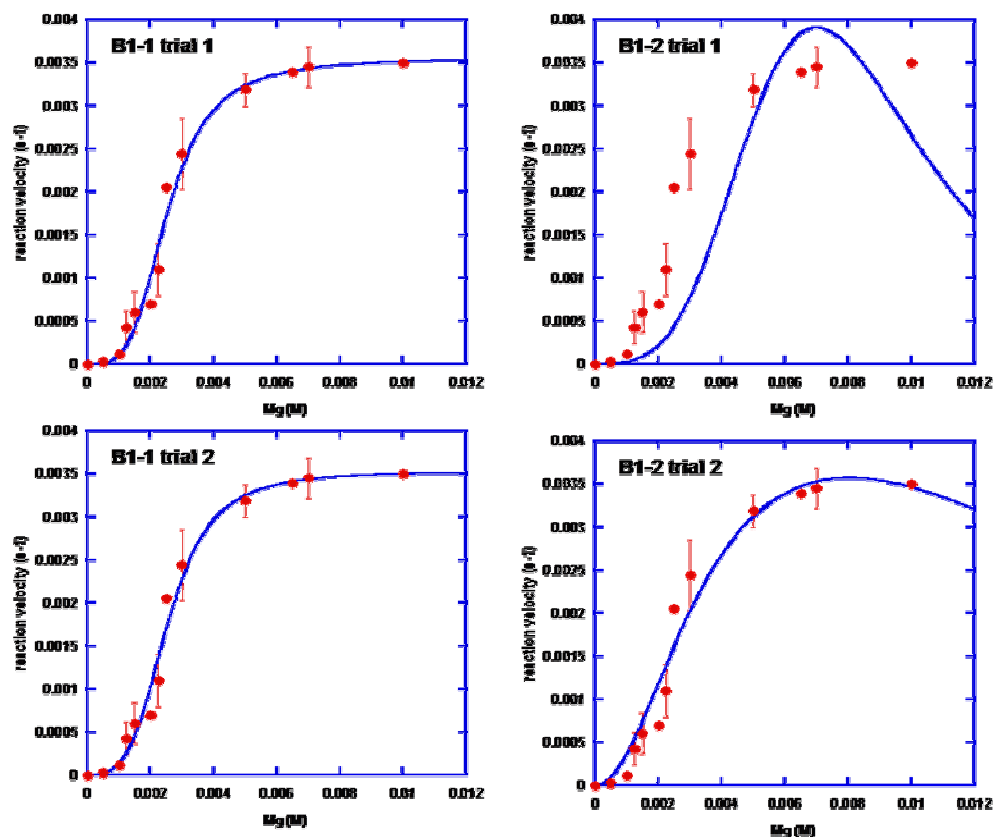


**Figure 4.9.** The best fit to the Mg(II)-steady state velocity profile by two models **B1-1** and **B1-2**. The experimental conditions were 75 nM DNA and 1 or 2 nM enzyme with buffers containing various Mg(II) concentrations. The reactions were usually monitored for about 15 to 20 minutes. The experimental velocities were calculated by the slope of linear phase in the reaction courses and normalized by enzyme concentrations. In global fits, the steady state reaction velocity were calculated when the reaction lasted 500 seconds.

---

that model B1-1 fits better and the product release is independent of the metal dissociation from the active site.

*Global Fits With Pre-steady State Reaction Time Courses.* Both single turnover and multiple turnovers are monitored in the pre-steady state progress curves, indicated by burst phase and linear phase, respectively. The best fit model for single turnover and steady state kinetics should also fit well with pre-steady state kinetic data. A series of progress curves of pre-steady state data have been collected at Mg(II) concentrations from 2 mM to 10 mM with substrate concentrations in at least 5 fold excess over enzyme concentration. Global fits have been performed with this series of pre-steady state progress curves using models B1-1 and B1-2 in **Scheme 4.4**. The assignments of floating and fixed kinetic parameters are the same as described as in steady state kinetics section. The plots of global fits to pre-steady state progress curves are shown in **Figure 4.10**.

*Comments On Pre-Steady State Kinetics.* It is obvious that model B1-1 shows a much better fit quality than model B1-2 regardless of two trials. It can be concluded that model B1-1 is the best model to fit pre-steady state experimental data. The errors status and derived unknown kinetic parameters are summarized in **Table 4.7**. The local fit using model B1-1 with steady state kinetic data shows a higher error status with metal association rate constant ( $k_1$  or  $k_3$ ) than the global fit with pre-steady state kinetic data using the same model. This indicates that global fit can effectively improve the error status when floating multiple kinetic parameters. The

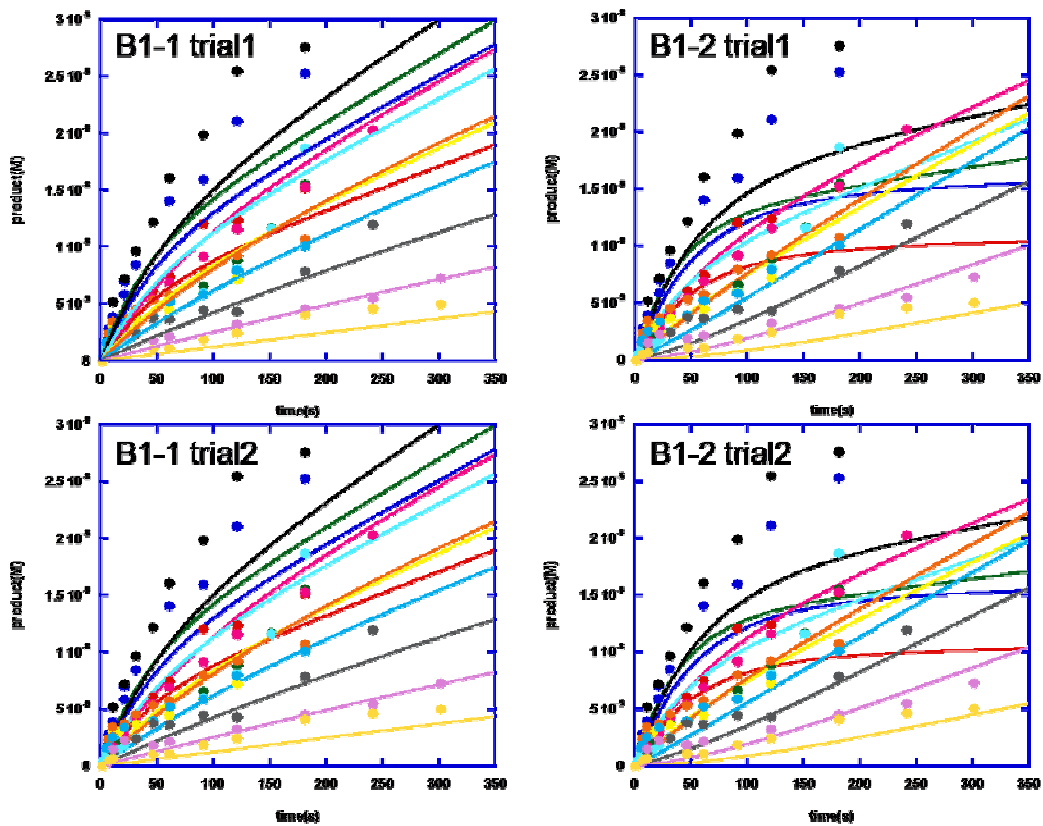


**Figure 4.10. Global fit of pre-steady state time courses under various Mg(II) concentration.** From bottom to top, the experiment data are collected under reaction conditions ( $[E]/[S]$  nM/nM) including 20/100 at 2, 2.5, 3, 4 mM Mg(II), 15/150 and 20/100 at 4, 5 and 7 mM Mg(II), 10/100 and 15/100 at 10 mM Mg(II).

**Table 4.7. The best fit results of steady state and pre-steady state kinetics with model B1-1 and B1-2.**

Model	Steady state kinetics		Pre-steady state kinetics	
	B1-1	B1-2	B1-1	B1-2
<b>Trial 1</b>				
<b>k1 (M<sup>-2</sup>s<sup>-1</sup>)</b>	3.2e7 (170%)	2.5e7 (260%)	4.0e7 (60%)	4.8e6 (610%)
<b>k3 (M<sup>-2</sup>s<sup>-1</sup>)</b>	2.2e8 (160%)	2.9e7 (180%)	5.6e7 (43%)	7.5e8 (600%)
<b>k7/k8<sup>a</sup> (s<sup>-1</sup>)</b>	0.0047 (6.5%)	0.040 (150%)	0.0054 (34%)	0.011 (38%)
<b>Trial 2</b>				
<b>k1 (M<sup>-2</sup>s<sup>-1</sup>)</b>	1.2e7 (130%)	5.4e7 (14%)	1.6e7 (34%)	4.8e6 (290%)
<b>k3 (M<sup>-2</sup>s<sup>-1</sup>)</b>	4.7e8 (150%)	746600 (570%)	7.7e7 (39%)	7.8e8 (290%)
<b>k7/k8 (s<sup>-1</sup>)</b>	0.0047 (4.8%)	0.077 (100%)	0.0062 (30%)	0.0093 (32%)

Percentage errors are indicated in the bracket. As shown in **Scheme 4.4**, k7 is for model B1-1 and k8 is for model B1-2. In those global fits, step 8 is regarded as irreversible step with one kinetic parameter k8, not like in **Scheme 4.4**.

---

error status of product release rate constant ( $k_7$  or  $k_8$ ) is low and does not differ away data sets. For model B1-1, most of the errors in global fits with pre-steady state time courses were well below 50% (except  $k_1$  in trial 1). But global fits with model B1-2 is generally higher than 100% (except  $k_7$ ). Those results demonstrate that model B1-1 can account for both steady state and pre-steady state data sets, and the derived product release rate constants are consistent when using the same kinetic model.

*Global Fits With Binding Equilibrium For EP.* It seems that model B1-1 works well with most of the kinetic data, so there is no need to explore model B1-3 since model B1-1 is the part of it. However, there are two small variations between modeling and experimental evidence. It is mentioned above that step 8 in models B1-2 and B1-3 (**Scheme 4.4**) is a weak equilibrium with micromolar binding affinity, rather than irreversible. Does this small variation change our conclusion that model B1-1 fits experimental data better than B1-2? In model B1-2, E ( $EM_2$ ) and EP ( $EM_2P$ ) are assumed to have the same metal binding affinities. What are the metal binding affinities of EP and  $EM_2P$  if they are floating as unknown parameters (model B1-3 in **Scheme 4.4**)?

Model B1-2\* (to distinguish the previously discussed B1-2) is constructed by assigning step 8 as an equilibrium characterized by two kinetic parameters ( $k_8$  and  $k_{-8}$ ).  $k_8$  is still floating as in the previous global fit (**Table 4.7**), and  $k_{-8}$  is fixed to be  $300 \text{ M}^{-1}\text{s}^{-1}$ . The DNA binding association rate constant for cognate DNA under metal free conditions is about  $3000 \text{ M}^{-1}\text{s}^{-1}$  (in **Table 4.5**), and a 10 fold decrease should make sense for a product association rate constant since binding affinity of

---

cognate DNA and product to apo enzyme are about 300 nM (**Table 4.1**) and 10  $\mu\text{M}$  (averaged values from binding experiments in **Figure 4.8**), respectively. The comparison of global fits with model B1-2 and B1-2\* is summarized in **Table 4.8A** including derived kinetic parameters and standard deviations. It is obvious that treating step 8 as equilibrium or irreversible product dissociation really makes no difference in global fit results using model B1-2.

Two trials of global fits have been conducted with pre-steady progress curves in order to estimate the unknown metal binding affinity of EP ( $\text{EM}_2\text{P}$ ) and examine if treating step 8 as equilibrium or irreversible step makes any difference for model B1-3. In trial 1,  $k_9$ ,  $k_{10}$ ,  $k_7$  are floating, and equilibrium of step 8 has been characterized by on and off rate constants ( $k_8$  is fixed as  $0.003 \text{ s}^{-1}$  and  $k_{-8}$  is fixed as  $300 \text{ s}^{-1}$ ). In trial 2,  $k_9$ ,  $k_{10}$ ,  $k_7$  and  $k_8$  (irreversible step) are all floating.  $k_1$  and  $k_3$  are both fixed from the derived Mg(II) binding association rate constant from model B1 in **Table 4.5**. **Table 4.8B** summarizes the derived kinetic parameters and error status for both trials. Derived parameters do not make any difference in derived kinetic parameters. Even derived  $k_8$  from trial 2 is the same as fixed  $k_8$  in trial 1. Those two trials fully demonstrate that assuming step 8 is irreversible in previous global fits (**Table 4.7**) is valid and should not cause any problems. It is also noticeable that the derived metal binding affinity of EP ( $\text{EM}_2\text{P}$ ) is within the same range as apo E ( $\text{EM}_2$ ) (**Table 4.8B**).

These results are expected because in either steady state kinetics or pre-steady

**Table 4.8. The potential influence of weak equilibrium between apo enzyme and product on global fit results. A: influence on model B1-2, B: influence on model B1-3.**

A. Comparison of model B1-2 and B1-2\* by the best fit of steady state kinetic and pre-steady state kinetics.

Model	Standard deviation	k1 (M <sup>-2</sup> s <sup>-1</sup> )	k3 (M <sup>-2</sup> s <sup>-1</sup> )	k8 (s <sup>-1</sup> )
Steady State Kinetics				
B1-2	2.49e-4	5.4e7 (14%)	7.5e5 (570%)	0.077 (100%)
B1-2*	2.49e-4	5.4e7 (14%)	7.5e5 (570%)	0.077 (100%)
Pre-steady state Kinetics				
B1-2	2.72e-9	4.8e6 (290%)	7.8e8 (290%)	0.0093 (32%)
B1-2*	2.72e-9	4.4e6 (310%)	8.5e8 (320%)	0.01 (32%)

B. Comparison of global fit results with step 8 as equilibrium and irreversible on model B1-3. The pre-steady state kinetic data is the same shown in **Figure 4.10**. k1 and k3 are fixed according to global fit of model B1 in **Table 4.5B**.

Model	Standard deviation	k9 <sup>a</sup> (M <sup>-2</sup> s <sup>-1</sup> )	k10 <sup>b</sup> (M <sup>-2</sup> s <sup>-1</sup> )	k7 (s <sup>-1</sup> )	k8 (s <sup>-1</sup> )
Trial 1	2.5e-4	1.5e7 (170%)	5.74e7 (38%)	0.0063 (29%)	n/a
Trial 2	2.5e-4	1.55e7 (270%)	5.72e7 (70%)	0.0063 (38%)	0.0030 (110%)

- k9 is the association rate constant of step 9 (EP + 2M <->EM<sub>2</sub>P) in model B1-3 of **Scheme 4.4**. The calculated K<sub>d</sub> for step 9 is 8.2 mM.
- k10 is the association rate constant for step 10 (EM<sub>2</sub>P + 2M <->EM<sub>4</sub>P) in B1-3 of **Scheme 4.4**. The calculated K<sub>d</sub> for step 10 is 4.2 mM.

---

state kinetics, the concentration of enzyme (<50 nM) and DNA (<200 nM) is too low to form a large proportion of EP complex (micromolar binding affinity). Since there is little EP complex, the product dissociation can be treated as irreversible without affecting any global fit results.

**Possibility of One Unique Kinetic Model For Single Turnover Kinetics, Steady State Kinetics And Pre-Steady State Kinetics.**

Returning to our goal of using one unique, complete kinetic model to unify all metal dependence of specific DNA binding and cleavage by *PvuII*, a kinetic model B1-1 shown in **Scheme 4.4** seems to be our answer. The following assumptions have been made to reduce unknown parameters in order to improve fitting quality. The number of Mg(II) ions bound in the post-reactive complex may not affect the product dissociation rate constants (in model B1-1, the product dissociation rate constant  $k_7$  is used for both  $EM_2P$  and  $EM_4P$ ). Substrate dissociation rate constants were measured experimentally and assumed to be the same for all DNA dissociation steps (**Table 4.2**). Metal ion dissociation rate constants were obtained from references and assumed to be the same for all metal dissociation steps (**Table 4.4**)

The following conclusions can be drawn from the kinetic modeling. In the reaction, metal ion association mostly occurs prior to the DNA association, a sequence which has been proven to be kinetically more favorable. The binding mechanism of DNA association prior to metal ions is shown to be kinetically unfavorable (model A2/B2 or A3/B3 for single turnover kinetics). Two separate trials have been conducted with different DNA association rate constants for  $EM_2$ , and trial 2 actually

---

is more reasonable than trial 1 ( $K_d = 100$  nM in trial 1 and 10 nM in trial 2 for  $EM_2$ ) because assumed 100 nM DNA binding affinity in trial 1 is too close to determined affinity ( $307 \pm 146$ ) nM under metal free conditions and probably is not valid in the case of one metal binding site occupied.

Model B1 supports enzymatic activity when one metal binding site is occupied. Two different turnover rate constants (**Table 4.5**) have been derived ( $k_5=1.128$  s<sup>-1</sup> for  $EM_4$  and  $k_6=0.02$  s<sup>-1</sup> for  $EM_2$ ) from global fit, which indicates that one-metal ion catalytic activity is about 50 fold slower than two-metal ion catalytic activity. The presence of second metal ion in the active site seems to effectively lower the activation energy barrier. This can be attributed to protonation of the leaving group and stabilization of the transition state by electrostatic interactions. For the multiple turnover reactions, enzyme dissociates from the product and metal ions are still bound in the active site.

The derived metal binding affinities are summarized in **Table 4.9** in order to examine if the unique model can accounts for all the experimental data. Except for Ca(II) binding experiments with metal ion binding affinities of micromolar, all other kinetic experiments generate metal binding affinities for two sequential Mg(II) binding steps within a range from 1 to 10 mM (**Table 4.9**). In trial 2,  $K_{d1}$  is always higher than  $K_{d3}$ , regardless of the data sets used in global fits, and similar metal binding affinities have been obtained for three different data sets. These comparisons provide the confidence that model B1-1 probably is the unique kinetic

**Table 4.9. Best fit derived metal binding equilibrium constants and product release rate for DNA binding, single turnover kinetics, steady state kinetics and pre-steady state kinetics.**

Derived kinetic parameters	DNA binding	Single turnover kinetics	Pre-steady state kinetics	Steady state kinetics
Scheme	4.1	4.2	4.4	4.4
<b>Trial 1</b>				
Metal ion	Ca(II)	Mg(II)	Mg(II)	Mg(II)
$K_{d1}$ (mM)	0.087	2.7	5.0	5.6
$K_{d3}$ (mM)	4.3	4.5	4.2	2.2
$k_7$ (sec <sup>-1</sup> )	n/a	n/a	0.0054	0.0047
<b>Trial 2</b>				
Metal ion	Ca(II)	Mg(II)	Mg(II)	Mg(II)
$K_{d1}$ (mM)	0.12 <sup>a</sup>	7.9	7.9	9.4
$K_{d3}$ (mM)	2.1 <sup>a</sup>	2.1	3.6	1.5
$k_7$ (sec <sup>-1</sup> )	n/a	n/a	0.0062	0.0047

The global fit results are summarized in trial 1 and trial 2, respectively. The meaning of trial 1 and trial 2 are different for Ca(II) dependent DNA association data and Mg(II) dependent cleavage data (see Results **Table 4.1**, **Table 4.5** and **Table 4.7**). The Ca(II) binding affinities in trial 2 are fixed in the global fit and are obtained from ITC experiments. The applied reaction scheme for each global fit is indicated.

a. (Jose, et al., 1999)

---

model for single turnover, steady state and pre-steady state kinetics. The DNA binding equilibrium constants used in global fits could not be measured directly, and are estimated from steady state kinetics data (**Table 4.3**). These approximations can contribute to uncertainty in the global fits and contribute to the differences on the metal binding affinities derived from single turnover, steady state and pre-steady state data sets.

---

## DISCUSSION

**Ca(II) Dependence of Specific DNA Binding.** Ca(II) is the metal cofactor used in the specific DNA binding measurements for type II restriction endonucleases since it does not support hydrolysis (Engler, et al., 1997; Engler, et al., 2001; Reid, et al., 2001; Conlan & Dupureur, 2002b; Conlan & Dupureur, 2002a). The two Ca(II) binding sites for each subunit in the crystallographic structure of *PvuII*-DNA complex agree well with Hill analysis ( $n_H = 3.6$  per dimer) of the sigmoidal DNA association constants as a function of Ca(II) concentration (**Figure 4.2**) (Conlan & Dupureur, 2002b). As shown in **Scheme 4.1**, DNA binding in the presence of Ca(II) is described as stepwise, excluding the possible DNA binding to apo-enzyme prior to the metal ion association. Global fit yields the DNA association constant (10 nM in **Table 4.1**) when one metal binding site is occupied, which was not available experimentally. The DNA binding affinity to *PvuII* is enhanced by 30 fold when filling the first site and by 50 (in trial 1 of **Table 4.1**) or 80 fold (in trial 2 of **Table 4.1**) when filling the second site. This indicates that the contribution of the first and second Ca(II) ions to the DNA dissociation are similar. The crystallographic structure of *PvuII* (1F0O) shows that both Ca(II) ions coordinate with Asp58, Glu68 and oxygen O2P of the scissile phosphate, supporting the similar geometry for their coordinations (**Figure 4.1A**) (Horton & Cheng, 2000). The derived Ca(II) binding affinities for two sites from the global fits shows good agreement with binding affinities obtained with ITC data (Jose, et al., 1999). ITC data fitted to two independent site equation yields a strong site with an affinity of 120  $\mu$ M and a weak

---

site with an affinity of 2.1 mM, while global fit resulted in Ca(II) binding affinities of 120  $\mu$ M and 4.3 mM (**Table 4.1**). The observation of a strong and weak metal binding site may be attributed to the repulsive interactions between two Ca(II) ions.

**Ca(II) vs Mg(II).** It is known that the addition of Ca(II) inhibits the enzymatic activity in a 5 mM Mg(II) background (unpublished results), which indicates that Ca(II) ions can effectively substitute the bound Mg(II) ions in the *PvuII* active site. This may be attributed to the different metal binding affinities of *PvuII* with Ca(II) and Mg(II).

*Ca(II) and Mg(II) Binding Affinities.*

The Ca(II) titration with *PvuII* using ITC shows a strong site with micromolar affinity and a weak site with millimolar affinity (**Table 4.1**). The global fits with Mg(II) dependent kinetic data show millimolar affinities for both sites (**Table 4.9**). The binding affinities of Mg(II) for some metallonucleases are summarized in **Table 4.10A**. The typical Mg(II) binding affinity for metallonucleases is within a range from sub-millimolar to a few millimolar. **Table 4.10B** compares the binding affinities between Mg(II) and Ca(II) for the same enzymes. For the metallonucleases, there are no dramatic differences in Ca(II) and Mg(II) binding affinities since both are divalent metal ions. However, parvalbumin is an exception in that Ca(II) binding affinity is over 20 fold higher than Mg(II).

---

**Table 4.10 A. Mg(II) binding affinities of enzymes.**

---

Enzyme	Methods	Binding affinity (mM)	Reference
Klenow	ITC	0.16	(Cowan, 1997)
Klenow	ITC	0.4	(Cowan, 1997)
Ribonuclease H	<sup>25</sup> Mg NMR	0.06	(Cowan, et al., 1997)
Ribonuclease H	<sup>1</sup> H NMR	0.2	(Cowan, et al., 1997)
exo III	ITC	0.91	(Black & Cowan, 1998)
EcoRI ENase	Kinetics	3.1	(JenJacobson, et al., 1996)
EcoRV Enase	Kinetics	5	(Engler, et al., 1997)
EcoRV Enase	Kinetics	1.3	(Groll, et al., 1997)
BamI Enase	Kinetics	4.7	(Engler, et al., 1997)
<i>PvuII</i> Enase	<sup>25</sup> Mg NMR	1.9	(Dupureur & Conlan, 2000)
Pyrophosphatase	Dialysis	0.083	(Kapyła, et al., 1995)
Pyrophosphatase	Dialysis	1.67	(Kapyła, et al., 1995)
Parvalbumin	ITC	0.01	(Moeschler, et al., 1980)
T7 RNA Polymerase	EPR	2	(Woody, et al., 1996)
Farnesyltransferase	Kinetics	4	(Pickett, et al., 2003)
Hepatitis Delta Virus Ribozyme	Kinetics	2.4	(Nakano, et al., 2000)

---

**Table 4.10 B. The comparison of Mg(II) and Ca(II) binding affinities for the same enzyme.**

Enzyme	K <sub>d</sub> of Ca(II) (mM)	K <sub>d</sub> of Mg(II) (mM)	Experiments	Reference
Exo III	1.8	0.91	ITC	(Black & Cowan, 1998)
<i>Pvu</i> II Enase	1.3	1.9	ITC and <sup>25</sup> Mg NMR	(Dupureur & Conlan, 2000) (Jose, et al., 1999)
Parvalbumin	3.7*10 <sup>-4</sup>	0.01	ITC	(Moeschler, et al., 1980)
Rat α PV	8.3*10 <sup>-3</sup>	0.105	ITC	(Henzl, et al., 2003)
Rat β PV	4.55*10 <sup>-2</sup>	0.091	ITC	(Henzl, et al., 2003)

---

The ionic radius of Ca(II) is 0.34 Å larger than that of Mg(II), and Ca(II) prefers a longer coordination distance (2.5 Å) than Mg(II) (2.0 Å) (Horton & Cheng, 2000). For two metal binding sites, the difference in binding affinity between the strong and weak sites for Mg(II) is not as dramatic as that for Ca(II). For the derived Mg(II) binding affinities in global fits (**Table 4.9**, trial 2), the difference in binding affinities between strong and weak binding sites is between 2 and 6 fold, and two sites tend to have similar metal ion binding affinities.

The distances between two metal ions captured in the crystal structures for metallonucleases are summarized in **Table 4.11**. It seems that the distance between two metal ions regardless of Ca(II) or Mg(II) is ranging from 3.5 Å to 5.5 Å, which demonstrates that the geometry and configurations of two Ca(II) and Mg(II) ions in the active sites are similar for most of metallonucleases. Carboxylic groups (Asp and Glu) are the common ligands for both metal ions. The difference of ligation between Ca(II) and Mg(II) is the extensive hydration of Mg(II) and possible outer-sphere interactions between Mg(II) ions and their binding sites (Cowan, 1998). In the crystallographic structure of *PvuII*-Ca(II)-DNA, the direct Ca(II) phosphate contact is observed and the Ca(II) ions follow inner-sphere interactions in this case (Horton & Cheng, 2000).

*Ca(II) and Mg(II) Dependent DNA Association.*

In the presence of 10 mM Ca(II), the DNA dissociation constant is about 100 pM (**Table 4.1**), whereas the derived DNA dissociation constant is about 5 nM (**Table 4.4**) in the presence of the same concentration of Mg(II). **Table 4.12** lists

**Table 4.11. The summary of distance between two metal ions in the crystal structures of nucleases.**

Enzyme	Metal ions	Distance (Å)	pdb code	Remark
<i>Pvu</i> II	Ca(II)	3.5	1F0O	Subunit A
<i>Pvu</i> II	Ca(II)	4.2	1F0O	Subunit B
Bgl I	Ca(II)	4.3	1DMU	
BamHI	Ca(II)	4.3	2DAM	
BamHI	Mn(II)	3.9	3BAM	
EcoRV	Ca(II)	5.4	1BSS	
EcoRV	Mg(II)	5.43	1RVS	
EcoRV	Mn(II)	3.62	1SX5	Subunit A
T7 Enase I	Mn(II)	3.52	1M0D	
TnsA	Mg(II)	4.0	1F1Z	
NgoMIV	Mg(II)	3.7	1FIU	
Vsr endonuclease	Mg(II)	4.0	1CW0	
HincII	Mn(II)	4.1	1XHV	

List of references for pdb files:

1F0O (Horton & Cheng, 2000), 1DMU (Newman, et al., 1998), 2DAM (unpublished result), 3BAM (Viadiu & Aggarwal, 1998), 1BSS (Horton, et al., 1998), 1RVS (Jaroniec, et al., 2004), 1SX5 (Horton & Perona, 2004), 1M0D (Hadden, et al., 2002), 1F1Z (Tranter, et al., 2000), 1FIU ((Deibert, et al., 2000), 1CW0 (Tsutakawa, 1999), 1XHV (Etzkorn & Horton, 2004).

**Table 4.12. Summary of Ca(II) and Mg(II) dependence on DNA binding affinity.**

Substrate	Relative DNA binding affinity <sup>a</sup>	Endonuclease	Reference
3'-S-phosphorothiolate	175	EcoRV (WT)	(Engler, et al., 1997)
4'-thiodeoxyribose	92.5	EcoRV (WT)	(Engler, et al., 1997)
UA instead of TA	3.6	EcoRV (WT)	(Martin, et al., 1999a)
UA instead of TA	93	EcoRV (K38A)	(Martin, et al., 1999a)
CI (inosine) instead of TA	24	EcoRV (K38A)	(Martin, et al., 1999a)
CG instead of TA	1.1	EcoRV (K38A)	(Martin, et al., 1999a)
Nsp <sup>b</sup> strand	1	EcoRV (K38A)	(Martin, et al., 1999a)
phosphoramidate	50	<i>PvuII</i> (WT)	(King, et al., 2004)

a. Relative DNA binding affinity is the ratio of DNA binding affinity at the same concentration of Ca(II) and Mg(II):  $K_a(\text{Ca}^{2+})/K_a(\text{Mg}^{2+})$ . b. Nsp means non specific DNA sequence for endonucleases. The non-hydrolyzable substrates have been used in the measurement of binding affinity in the presence of Mg(II).

---

determined DNA binding affinities with Ca(II) and Mg(II) at the same concentration for restriction endonucleases. For the non-hydrolysable DNA, Ca(II) stimulates a nearly 200 fold binding enhancement of DNA association compared with the same concentration of Mg(II) (Engler, et al., 1997). The inactive mutant K38A of *EcoRV* also shows a 50 fold enhancement of DNA binding affinity with Ca(II) compared to Mg(II) at the same concentration (Martin, et al., 1999a). It seems electrostatic interactions can not solely account for this enhancement on DNA association since Ca(II) and Mg(II) both are divalent ions. The reason may be the different type of ligation (inner vs. outer sphere interactions) and different size between Ca(II) and Mg(II). The size of Ca(II) is slightly larger and Ca(II) may better coordinate with the bending of DNA molecules upon binding.

**The Number of Metal Ions Required In Catalysis.** It is certain that there are two metal ions involved in DNA binding, whereas the number of metal ions required in catalysis has been unclear. To address this problem, the kinetic models are divided into group A and group B; group A contains one chemistry step which requires both metal binding sites to be occupied. Group B contains two chemistry steps which require at least one metal binding site to be occupied. It is found that group B fits the experimental single turnover data better than group A, which indicates that one metal ion occupied in the active site is able to support catalysis with reduced activity. The kinetic model B1 yields a turnover rate constant  $1.13 \text{ s}^{-1}$  ( $k_5$  in **Table 4.5B** trial 2) when both sites are filled and turnover rate constant  $0.02 \text{ s}^{-1}$  ( $k_6$  in **Table 4.5B** trial 2) when one site is filled. An enhancement of 50 fold in enzymatic

---

activity is estimated upon to the addition of the second Mg(II) ion. The turnover rate  $k_5$  is considered as the intrinsic and the maximal activity for *PvuII* with given pH (7.5) and temperature (37 °C), which is independent of Mg(II) concentration. It is noted that the derived  $k_5$  is higher than the measured single turnover rate constant of 0.24 s<sup>-1</sup> with 2 μM enzyme and 0.47 s<sup>-1</sup> with 5 μM enzyme at 10 mM Mg(II). This indicates that the measured rate constant is still influenced by the enzyme concentration because DNA association step is not fast enough to be neglected, which is in a good agreement with a slow DNA association rate ( $k_4 = 2 \cdot 10^5 \text{ M}^{-1}\text{s}^{-1}$  in **Table 4.5**) constant used in global fits. For plasmid cleavage by *MunI*, the maximal single turnover activity is reported to be 1.9 s<sup>-1</sup> (Sasnauskas, et al., 1999). For *EcoRV*, the measured single turnover rate is 0.62 s<sup>-1</sup> at 10 mM Mg(II) with 150 nM enzyme and 50 nM oligonucleotides (Sam & Perona, 1999a). The determined rate constants with *PvuII* seems slower than those published data, and derived  $k_5$  agrees well with them.

The mixing procedure to initiate the reaction may affect the measured single turnover rates. Three different mixing protocols have been used in our lab to address the potential influence of order addition on the measured activity. It was observed that reactions initiated by Mg(II) are generally slower than reactions initiated by enzyme, regardless of enzyme is pre-mixed with Mg(II) or not (Baldwin, et al., 1995; Sam & Perona, 1999a). As shown in **Table 4.13**, most of the cleavage rate constants using protocol 1 are higher or similar to those values using protocol 2 except at 2 mM Mg(II). At 1 mM Mg(II), the average rate using protocol 1 falls within the range of

**Table 4.13. The summary of measured *Pvu*II enzyme activity for different mixing protocols.**

Mg(II) (mM)	Average $k_{\text{obs}}$ under single turnover reaction conditions ( $\text{s}^{-1}$ )		
	Mixing protocol # 1	Mixing protocol # 2	Mixing protocol # 3
	E + MS	ES + M	EM + SM
0.5	0.0024	0.005 <sup>a</sup>	n/a
1	0.0027	0.024 <sup>b</sup>	n/a
2	0.015	0.035 <sup>b</sup>	n/a
3	0.053	0.039 <sup>b</sup>	n/a
10	0.23	n/a	0.26

E, S and M represents enzyme dimer, substrate and Mg(II) cofactors. MS means pre-mixing metal cofactor with substrate. ES means pre-mixing apo enzyme and substrate without the presence of Mg(II) cofactor. EM and ES means both enzyme and substrate containing Mg(II) cofactor. The single turnover conditions are 2  $\mu\text{M}$  enzyme and 300 nM substrate, pH 7.5 at 37 °C.

a. The three trials are 0.0047, 0.008, 0.0017  $\text{s}^{-1}$  and the average rate constant in protocol #1 actually falls within it.

b. The error bar of those average values are within 0.005  $\text{s}^{-1}$  for three trials.

---

three trials using protocol 2 (see notes of **Table 4.13**). This is consistent with observations that reactions initiated by adding Mg(II) into enzyme-DNA complex are generally slower. Protocol 1 and protocol 3 yield similar rate constants at 10 mM Mg(II) in. So pre-mixing enzyme with metal ions or not does not affect the measured cleavage rate since DNA association is rate limiting step in the formation of EM<sub>n</sub>S complex.

**Figure 4.5A** clearly shows that all the plots of Mg(II)-k<sub>obs</sub> are sigmoidal shape, regardless of the number of chemistry steps. Since the apparent cleavage rate is a result of binding and catalysis, the two sequential metal ion binding steps in the two-site kinetic models seems sufficient to provide the sigmoidal shape. The sigmoidal dependence can also be the result of cooperativity between multiple sites, which complicates the dissection of the number of metal ions in catalysis.

For *EcoRV*, which is structurally similar to *PvuII*, Pingoud was not convinced that a second metal ion was directly relevant to catalysis because Ala mutation on a metal binding site E45 yielded cleavage activity reduced by only 1.8 fold compared with WT (Groll, et al., 1997). Fuxreiter probed the Mg(II) positions in the active site of *BamHI* by molecular dynamics simulations and suggested a single metal ion is critical in catalysis and a second metal ion serves a regulatory function (Mones, et al., 2007c). Although *EcoRV*, *BamHI* and *PvuII* structurally can tolerate two metal ions in their active sites, they may just need one metal ion for catalysis. Different approaches (mutagenesis, molecular dynamics simulation and kinetic modeling) surprisingly appear to draw the same conclusion (Groll, et al., 1997; Mones, et al.,

---

2007a; Mones, et al., 2007b).

**Two Distinct Sites (A and B) In *PvuII*.** As shown in **Scheme 4.3**, two distinctive metal binding sites are distinguished in the kinetic models and finally conclude two sites equivalent with positive cooperativity (best fit model C1). Two equivalent sites can be interpreted from the *PvuII* crystal structures containing two Ca(II) ions each subunit, which shares the same ligands and geometries. In **Table 4.6B** for model C1, the interaction factor differs in two trials depending on DNA binding affinity of EM<sub>2</sub> (100 nM in trial 1 and 10 nM in trial 2). The tighter DNA binding for EM<sub>2</sub> in trial 2 resulted in a stronger cooperativity between two sites. This suggests that the cooperativity between two metal binding sites may be a result of DNA binding rather than the repulsive interactions between two Mg(II) ions since negatively cooperative metal ions binding affinities would be expected due to repulsive interactions. The scissile phosphates provide additional metal binding ligands, and cause dramatic conformational changes in restriction enzymes (Horton & Cheng, 2000; Spyridaki, et al., 2003; Dupureur, 2005).

The global fits for four reaction pathways (from B1 to B4) appear to support the subsequent metal binding mechanism and metal binding steps are prior to DNA binding. If the bound DNA enhances the binding affinities of the second metal ion, DNA must bind before the second metal ion as modeled in candidate B3 or they binds to the enzyme simultaneously. Since model B3 has the large standard deviations and error status, the simultaneous binding of the second metal ion and DNA probably occurs when the second site is filled up. The only related experimental evidence

---

about two metal binding order is stop flow experiments on *EcoRV* (Baldwin, et al., 1995), which identified two metal dependent transitions. The affinities of site A and site B can be estimated from trial 2 using model C1 (**Table 4.6**), similar to derived metal binding affinities using model B1 (**Table 4.5**). Without filling up another site, Mg(II) in one site can solely support the cleavage and this cleavage rate is indicated by rate constant  $k_6$ , which is derived ranging from 0.01 up to 0.049 s<sup>-1</sup> depending on trials.

**Mg(II) Ion Included In Post-Reactive Complex.** The best fit kinetic model B1-1 with multiple turnover data sets strongly suggests that metal ions remain bound in the post-reactive complex, and product release occurs without the dissociation of metal ions in the active site. This conclusion is also supported by the crystal structures of a post-reactive complex containing Mg(II) ions in *EcoRV* (Kostrewa & Winkler, 1995). The measured steady state velocity at saturated Mg(II) concentrations is comparable with the cognate DNA dissociation rate constant (in **Table 4.2**). The similarity of those two rate constants implies that the product release measured in steady state kinetics is fully a physical process. Compared with the binding step and the chemistry step, product release is much slower and is considered the rate limiting step in overall reaction scheme. So a burst phase in the pre-steady state kinetics can be visualized (**Figure 4.7**). The crystal structure of pre-reactive complexes and post-reactive complexes shows the Mg(II) ions binding at different sites, which reflects the change of the Mg(II) binding environment once the scissile phosphate is broken (Kostrewa & Winkler, 1995). It is worth noting that

---

the fits of B1-2 were conducted based on the assumption that metal ion binding affinities of the enzyme product complex are the same as apo-enzyme. This might not be true because the metal-phosphate contact is absent in the *PvuII*-Mg(II) complex but present in the post-reactive complex of *EcoRV* (Kostrewa & Winkler, 1995). A global fit using model B1-3 in **Scheme 4.4** performed with pre-steady state reaction courses with fixing  $k_1$  and  $k_3$  (from **Table 4.5B** model B1) generated metal binding affinities for EP and  $EM_2P$  which are about 4 mM and 8 mM, respectively (derived from **Table 4.8B**,  $k_9$  and  $k_{10}$  are metal binding association rate constants for EP and  $EM_2P$ , respectively). This indicates that although enzyme product complex may not have the same metal binding affinity as apo enzyme, the values are still within 10 mM and do not change much.

Although the kinetic models B1 and B1-1 are limited by the assumptions and approximations of fixing kinetic parameters, the global fits with this kinetic model produced the unknown kinetic parameters which are hard to measure experimentally with small error status. The outputs are similar for single turnover, steady state and pre-steady state kinetics. The derived metal ion binding affinities and kinetic behavior supports one-metal ion catalytic mechanism with the assumption of one catalytic site and one regulatory site, which shows good agreement with work on other type II endonucleases.

---

## Reference

- Aaqvist, J. and A. Warshel (1990). "Free energy relationships in metalloenzyme-catalyzed reactions. Calculations of the effects of metal ion substitutions in staphylococcal nuclease." *J. Am. Chem. Soc.* **112**(8): 2860-2868.
- Alexov, E. G. and M. R. Gunner (1997). "Incorporating protein conformational flexibility into the calculation of pH-dependent protein properties." *Biophys J* **72**(5): 2075-93.
- Alexov, E. G. and M. R. Gunner (1999). "Calculated protein and proton motions coupled to electron transfer: Electron transfer from Q(A)(-) to Q(B) in bacterial photosynthetic reaction centers." *Biochemistry* **38**(26): 8253-8270.
- Anderson, J. E. (1993). "Restriction Endonucleases and Modification Methylases." *Current Opinion in Structural Biology* **3**(1): 24-30.
- Andersson, T., T. Drakenberg, S. Forsen, E. Thulin and M. Swaerd (1982). "Direct observation of the calcium-43 NMR signals from calcium(2+) bound to proteins " *J. Am. Chem. Soc.* **104**(2): 576-580.
- Andersson, T., T. Drakenberg, S. Forsen, T. Wieloch and M. Lindstrom (1981). "Calcium binding to porcine pancreatic phospholipase A2 studied by <sup>43</sup>Ca NMR." *FEBS Lett* **123**(1): 115-7.
- Antosiewicz, J., J. M. Briggs, A. H. Elcock, M. K. Gilson and J. A. McCammon (1996a). "Computing ionization states of proteins with a detailed charge model." *Journal of Computational Chemistry* **17**(14): 1633-1644.
- Antosiewicz, J., J. A. McCammon and M. K. Gilson (1994). "Prediction of pH-dependent properties of proteins." *J Mol Biol* **238**(3): 415-36.
- Antosiewicz, J., J. A. McCammon and M. K. Gilson (1996b). "The determinants of pK(a)s in proteins." *Biochemistry* **35**(24): 7819-7833.
- Baldwin, G. S., I. B. Vipond and S. E. Halford (1995). "Rapid reaction analysis of the catalytic cycle of the EcoRV restriction endonuclease." *Biochemistry* **34**(2): 705-14.
- Bastock, J. A., M. Webb and J. A. Grasby (2007). "The pH-dependence of the Escherichia coli RNase HII-catalysed reaction suggests that an active site carboxylate group participates directly in catalysis." *J Mol Biol* **368**(2): 421-33.
- Bertrand, H. O., A. Pullman, K. Zakrzewska, B. Hartmann and S. Femandjian (1999). "Determination of a set of parameters for the molecular modelling of phosphorothioate DNA." *Theor Chem Acc* **101**: 269-273.
- Black, C. B. and J. A. Cowan (1998). "A critical evaluation of metal-promoted Klenow 3'-5' exonuclease activity: calorimetric and kinetic analyses support a one-metal-ion mechanism." *Journal of Biological Inorganic Chemistry* **3**(3): 292-299.
- Bowen, L. M. and C. M. Dupureur (2003). "Investigation of restriction enzyme cofactor requirements: a relationship between metal ion properties and

- 
- sequence specificity." *Biochemistry* **42**(43): 12643-53.
- Braunlin, W. H., T. Drakenberg and S. Forsen (1985). "Metal Ion NMR: Application To Biological Systems." *Current Topics in Bioenergetics* **14**: 97-147.
- Briggs, J. M., J. D. Madura, M. E. Davis, M. K. Gilson, J. Antosiewicz, B. A. Luty, R. C. Wade, B. Bagheri, A. Ilin, R. C. Tan and J. A. McCammon (1989). "University of Houston Brownian Dynamics Program User's Guide and Programmer's Manual Release 5.1."
- Cieplak, P., W. D. Cornell, C. Bayly and P. A. Kollman (1994). "Application of the multimolecule and multiconformational RESP methodology to biopolymers: Charge derivation for DNA, RNA, and proteins." *Journal of Computational Chemistry* **16**(11): 1357-1377.
- Conlan, L. H. and C. M. Dupureur (2002a). "Dissecting the metal ion dependence of DNA binding by PvuII endonuclease." *Biochemistry* **41**(4): 1335-42.
- Conlan, L. H. and C. M. Dupureur (2002b). "Multiple metal ions drive DNA association by PvuII endonuclease." *Biochemistry* **41**(50): 14848-55.
- Cowan, J. A. (1997). "Metal-mediated hydrolysis of biological phosphate esters: A critical analysis of the essential metal ion stoichiometry for magnesium-dependent nuclease activation." *JBIC* **2**: 168-176.
- Cowan, J. A. (1998). "Metal Activation of Enzymes in Nucleic Acid Biochemistry." *Chem Rev* **98**(3): 1067-1088.
- Cowan, W. K., P. Kelly, A. Sawan, W. J. Cunliffe, L. Henry, M. J. Higgs, L. G. Lunt, J. R. Young, C. H. Horne and B. Angus (1997). "The pathological and biological nature of screen-detected breast carcinomas: a morphological and immunohistochemical study." *J Pathol* **182**(1): 29-35.
- Dahm, S. C., W. B. Derrick and O. C. Uhlenbeck (1993). "Evidence for the role of solvated metal hydroxide in the hammerhead cleavage mechanism." *Biochemistry* **32**(48): 13040-5.
- Deibert, M., S. Grazulis, G. Sasnauskas, V. Siksnys and R. Huber (2000). "Structure of the tetrameric restriction endonuclease NgoMIV in complex with cleaved DNA." *Nat Struct Biol* **7**(9): 792-9.
- Drakenberg, T., T. Andersson, S. Forsen and T. Wieloch (1984). "Calcium ion binding to pancreatic phospholipase A2 and its zymogen: a  $^{43}\text{Ca}$  NMR study." *Biochemistry* **23**(11): 2387-92.
- Dupureur, C. M. (2005). "NMR studies of restriction enzyme-DNA interactions: role of conformation in sequence specificity." *Biochemistry* **44**(13): 5065-74.
- Dupureur, C. M. and L. H. Conlan (2000). "A catalytically deficient active site variant of PvuII endonuclease binds Mg(II) ions." *Biochemistry* **39**(35): 10921-7.
- Dupureur, C. M. and L. M. Hallman (1999). "Effects of divalent metal ions on the activity and conformation of native and 3-fluorotyrosine-PvuII endonucleases." *Eur J Biochem* **261**(1): 261-8.
- Engler, L. E., P. Sapienza, L. F. Dorner, R. Kucera, I. Schildkraut and L. Jen-Jacobson (2001). "The energetics of the interaction of BamHI endonuclease with its recognition site GGATCC." *J Mol Biol* **307**(2): 619-36.
- Engler, L. E., K. K. Welch and L. Jen-Jacobson (1997). "Specific binding by EcoRV

- 
- endonuclease to its DNA recognition site GATATC." *J Mol Biol* **269**(1): 82-101.
- Erskine, S. G., G. S. Baldwin and S. E. Halford (1997). "Rapid-reaction analysis of plasmid DNA cleavage by the EcoRV restriction endonuclease." *Biochemistry* **36**(24): 7567-76.
- Etzkorn, C. and N. C. Horton (2004). "Mechanistic insights from the structures of HincII bound to cognate DNA cleaved from addition of Mg<sup>2+</sup> and Mn<sup>2+</sup>." *J Mol Biol* **343**(4): 833-49.
- Fierke, C. A. and G. G. Hammes (1995). "Transient kinetic approaches to enzyme mechanisms." *Methods Enzymol* **249**: 3-37.
- Fitch, C. A., D. A. Karp, K. K. Lee, W. E. Stites, E. E. Lattman and E. B. Garcia-Moreno (2002). "Experimental pK(a) values of buried residues: analysis with continuum methods and role of water penetration." *Biophys J* **82**(6): 3289-304.
- Follope, N. and J. Alexander D. Mackerell (1999). "All-Atom Empirical Force Field for Nucleic Acids: I. Parameter Optimization Based on Small Molecule and Condensed Phase Macromolecular Target Data." *Journal of Computational Chemistry* **21**(2): 86-104.
- Forsen, S., A. Andersson, T. Drakenberg, O. Teleman, E. Thulin and H. J. Volgel (1983). Calcium Binding Proteins. Amsterdam, Elsevier.
- Fuxreiter, M. and R. Osman (2001). "Probing the general base catalysis in the first step of BamHI action by computer simulations." *Biochemistry* **40**(49): 15017-23.
- Gilson, M. K. (1993). "Multiple-site titration and molecular modeling: two rapid methods for computing energies and forces for ionizable groups in proteins." *Proteins* **15**(3): 266-82.
- Gilson, M. K. and B. H. Honig (1986). "The dielectric constant of a folded protein." *Biopolymers* **25**(11): 2097-119.
- Gorfe, A. A., P. Ferrara, A. Caflisch, D. N. Marti, H. R. Bosshard and I. Jelesarov (2002). "Calculation of protein ionization equilibria with conformational sampling: pK(a) of a model leucine zipper, GCN4 and barnase." *Proteins-Structure Function and Genetics* **46**(1): 41-60.
- Grigorescu, A., Horvath M., Wilkosz P. A., C. K. and R. J. M. (2004). The integration of recognition and cleavage: X-ray structures of the pre-transition state complex, post-reactive complex and the DNA-free endonuclease. Berlin, Springer.
- Groll, D. H., A. Jeltsch, U. Selent and A. Pingoud (1997). "Does the restriction endonuclease EcoRV employ a two-metal-Ion mechanism for DNA cleavage?" *Biochemistry* **36**(38): 11389-401.
- Guex, N. and M. C. Peitsch (1997). "SWISS-MODEL and the Swiss-PdbViewer: An environment for comparative protein modeling." *Electrophoresis* **18**: 2714-2733.
- Hadden, J. M., A. C. Declais, S. E. Phillips and D. M. Lilley (2002). "Metal ions bound at the active site of the junction-resolving enzyme T7 endonuclease I."

- 
- Embo J **21**(13): 3505-15.
- Haq, I., R. O'Brien, A. Lagunavicius, V. Siksnys and J. E. Ladbury (2001). "Specific DNA recognition by the type II restriction endonuclease MunI: the effect of pH." *Biochemistry* **40**(49): 14960-7.
- Henzl, M. T., J. D. Larson and S. Agah (2003). "Estimation of parvalbumin Ca(2+)- and Mg(2+)-binding constants by global least-squares analysis of isothermal titration calorimetry data." *Anal Biochem* **319**(2): 216-33.
- Hiller, D. A., J. M. Fogg, A. M. Martin, J. M. Beechem, N. O. Reich and J. J. Perona (2003). "Simultaneous DNA binding and bending by EcoRV endonuclease observed by real-time fluorescence." *Biochemistry* **42**(49): 14375-85.
- Honig, B. and A. Nicholls (1995). "Classical Electrostatics in Biology and Chemistry." *Science* **268**(5214): 1144-1149.
- Horton, K. J. Newberry and J. J. Perona (1998). "Metal ion-mediated substrate-assisted catalysis in type II restriction endonucleases." *Proc Natl Acad Sci U S A* **95**(23): 13489-94.
- Horton, J. R. and X. Cheng (2000). "PvuII endonuclease contains two calcium ions in active sites." *J Mol Biol* **300**(5): 1049-56.
- Horton, N. C., Connolly, B. A., and Perona, J. J. (2000). "Inhibition of EcoRV endonuclease by deoxyribo-3 $\phi$ -S-phosphorothiolates: A high-resolution X-ray-crystallographic study." *J. Am. Chem. Soc.* **122**: 3314-3324.
- Horton, N. C. and J. J. Perona (2004). "DNA cleavage by EcoRV endonuclease: two metal ions in three metal ion binding sites." *Biochemistry* **43**(22): 6841-57.
- Huyghues-Despointes, B. M., R. L. Thurlkill, M. D. Daily, D. Schell, J. M. Briggs, J. M. Antosiewicz, C. N. Pace and J. M. Scholtz (2003). "pK values of histidine residues in ribonuclease Sa: effect of salt and net charge." *J Mol Biol* **325**(5): 1093-105.
- Jaroniec, C. P., C. E. MacPhee, V. S. Bajaj, M. T. McMahon, C. M. Dobson and R. G. Griffin (2004). "High-resolution molecular structure of a peptide in an amyloid fibril determined by magic angle spinning NMR spectroscopy." *Proc Natl Acad Sci U S A* **101**(3): 711-6.
- Jeltsch, A., J. Alves, H. Wolfes, G. Maass and A. Pingoud (1993). "Substrate-assisted catalysis in the cleavage of DNA by the EcoRI and EcoRV restriction enzymes." *Proc Natl Acad Sci U S A* **90**(18): 8499-503.
- JenJacobson, L., L. E. Engler, D. R. Lesser, M. R. Kurpiewski, C. Yee and B. McVerry (1996). "Structural adaptations in the interaction of EcoRI endonuclease with methylated GAATTC sites." *Embo Journal* **15**(11): 2870-2882.
- Johnson, K. A. (1998). "Advances in transient-state kinetics." *Curr Opin Biotechnol* **9**(1): 87-9.
- Jose, T. J., L. H. Conlan and C. M. Dupureur (1999). "Quantitative evaluation of metal ion binding to PvuII restriction endonuclease." *J Biol Inorg Chem* **4**(6): 814-23.
- Kapyla, J., T. Hyytia, R. Lahti, A. Goldman, A. A. Baykov and B. S. Cooperman (1995). "Effect of D97E substitution on the kinetic and thermodynamic

- 
- properties of Escherichia coli inorganic pyrophosphatase." *Biochemistry* **34**(3): 792-800.
- Kim, J., J. Mao and M. R. Gunner (2005). "Are acidic and basic groups in buried proteins predicted to be ionized?" *J Mol Biol* **348**(5): 1283-98.
- King, J. B., L. M. Bowen and C. M. Dupureur (2004). "Binding and conformational analysis of phosphoramidate-restriction enzyme interactions." *Biochemistry* **43**(26): 8551-9.
- Kostrewa, D. and F. K. Winkler (1995). "Mg<sup>2+</sup> binding to the active site of EcoRV endonuclease: a crystallographic study of complexes with substrate and product DNA at 2 Å resolution." *Biochemistry* **34**(2): 683-96.
- Kuzmic, P. (1996). "Program DYNAFIT for the analysis of enzyme kinetic data: application to HIV proteinase." *Anal Biochem* **237**(2): 260-73.
- Lagunavicius, A., S. Grazulis, E. Balciunaite, D. Vainius and V. Siksnyus (1997). "DNA binding specificity of MunI restriction endonuclease is controlled by pH and calcium ions: involvement of active site carboxylate residues." *Biochemistry* **36**(37): 11093-9.
- Lakowicz, J. R. and R. B. Thompson (1983). "Differential polarized phase fluorometric studies of phospholipid bilayers under high hydrostatic pressure." *Biochim Biophys Acta* **732**(2): 359-71.
- Lamotte-Brasseur, J., V. Lounnas, X. Raquet and R. C. Wade (1999). "pKa calculations for class A beta-lactamases: influence of substrate binding." *Protein Sci* **8**(2): 404-9.
- Lanter, F., D. Erne, D. Ammann and W. Simon (1980). "Neutral Carrier Based Ion-Selective Electrode for Intracellular Magnesium Activity Studies." *Anal. Chem.* **52**: 2400-2402.
- Laurents, D. V., B. M. Huyghues-Despointes, M. Bruix, R. L. Thurlkill, D. Schell, S. Newsom, G. R. Grimsley, K. L. Shaw, S. Trevino, M. Rico, J. M. Briggs, J. M. Antosiewicz, J. M. Scholtz and C. N. Pace (2003). "Charge-charge interactions are key determinants of the pK values of ionizable groups in ribonuclease Sa (pI=3.5) and a basic variant (pI=10.2)." *J Mol Biol* **325**(5): 1077-92.
- Lee, M. E. and T. Nowak (1992). "Mg-25 Nmr-Studies of Yeast Enolase and Rabbit Muscle Pyruvate-Kinase." *Archives of Biochemistry and Biophysics* **293**(2): 264-273.
- Lott, W. B., B. W. Pontius and P. H. von Hippel (1998). "A two-metal ion mechanism operates in the hammerhead ribozyme-mediated cleavage of an RNA substrate." *Proc Natl Acad Sci U S A* **95**(2): 542-7.
- Lukacs, C. M., R. Kucera, I. Schildkraut and A. K. Aggarwal (2000). "Understanding the immutability of restriction enzymes: crystal structure of BglIII and its DNA substrate at 1.5 Å resolution." *Nat Struct Biol* **7**(2): 134-40.
- MacKerell, A. D., J. W.-K. Jr. and M. Karplus (1995). "An All-Atom Empirical Energy Function for the Simulation of Nucleic Acids." *J. Am. Chem. Soc* **117**: 11946-1 1975.
- Mandel, M. (1964). "The Effect of Temperature on the Proton Magnetic Resonance Spectra of Ribonuclease, Oxidized Ribonuclease, and Lysozyme." *Proc Natl*

- 
- Acad Sci U S A **52**: 736-41.
- Mandel, M. (1965). "Proton Magnetic Resonance Spectra of Some Proteins. I. Ribonuclease, Oxidized Ribonuclease, Lysozyme, and Cytochrome C." *J Biol Chem* **240**: 1586-92.
- Martin, A. M., N. C. Horton, S. Lusetti, N. O. Reich and J. J. Perona (1999a). "Divalent metal dependence of site-specific DNA binding by EcoRV endonuclease." *Biochemistry* **38**(26): 8430-9.
- Martin, A. M., M. D. Sam, N. O. Reich and J. J. Perona (1999b). "Structural and energetic origins of indirect readout in site-specific DNA cleavage by a restriction endonuclease." *Nat Struct Biol* **6**(3): 269-77.
- Minasov, G, V. Tereshko and M. Egli (1999). "Atomic-resolution crystal structures of B-DNA reveal specific influences of divalent metal ions on conformation and packing." *J Mol Biol* **291**(1): 83-99.
- Moeschler, H. J., J. J. Schaer and J. A. Cox (1980). "A thermodynamic analysis of the binding of calcium and magnesium ions to parvalbumin." *Eur J Biochem* **111**(1): 73-8.
- Mones, L., P. Kulhanek, J. Florian, I. Simon and M. Fuxreiter (2007a). "Probing the Two-Metal Ion Mechanism in the Restriction Endonuclease BamHI." *Biochemistry* **46**(50): 14514-23.
- Mones, L., I. Simon and M. Fuxreiter (2007b). "Metal-binding sites at the active site of restriction endonuclease BamHI can conform to a one-ion mechanism." *Biol Chem* **388**(1): 73-8.
- Mones, L., I. n. Simon and M. Fuxreiter (2007c). "Metal-binding sites at the active site of restriction endonuclease BamHI can conform to a one-ion mechanism." *Biol. Chem.* **388**(1): 73-78.
- Moss, M. L., P. Kuzmic, J. D. Stuart, G. Tian, A. G. Peranteau, S. V. Frye, S. H. Kadwell, T. A. Kost, L. K. Overton and I. R. Patel (1996). "Inhibition of human steroid 5alpha reductases type I and II by 6-aza-steroids: structural determinants of one-step vs two-step mechanism." *Biochemistry* **35**(11): 3457-64.
- Nakano, S., D. M. Chadalavada and P. C. Bevilacqua (2000). "General acid-base catalysis in the mechanism of a hepatitis delta virus ribozyme." *Science* **287**(5457): 1493-7.
- Nastri, H. G., P. D. Evans, I. H. Walker and P. D. Riggs (1997). "Catalytic and DNA binding properties of PvuII restriction endonuclease mutants." *J Biol Chem* **272**(41): 25761-7.
- Newman, M., K. Lunnen, G. Wilson, J. Greci, I. Schildkraut and S. E. Phillips (1998). "Crystal structure of restriction endonuclease BglII bound to its interrupted DNA recognition sequence." *Embo J* **17**(18): 5466-76.
- Nicholls, A. and B. Honig (1991). "A Rapid Finite-Difference Algorithm, Utilizing Successive over-Relaxation to Solve the Poisson-Boltzmann Equation." *Journal of Computational Chemistry* **12**(4): 435-445.
- Nicholls, A., K. A. Sharp and B. Honig (1991). "Protein Folding and Association - Insights from the Interfacial and Thermodynamic Properties of

- 
- Hydrocarbons." *Proteins-Structure Function and Genetics* **11**(4): 281-296.
- Nielsen, J. E., K. V. Andersen, B. Honig, R. W. W. Hooft, G. Klebe, G. Vriend and R. C. Wade (1999). "Improving macromolecular electrostatics calculations." *Protein Engineering* **12**(8): 657-662.
- Nielsen, J. E., T. V. Borchert and G. Vriend (2001). "The determinants of alpha-amylase pH-activity profiles." *Protein Eng* **14**(7): 505-12.
- Nielsen, J. E. and J. A. McCammon (2003). "On the evaluation and optimization of protein X-ray structures for pKa calculations." *Protein Science* **12**(2): 313-326.
- Nielsen, J. E. and G. Vriend (2001). "Optimizing the hydrogen-bond network in Poisson-Boltzmann equation-based pK(a) calculations." *Proteins* **43**(4): 403-12.
- Noble, M. A., S. Gul, C. S. Verma and K. Brocklehurst (2000). "Ionization characteristics and chemical influences of aspartic acid residue 158 of papain and caricain determined by structure-related kinetic and computational techniques: multiple electrostatic modulators of active-centre chemistry." *Biochem J* **351 Pt 3**: 723-33.
- Pace, C. N., F. Vajdos, L. Fee, G. Grimsley and T. Gray (1995). "How to measure and predict the molar absorption coefficient of a protein." *Protein Sci* **4**(11): 2411-23.
- Papadakos, G. A., H. Nastri, P. Riggs and C. M. Dupureur (2007). "Uncoupling metallonuclease metal ion binding sites via nudge mutagenesis." *J Biol Inorg Chem* **12**(4): 557-69.
- Pickett, J. S., K. E. Bowers, H. L. Hartman, H. W. Fu, A. C. Embry, P. J. Casey and C. A. Fierke (2003). "Kinetic studies of protein farnesyltransferase mutants establish active substrate conformation." *Biochemistry* **42**(32): 9741-8.
- Pingoud, A., M. Fuxreiter, V. Pingoud and W. Wende (2005). "Type II restriction endonucleases: structure and mechanism." *Cell Mol Life Sci* **62**(6): 685-707.
- Pyle, A. M. (1993). "Ribozymes: a distinct class of metalloenzymes." *Science* **261**(5122): 709-14.
- Record, M. T., L. T. M. and d. H. Pieter (1976). "Ion effects on ligand-nucleic acid interactions." *Journal of Molecular Biology* **107**(2): 145-158.
- Reid, S. L., D. Parry, H. H. Liu and B. A. Connolly (2001). "Binding and recognition of GATATC target sequences by the EcoRV restriction endonuclease: a study using fluorescent oligonucleotides and fluorescence polarization." *Biochemistry* **40**(8): 2484-94.
- Reid, S. S. and J. A. Cowan (1990). "Biostructural chemistry of magnesium ion: characterization of the weak binding sites on tRNA(Phe)(yeast). Implications for conformational change and activity." *Biochemistry* **29**(25): 6025-32.
- Roychowdhury-Saha, M. and D. H. Burke (2006). "Extraordinary rates of transition metal ion-mediated ribozyme catalysis." *Rna* **12**(10): 1846-52.
- Sam, M. D. and J. J. Perona (1999a). "Catalytic roles of divalent metal ions in phosphoryl transfer by EcoRV endonuclease." *Biochemistry* **38**(20): 6576-86.
- Sam, M. D. and J. J. Perona (1999b). "Mn<sup>2+</sup>-dependent Catalysis by Restriction Enzymes: Pre-Steady-State Analysis of EcoRV Endonuclease Reveals Burst

- 
- Kinetics and the Origins of Reduced Activity." *J. Am. Chem. Soc.* **121**(7): 1444-1447.
- Sasnauskas, G., A. Jeltsch, A. Pingoud and V. Siksnys (1999). "Plasmid DNA cleavage by MunI restriction enzyme: single-turnover and steady-state kinetic analysis." *Biochemistry* **38**(13): 4028-36.
- Spassov, V. Z., H. Luecke, K. Gerwert and D. Bashford (2001). "pK(a) Calculations suggest storage of an excess proton in a hydrogen-bonded water network in bacteriorhodopsin." *J Mol Biol* **312**(1): 203-19.
- Spyridaki, A., C. Matzen, T. Lanio, A. Jeltsch, A. Simoncsits, A. Athanasiadis, E. Scheuring-Vanamee, M. Kokkinidis and A. Pingoud (2003). "Structural and biochemical characterization of a new Mg(2+) binding site near Tyr94 in the restriction endonuclease PvuII." *J Mol Biol* **331**(2): 395-406.
- Sreedhara, A. and J. A. Cowan (2002). "Structural and catalytic roles for divalent magnesium in nucleic acid biochemistry." *Biomaterials* **15**(3): 211-23.
- Steitz, T. A. and J. A. Steitz (1993). "A general two-metal-ion mechanism for catalytic RNA." *Proc Natl Acad Sci U S A* **90**(14): 6498-502.
- Tang, C. L., E. Alexov, A. M. Pyle and B. Honig (2007). "Calculation of pKas in RNA: on the structural origins and functional roles of protonated nucleotides." *J Mol Biol* **366**(5): 1475-96.
- Thorogood, H., J. A. Grasby and B. A. Connolly (1996). "Influence of the phosphate backbone on the recognition and hydrolysis of DNA by the EcoRV restriction endonuclease. A study using oligodeoxynucleotide phosphorothioates." *J Biol Chem* **271**(15): 8855-62.
- Tock, M. R. and D. T. Dryden (2005). "The biology of restriction and anti-restriction." *Curr Opin Microbiol* **8**(4): 466-72.
- Tock, M. R., E. Frary, J. R. Sayers and J. A. Grasby (2003). "Dynamic evidence for metal ion catalysis in the reaction mediated by a flap endonuclease." *Embo J* **22**(5): 995-1004.
- Tolbert, B. S., S. G. Tajc, H. Webb, J. Snyder, J. E. Nielsen, B. L. Miller and R. Basavappa (2005). "The active site cysteine of ubiquitin-conjugating enzymes has a significantly elevated pKa: functional implications." *Biochemistry* **44**(50): 16385-91.
- Tranter, R., J. A. Read, R. Jones and R. L. Brady (2000). "Effector sites in the three-dimensional structure of mammalian sperm beta-acrosin." *Structure* **8**(11): 1179-88.
- Tsai, M. D., T. Drakenberg, E. Thulin and S. Forsen (1987). "Is the binding of magnesium (II) to calmodulin significant? An investigation by magnesium-25 nuclear magnetic resonance." *Biochemistry* **26**(12): 3635-43.
- Tsutakawa, S. E., Jingami, H., Morikaw (1999). "CRYSTAL STRUCTURE ANALYSIS OF VERY SHORT PATCH REPAIR (VSR) ENDONUCLEASE IN COMPLEX WITH A DUPLEX DNA." *cell* **99**: 615-623.
- Viadiu, H. and A. K. Aggarwal (1998). "The role of metals in catalysis by the restriction endonuclease BamHI." *Nat Struct Biol* **5**(10): 910-6.
- Vipond, I. B., G. S. Baldwin and S. E. Halford (1995a). "Divalent metal ions at the

- 
- active sites of the EcoRV and EcoRI restriction endonucleases." *Biochemistry* **34**(2): 697-704.
- Vipond, I. B., G. S. Baldwin, M. Oram, S. G. Erskine, L. M. Wentzell, M. D. Szczelkun, T. J. Nobbs and S. E. Halford (1995b). "A general assay for restriction endonucleases and other DNA-modifying enzymes with plasmid substrates." *Mol Biotechnol* **4**(3): 259-68.
- Vriend, G. (1990). "WHAT IF: A molecular modeling and drug design program." *J. Mol. Graph.* **8**(52): 56.
- Wilcox, D. E. (1996). " Binuclear Metallohydrolases." *Chem. Rev.* **96**(7): 2435-2458.
- Woody, A. Y., S. S. Eaton, P. A. Osumi-Davis and R. W. Woody (1996). "Asp537 and Asp812 in bacteriophage T7 RNA polymerase as metal ion-binding sites studied by EPR, flow-dialysis, and transcription." *Biochemistry* **35**(1): 144-52.
- Xia, Z., H. F. Azurmendi and A. S. Mildvan (2005). "Transient state kinetic studies of the MutT-catalyzed nucleoside triphosphate pyrophosphohydrolyase reaction." *Biochemistry* **44**(46): 15334-44.
- Yao, L., S. Sklenak, H. Yan and R. I. Cukier (2005). "A molecular dynamics exploration of the catalytic mechanism of yeast cytosine deaminase." *J Phys Chem B* **109**(15): 7500-10.
- You, T. J. and D. Bashford (1995). "Conformation and hydrogen ion titration of proteins: a continuum electrostatic model with conformational flexibility." *Biophys J* **69**(5): 1721-33.
- Zebala, J. A., J. Choi and F. Barany (1992). "Characterization of steady state, single-turnover, and binding kinetics of the TaqI restriction endonuclease." *J Biol Chem* **267**(12): 8097-105.
- Zhou, H. X. and M. Vijayakumar (1997). "Modeling of protein conformational fluctuations in pKa predictions." *J Mol Biol* **267**(4): 1002-11.

---

## Appendix I

### Scripts for global fit.

[task]<sup>a</sup>

data = progress  
task = fit

[mechanism]

```
E + M + M <--> EM2      :   k1  k-1
EM2 + S <--> EM2S       :   k2  k-2
EM2 + M + M <--> EM4    :   k3  k-3
EM4 + S <--> EM4S       :   k4  k-4
EM4S --> P              :   k5
EM2S --> P              :   k6
```

[constants]

```
k1 = 1E8 ?,      k-1 = 1000
k2 = 1E+5 ,      k-2 = 0.001
k3 = 1E8 ?,      k-3 = 1000
k4 = 2E+05 ,     k-4 = 0.001
k5 = 0.6 ?
k6 = 0.05 ?
```

[responses]

P = 1

[progress]<sup>b</sup>

```
offset auto
directory ./examples/fuqian/sto/data/
extension txt
```

```
file      fx61214(3.5)
  conc.    E = 2000e-9 , S = 300e-9 , M = 3.5E-3
file      fx61207(3.5)
  conc.    E = 2000e-9 , S = 300e-9 , M = 3.5E-3
file      fx61112(4)
  conc.    E = 2000e-9 , S = 300e-9 , M = 4E-3
file      fx61214(4)
  conc.    E = 2000e-9 , S = 300e-9 , M = 4E-3
file      fx70108(5)
```

---

conc. E = 2000e-9 , S = 300e-9 , M = 5E-3  
file fx70109(5)  
conc. E = 2000e-9 , S = 300e-9 , M = 5E-3  
file fx61204(7)  
conc. E = 2000e-9 , S = 300e-9 , M = 7E-3  
file fx61207(7)  
conc. E = 2000e-9 , S = 300e-9 , M = 7E-3  
file fx70103(10)  
conc. E = 2000e-9 , S = 300e-9 , M = 10E-3  
file fx71011(12)  
conc. E = 2000e-9 , S = 300e-9 , M = 12E-3

delay 1.5<sup>c</sup>

file fx61207(0.1)  
conc. E = 2000e-9 , S = 300e-9 , M = 0.1E-3  
file fx61204(0.5)  
conc. E = 2000e-9 , S = 300e-9 , M = 0.5E-3  
file 60712(1)  
conc. E = 2000e-9 , S = 300e-9 , M = 1E-3  
file 60713(1)  
conc. E = 2000e-9 , S = 300e-9 , M = 1E-3  
file 60706(1.5)  
conc. E = 2000e-9 , S = 300e-9 , M = 1.5E-3  
file 60713(1.5)  
conc. E = 2000e-9 , S = 300e-9 , M = 1.5E-3  
file fx61122(2)  
conc. E = 2000e-9 , S = 300e-9 , M = 2E-3  
file 50415(2.5)  
conc. E = 2000e-9 , S = 300e-9 , M = 2.5E-3  
file fx61207(3)  
conc. E = 2000e-9 , S = 300e-9 , M = 3E-3  
file fx61205(3)  
conc. E = 2000e-9 , S = 300e-9 , M = 3E-3

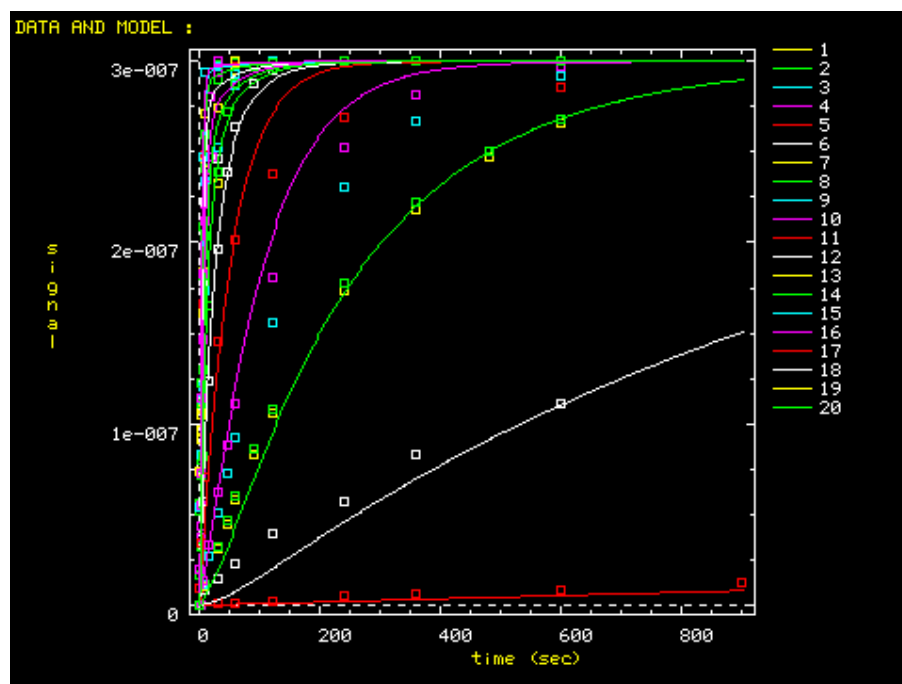
[output]

directory ./examples/fuqian/sto/b1

[settings]

<Filter>  
Scale = seconds

The best fit of reaction courses at various Mg(II) concentrations given by Dynafit.



The standard error status of floating four kinetic parameters.

Formal Standard Errors					
Set	Parameter	Initial	Fit	Error	%
	$k_1$	1e+008	1.5974e+007	1.533e+006	9.6
	$k_3$	1e+008	2.3218e+008	2.311e+007	10.0
	$k_5$	0.6	1.128	0.1449	12.8
	$k_6$	0.05	0.02004	0.004501	22.5

Note:

- The data type could be progress or equilibrium or velocity, task type could be either fit or simulate.
- All the data sets are listed as below, the number in the bracket indicate the metal ion concentrations. E, S and M represent enzyme dimer, substrate and metal ions. Their concentrations are given for each data set-a single reaction course.
- Reaction samples collected manually needs 1.5 seconds mixing time while reactions monitored by quench flow doesn't need since it is a real time experiment.

---

**Appendix II. The electrostatic potentials among four conserved active site residues: D58, E68, K70 and Y94.**

Refer the part “**Theory and Methods**” for the definition and instruction about electrostatic potential.  $pK_a$  calculations were performed based on 1F0O subunit A structure in the presence of two Mg(II) ions and one water molecules (W1035) as shown in **Figure 3.5**.

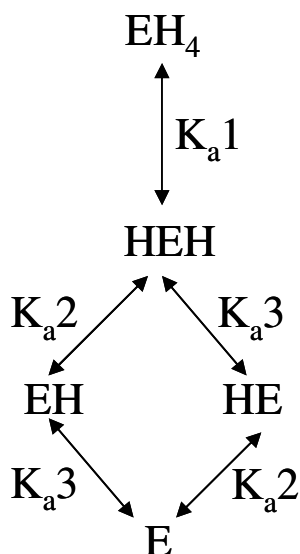
<b>Residue</b>	<b>Electrostatic potential</b>			
<b>D58</b>	n/a	-	-	-
<b>E68</b>	1.83269	n/a	-	-
<b>K70</b>	0.678835	1.82826	n/a	-
<b>Y94</b>	0.58314	1.62349	2.44791	n/a
	<b>D58</b>	<b>E68</b>	<b>K70</b>	<b>Y94</b>

**Appendix III. Summary of metal ligated water pK<sub>a</sub> on metallonucleases.**

Enzyme	pdb code	pK <sub>a, apparent</sub>	Model pK <sub>a</sub>	Operations	M(II)
<i>PvuII</i>	1H56(subunit A)	6.5	11.4	WT	One Mg <sup>2+</sup>
	1H56(subunit A)	9.8	11.4	K70A	One Mg <sup>2+</sup>
	1F0O(subunit A)	7.4	11.4	WT	Two Mg <sup>2+</sup>
	1F0O(subunit A)	9.9	11.4	K70A	Two Mg <sup>2+</sup>
	1F0O(subunit B)	9.3	11.4	WT	Two Mg <sup>2+</sup>
	1F0O(subunit B)	10.5	11.4	K70 off	Two Mg <sup>2+</sup>
	1F0O(subunit B)	8.7	11.4	K70Q	Two Mg <sup>2+</sup>
	1F0O(subunit B)	10.7	11.4	Q70 off	Two Mg <sup>2+</sup>
<i>HincII</i>	1HXV(subunit A)	10.8	14	WT	Two Mn <sup>2+</sup>
	1HXV(subunit A)	12.2	14	K129A	Two Mn <sup>2+</sup>
	1HXV(subunit A)	7.1	11.4	WT	Two Mn <sup>2+</sup>
	1HXV(subunit A)	8.2	11.4	K129A	Two Mn <sup>2+</sup>
	1HXV(subunit A)	6.3	10.6	WT	Two Mn <sup>2+</sup>
	1HXV(subunit A)	7.4	10.6	K129A	Two Mn <sup>2+</sup>
<i>EcoRV</i>	1EO4(subunit A)	7.3	10.6	WT	Two Mn <sup>2+</sup>
	1EO4(subunit A)	8.5	10.6	K91A	Two Mn <sup>2+</sup>
	1EON(subunit A)	8.6	11.4	WT	Two Mg <sup>2+</sup>
	1EON(subunit A)	10.7	11.4	K91A	Two Mg <sup>2+</sup>
	1RVB(subunit B)	8.9	11.4	WT	Two Mg <sup>2+</sup>
	1RVB(subunit B)	10.1	11.4	K91 off	Two Mg <sup>2+</sup>
	1SX5(subunit A)	9.5	14	A38K	Two Mn <sup>2+</sup>
	1SX5(subunit A)	11.6	14	K91off	Two Mn <sup>2+</sup>
	1SX8(subunit B)	6.6	10.6	WT	Two Mn <sup>2+</sup>
1SX8(subunit B)	8.3	10.6	K92A	Two Mn <sup>2+</sup>	
<i>TnsA</i>	1F1Z(subunit A)	6.3	11.4	WT	Two Mg <sup>2+</sup>
	1F1Z(subunit A)	7.9	11.4	K132 off	Two Mg <sup>2+</sup>
T7 Endo I	1MOD(subunit A)	6.3	10.6	WT	Two Mn <sup>2+</sup>
	1MOD(subunit A)	7.9	10.6	K67 off	Two Mn <sup>2+</sup>
<i>EcoRI</i>	1QPS(subunit A)	7.5	10.6	WT	One Mn <sup>2+</sup>
	1QPS(subunit A)	8.1	10.6	K113A	One Mn <sup>2+</sup>
NgoMIV	1F1U(subunit A)	5.6	11.4	WT	Two Mg <sup>2+</sup>
	1F1U(subunit A)	7.2	11.4	K187 off	Two Mg <sup>2+</sup>

The pdb files are downloaded from [www.rcsb.org](http://www.rcsb.org). The subunit of the crystal structures are modified according to the “mutation” or “off” operations as described in Experiments and Methods.

**Appendix IV. pH dependent activity equation (3).**



The ionizations scheme is shown as above. The assumptions include:

- 1).  $\text{EH}_4$  loses one proton through intermediate  $\text{EH}_3$  step by step with apparent equilibrium constant  $K_{a1}$ .
- 2). E has two proton binding sites corresponding to general base and general acid catalysis. EH is active and HE is inactive.

The apparent activity  $k_{\text{obs}} = k_{\text{max}} \cdot \text{EH} / \text{E}_{\text{total}}$ .

$$\text{E}_{\text{total}} = \text{EH}_4 + \text{HEH} + \text{EH} + \text{HE} + \text{E}$$

According to ionizations shown in the scheme,  $\text{EH}_4$ , HEH, HE and E all can be expressed as a function of EH.

$$\text{EH}_4 = \text{EH} \cdot 10^{2 \cdot \text{pKa}_1 + \text{pKa}_2 - 3 \cdot \text{pH}}$$

$$\text{HEH} = \text{EH} \cdot 10^{\text{pKa}_2 - \text{pH}}$$

$$\text{HE} = \text{EH} \cdot 10^{\text{pKa}_2 - \text{pKa}_3}$$

$$\text{E} = \text{EH} \cdot 10^{\text{pH} - \text{pKa}_3}$$

$$\text{Therefore, } k_{\text{obs}} = k_{\text{max}} / (1 + 10^{(2 \cdot \text{pKa}_1 + \text{pKa}_2 - 3 \cdot \text{pH})} + 10^{(\text{pKa}_2 - \text{pH})} + 10^{(\text{pH} - \text{pKa}_3)} + 10^{(\text{pKa}_2 - \text{pKa}_3)})$$

---

## VITA

Fuqian Xie was born on July 6, 1981 in city of Qufu, P.R. China. In 2002, Fuqian Xie received his Bachelor's degree in polymer chemistry from Zhejiang University, China. In the fall of 2003 he entered the graduate program of Chemistry and Biochemistry department at the University of Missouri-St. Louis and received his Master's degree in 2006.

### Permanent Address

Fuqian Xie  
8257 C Normandy Trace CT  
St. Louis MO 63121